DIMENSIONS OF CANCER:

IN VITRO MODELS OF THE TUMOR MICROENVIRONMENT

&

COMMUNITY ENGAGEMENT IN CANCER RESEARCH

A Dissertation

Presented to the Faculty of the Graduate School

of Cornell University

In Partial Fulfillment of the Requirements for the Degree of

Doctor of Philosophy

by

Peter Francis DelNero

December 2017

DIMENSIONS OF CANCER:

IN VITRO MODELS OF THE TUMOR MICROENVIRONMENT &

COMMUNITY ENGAGEMENT IN CANCER RESEARCH

Peter Francis DelNero

Cornell University 2017

Sustained research efforts have advanced our knowledge of the complexities that make cancer a highly diverse and clinically challenging disease. Of the many factors, the tissue microenvironment is increasingly appreciated for its crucial role in tumor initiation, progression, recurrence, and treatment response. The microvasculature is a critical determinant of tissue perfusion, with important consequences for cellular metabolism, drug delivery, and metastasis. To better understand how tissue perfusion contributes to tumor malignancy, I fabricated microphysiological *in vitro* models of the tumor-vascular microenvironment and assessed the differential regulation of tumor hypoxia response in 2D versus 3D culture. Results from these studies point to the value of tissue engineering approaches for deciphering the interdependence between cancer cells and their vascular microenvironment.

Laboratory-based research provides important insights on the biological mechanisms of disease, and these basic sciences approaches are strengthened by a broad understanding of the human and social dimensions of cancer. To this end, I helped initiate and sustain a community-based partnership that fosters dialogue between cancer patients and scientists. The partnership enables the mutual exchange of knowledge and experience across the community-campus boundary. This project led to several major outcomes, including a monthly seminar for non-academic audiences, a certificate program for public engagement, an undergraduate writing class about cancer, and several avenues for informal science education. The patient-researcher partnership has a sustained impact in graduate and postdoctoral training at Cornell and provides a valuable forum to our local cancer community.

BIOGRAPHICAL SKETCH

Peter Francis DelNero was born in Lebanon, PA. He graduated from Vanderbilt University with a bachelor's degree in Chemical and Biomolecular Engineering. As an undergraduate, Peter was involved in the Searle Systems Biology and Bioengineering Undergraduate Research Experience (Searle SYBBURE) program. Peter learned microfabrication, mammalian cell culture, microscopy and other experimental techniques in the laboratories of John Wikswo, Kevin Seale, Ann Richmond, John McLean, and Melody Swartz. His undergraduate work earned him the W. Dennis Threadgill Award for Outstanding Achievement in Chemical Engineering and the Thomas G. Arnold Prize for Biomedical Engineering Systems Design.

In 2011, Peter joined the Department of Biomedical Engineering at Cornell University. During his time as a graduate student, Peter accumulated a diversity of experiences that broadly enriched his education. He was a founding leader of the Cancer Brainstorming Club and helped initiate the Patient-Researcher Partnership. He taught an undergraduate seminar entitled *Dimensions of Cancer*, where students explored the many ways they can make a positive difference in the cancer community. He actively participated in programs related to education, social justice, and public engagement. These programs included leadership positions in the Cornell Participatory Action Research Network (cPARN), the Center for the Integration of Research, Teaching, and Learning (CIRTL) and the Center for Teaching Excellence (CTE), the Intergroup Dialogue Project (IDP), and the Office of Engagement Initiatives (OEI). Peter was also the founding admiral for the Big Red Pumpkin Regatta, a student organization dedicated to growing and racing giant pumpkins. Peter received the K. Patricia Cross Future Leaders Award from the Association of American Colleges and Universities "for exemplary promise as a future leader in higher education."

ACKNOWLEDGEMENTS

Thank you to my family, friends, and colleagues who made this degree possible. My deepest gratitude to Bob Riter, Bob Weiss, Alex McGregor, Jason Hungerford, Jojo DelNero, and Claudia Fischbach. Special thanks to Colleen McLinn and Richard Kiely, who went above and beyond in their support and mentorship. Also thanks to Jon Sipple and Janna Lamey, who helped me through difficult times. I gratefully acknowledge my thesis committee, labmates, collaborators, and community partners for their enduring support and mentorship. And many thanks to Riley Bear and the Dilmun Hill pumpkin patch that changed my life.

My work was generously supported by fellowships and grants from the National Science Foundation Graduate Research Fellowship Program, the National Cancer Institute, the John S. Knight Institute for Writing in the Disciplines, the Cornell Learning Initiative in Medicine and Bioengineering, and the Cornell Office of Engagement Initiatives.

AUTHOR CONTRIBUTIONS

Chapter 2: In vitro models of tumor vessels and matrix: engineering approaches to investigate transport limitations and drug delivery in cancer

Bo Ri Seo, Peter DelNero, and Claudia Fischbach conceived this review of literature. Bo Ri Seo and Peter DelNero collected, analyzed, and interpreted the literature. All authors drafted, critically revised, and gave final approval of the article.

Chapter 3: 3D culture regulates tumor hypoxia response and angiogenesis via pro-inflammatory pathways

Peter DelNero, Maureen Lane, Scott Verbridge, Brian Kwee, and Pouneh Kermani collected, analyzed, and interpreted the data. Peter DelNero, Maureen Lane, and Claudia Fischbach wrote the article. All authors designed the study and gave final approval of the article.

Chapter 4: Formation of microvascular networks in vitro

John Morgan, Peter DelNero, Ying Zheng, Scott Verbridge, Junmei Chen, Nak Wan Choi, Anthony Diaz-Santana., José López, Thomas Corso, Claudia Fischbach, and Abraham Stroock designed the research. John Morgan, Peter DelNero, Ying Zheng, Scott Verbridge, Junmei Chen, Michael Craven, Pouneh Kermani, and Barbara Hempstead performed research. John Morgan, Peter DelNero, Ying Zheng, Junmei Chen, Michael Craven, José Lopez, and Abraham Stroock analyzed data. John Morgan, Peter DelNero, Ying Zheng, and Abraham Stroock wrote the paper. Authors acknowledge the technical assistance of G. Swan, and thank C. Murry and S. Schwartz for helpful discussions.

Chapter 5: A physical sciences – oncology perspective on cancer metabolism

Peter DelNero, Ben Hopkins, and Claudia Fischbach conceived and wrote this perspective article. All authors critically reviewed and gave final approval of the article.

Chapter 6: From patients to partners

Bob Riter and Robert Weiss initiated and sustained the cancer patient-researcher partnership. Peter DelNero and Alexandra McGregor wrote the article. The authors gratefully acknowledge all the community members and students who have been involved in the partnership.

Chapter 7: Navigating a wayward path toward public engagement

Peter DelNero designed the study, collected and interpreted evidence, and wrote the article. The author gratefully acknowledges Richard Kiely for critical review and helpful discussions.

Appendix 1: Engineered tumours: roll-on scaffolds

Peter DelNero and Claudia Fischbach drafted, critically revised, and gave final approval of the article.

Appendix 2: Microengineered tumor models: insights and opportunities from a physical sciences – oncology perspective

Peter DelNero, Young Hye Song, and Claudia Fischbach designed this review of literature. Peter DelNero and Young Hye Song collected, analyzed, and interpreted the literature. All authors drafted, critically revised, and gave final approval of the article.

TABLE OF CONTENTS

CHAPTER 1

INTRODUCTION

Cancer is an intricate disease on all scales: at the microscopic level, malignant cells evolve within a complex biological landscape. At the human level, the diagnosis accompanies a cascade of physical, emotional, and financial stresses. On population and institutional levels, cancer constitutes a global epidemic (8.8M deaths worldwide, accounting for nearly 1 in 6 deaths in 2015), and enormous resources are exchanged in the relentless quest for effective treatments (total costs estimated at $1.16T globally in 2015). Due to its broad scope, cancer demands the mutual exchange of knowledge, skills, and ideas across many different groups, including physicians, researchers, patients, industries, and government officials.

The NCI Physical Sciences-Oncology Centers (PSOC) initiative is one strategy to foster dialogue between stakeholders that do not ordinarily interact with each other. The program disrupts traditional approaches to cancer research by encouraging radical ideas and transformative paradigms. In particular, the PSOC emphasizes the value of seeing cancer from many different perspectives. As a young investigator in the Cornell Center for the Microenvironment and Metastasis (now the Center for the Physics of Cancer Metabolism), I was enculturated into an academic community that values innovation and transdisciplinary collaboration, and this became the foundation for my graduate research experiences.

The following dissertation contains eight publications that I produced during my doctoral studies. These articles represent major academic milestones; in addition to these chapters, there are many aspects of my scholarship that I cannot directly translate into static documents, such as events, relationships, and personal development. Non-traditional scholarly products have contested value in academia; nevertheless, these elements make a substantial and original contribution toward knowledge of biomedical sciences and engineering.

Part 1: Tissue Engineering Models of Cancer

Within the PSOC, the Fischbach lab investigates a fundamental problem in cancer biology regarding the relationship between cancer cells and their surrounding tissue, including the links between cell metabolism and angiogenesis. As cancer cells proliferate, they eventually outgrow their blood supply. Without adequate vasculature, tumor growth is typically limited to 2 mm diameter. In order to continue growing, cancer cells secrete pro-angiogenic factors to promote new vessel growth and enable tumor progression.

In 1971, Judah Folkman proposed that interfering with angiogenic signaling might provide a way to cut off the blood supply and effectively starve the tumor. Several arguments support his idea, including that endothelial cells may be more susceptible than malignant epithelial cells. In 2004, the US FDA granted approval for Avastin (bevacizumab) for advanced colon cancer, the first pharmacological inhibitor of vascular endothelial growth factor (VEGF). The drug was later approved for lung, kidney, brain, and breast cancers. In the past 40 years, the principle of anti-angiogenic therapy was successfully translated into dozens of treatments for regulating vessel growth in cancer and other diseases. However, results were not all positive. In 2011, the FDA announced that the metastatic breast cancer indication for Avastin was withdrawn after finding no significant improvement in overall survival and an increased incidence of adverse effects.

The inconsistent benefits of anti-angiogenic therapy caused researchers to carefully reevaluate this treatment paradigm and the underlying mechanisms that regulate vessel growth. For example, Rakesh Jain proposed a conceptual shift from tumor starvation to vascular normalization. Rather than inhibit vessel growth, the same angiogenic compounds might instead be used to restore vessel maturation and tissue perfusion. According to Jain, a more stable endothelium might enhance drug delivery and radiation therapy. This idea was supported by

emerging evidence that angiogenic drugs work better in combination with chemotherapy and radiation, but are not effective by themselves. As the paradigm of anti-angiogenic therapy evolved, scientists and clinicians required a better understanding of microvascular regulation within the tumor microenvironment.

To address this problem, a subgroup from the Fischbach lab was working with Dr. Abraham Stroock to develop *in vitro* models of tumor vasculature. An expert in microfluidics, Dr. Stroock and his team were in the process of patterning microfluidic channels within cell-laden hydrogels. These channels provided a template for a biomimetic microvascular network, fully embedded within a biomaterial scaffold. In 2011, I joined this collaboration; the outcomes of my involvement are reported in Part I of this dissertation.

Chapter 2 provides the relevant background information for Part I. The article introduces the use of *in vitro* models to simulate the physical and fluid dynamic properties of a tumor, with special emphasis on the context of drug delivery. It reviews the biological characteristics, engineering principles, and *in vitro* model systems associated with microvascular and interstitial transport functions. The article also presents the limitations and future opportunities for microfluidic devices, patient-derived culture platforms, and integrating *in vitro* platforms with computer simulations.

Chapter 3 presents data from a comprehensive microarray gene expression analysis of tumor cells cultured in 2D and 3D environments. Oral squamous cell carcinoma (OSCC3) cells were embedded within microfabricated alginate discs or cultured on polystyrene and subjected to 1% or 17% O2. Gene expression and protein secretion of molecules of interest were validated by qPCR and ELISA with three additional tumor cell lines. 3D microwell invasion assays were used

to evaluate endothelial cell response to tumor-secreted soluble factors or corresponding inhibitors, including IL-8 and VEGF. Our results revealed strong coupling between culture dimensionality and hypoxic response, which was mediated in part by pro-inflammatory signaling pathways. In particular, IL-8 emerged as a major player in the microenvironmental regulation of the hypoxic program. Notably, this interaction between dimensionality and oxygen status via IL-8 exhibited pro-angiogenic consequences in a 3D endothelial invasion assay. Taken together, our data suggest that pro-inflammatory pathways may underlie the differential regulation of hypoxic response and facilitate tumor angiogenesis in 3D environments. These results highlight the importance of pathologically relevant tissue culture models to study the complex physical and chemical processes by which the cancer microenvironment mediates new vessel formation.

Chapter 4 is a protocol paper describing a method to fabricate microvascular networks *in vitro*. Despite its considerable therapeutic significance, the study of vascular biology lacks well-controlled experimental platforms to investigate microvascular growth, structure, and function in a physiologically appropriate context. We used soft lithography to fabricate explicit microvascular structures, fully embedded within remodelable hydrogel scaffolds. These platforms allowed the precise distribution of biomolecular signals, localized heterotypic cell seeding, and tunable matrix properties and fluid forces. The system supported multiday co-cultures and enabled in situ confocal microscopy of living or fixed tissues. Altogether, this model appropriately simulated the structure and function of microvascular networks in diseased tissue, and can be used to explore the interactions between tissue metabolism, angiogenesis, and microcirculation.

In chapter 5, I discuss the physical determinants of aberrant tumor metabolism and highlights how engineered culture models that recapitulate these properties may advance personalized drug screening. There is a demand for model systems to screen anti-cancer agents,

including drugs that target metabolic pathways, for precision medicine. In order to predict drug response, model systems must be attentive to tissue properties that regulate tumor metabolism. While much focus has been placed on the biochemical and cellular composition of the tumor microenvironment, physical aspects are similarly important. In particular, transport phenomena and matrix mechanics are major determinants of disease progression and treatment outcomes in general, and play an especially important role in regulating cell metabolism. In our article, we explain how engineered culture platforms allow modeling physical aspects of the tumor microenvironment in a relevant biological context and how these systems may help guide drug selection and dosing for precision oncology.

Part II: Public Engagement in Cancer Research

My involvement in the PSOC was not limited to the laboratory. I was also a founding leader of the Cancer Brainstorming Club (CBC), a student organization dedicated to coordinating education, outreach, and training programs for PS-OC young investigators. As a CBC officer, I planned various events to facilitate peer networking and information sharing, including exchange visits, journal clubs, and work-in-progress seminars. I also helped arrange workshops at two of the PSOC annual meetings and regularly contributed to NCI site visits, quarterly reports, and grant preparation.

In 2012, the CBC officers learned that colleagues at Moffitt were hosting a "Patient Night Out," where cancer patients and survivors would tour their labs and learn about research. Enchanted by this idea, Alex McGregor contacted our center's patient advocate to discuss the possibility of replicating this event at Cornell. After several unsuccessful inquiries, Alex decided to contact the executive director (Bob Riter) of a local cancer support center (the Cancer Resource Center of the Finger Lakes). Bob immediately responded to the idea. Coincidentally, he had

already started to build a relationship with cancer researchers at Cornell, led by Robert Weiss in the College of Veterinary Medicine. In March 2013, we all met together to discuss plans for the patient-researcher partnership.

The Patient-Researcher Partnership was a simple idea with powerful outcomes. Initially, we started hosting monthly seminars that were open to the public. These events encouraged interaction between scientists and community members, and we soon developed a deep appreciation for patients' perspectives. Our sustained relationship with the cancer community produced a continuous stream of new opportunities to strengthen and extend the partnership.

The partnership started as an outreach activity, but it gradually became an important part of my scholarship. I noticed that our program was part of a larger trend in higher education, which recognizes the value of collaborating with non-academic communities. Public engagement is particularly relevant in biomedical research. Because patients are at the center of the healthcare industry, it makes sense that aspiring researchers should interact with people who are affected by the diseases they study. This began my inquiry into public engagement in cancer research, which constitutes Part II of this dissertation.

In Chapter 6, Alex McGregor and I explain how a partnership transformed our graduate research experience. This article presents outcomes from our collaboration with Bob Riter, Robert Weiss, and the Cancer Resource Center. We argue that patient involvement contributes to all aspects of biomedical research, beginning with the training of new scientists. We hope that people who read our article will be encouraged to initiate or support similar programs at their own institutions.

Chapter 7 is a reflective essay that grapples with the concept of public engagement in biomedical engineering. The purpose of this article is to convey the *meaning* that I attached to my experiences as a "engaged scholar." As I began to deviate from a typical laboratory research career, I struggled to reconcile a new set of attitudes, priorities, and aspirations. Chapter 7 presents the messages that might have helped me as I learned to navigate this unfamiliar landscape. My goal was to provide affirmation and solidarity to students who found themselves in a similar situation.

Appendix

Appendix I is a commentary about an article that appeared in *Nature Materials*. The original paper presented a biocomposite scaffold for spatial analysis of cell metabolism within a molecular gradient. The "tumor roll" comprised a hydrogel-coated coffee filter wrapped around an aluminum spindle; as the material was unraveled, biochemical assays could be performed on each layer within the scaffold. This platform provides an extremely simple and reproducible method for investigating the relationship between cancer cells and their physical and soluble microenvironment. My article highlights the value of developing robust technologies that can be immediately adopted in non-engineering labs.

Appendix II is a review article about the using microfluidic biomaterials to recapitulate the tumor microenvironment. The article discusses materials and methods that can be used to generate physiologically-relevant *in vitro* culture models, and new opportunities that are afforded by these technologies.

CHAPTER 2

IN VITRO MODELS OF TUMOR VESSELS AND MATRIX: ENGINEERING APPROACHES TO INVESTIGATE TRANSPORT LIMITATIONS AND DRUG DELIVERY IN CANCER

Bo Ri Seo*, Peter DelNero*, and Claudia Fischbach. (2014) In vitro models of tumor vessels and matrix: engineering approaches to investigate transport limitations and drug delivery in cancer. *Advanced Drug Delivery Reviews* 69–70:205–16.

**Authors contributed equally.*

Abstract

Tumor-stroma interactions have emerged as critical determinants of drug efficacy. However, the underlying biological and physicochemical mechanisms by which the microenvironment regulates therapeutic response remain unclear, due in part to a lack of physiologically relevant *in vitro* platforms to accurately interrogate tissue-level phenomena. Tissue-engineered tumor models are beginning to address this shortcoming. By allowing selective incorporation of microenvironmental complexity, these platforms afford unique access to tumor-associated signaling and transport dynamics. This review will focus on engineering approaches to study drug delivery as a function of tumor-associated changes of the vasculature and extracellular matrix (ECM). First, we review current biological understanding of these components and discuss their impact on transport processes. Then, we evaluate existing microfluidic, tissue engineering, and materials science strategies to recapitulate vascular and ECM characteristics of tumors, and finish by outlining challenges and future directions of the field that may ultimately improve anti-cancer therapies.

Introduction

Given its extensive socioeconomic impact, cancer continues to be a major focus of drug development and delivery research. Nevertheless, clinical success of anti-cancer therapies remains limited, and most treatment strategies exhibit marginal efficacy, serious side effects, and the development of resistance. Moreover, complete tumor eradication is mostly impossible, and time until patient relapse or metastasis remains a tragic measure of clinical success. Targeted therapies interfering with specific genetic and molecular mechanisms of tumorigenesis have offered improvement relative to conventional cytotoxic therapy; however, cancer cells frequently evade therapy by assuming resistance mechanisms including secondary mutations and epigenetic modifications (1-3).

While many therapies directly target tumor cells, the microenvironment in which tumor cells reside is an equally important participant in disease progression. During health, normal "contextual cues" of the host microenvironment prevent the cancerous outgrowth of epithelial cells (4, 5). However, perturbation of this homeostasis, e.g., due to chronic inflammation, metabolic changes, or hormonal imbalance, enables the initiation and progression of malignancy (6-9) as well as the emergence of resistance (10, 11).

In addition to directly affecting tumor cell behavior, microenvironmental conditions may promote recurrence by simply preventing effective transport of therapeutics. When anti-cancer drugs are systemically administered, steps of drug delivery include transport (1) within the circulation, (2) across blood vessel walls, and (3) through the interstitial space to the tumor (12,

13). Alterations of microenvironmental conditions interfering with any of these processes may affect drug bioavailability with consequences on efficacy.

The physicochemical properties of the vasculature and the interstitial extracellular matrix (ECM) are key regulators of anti-cancer drug distribution and efficacy (14). As the primary conduits of perfusion, blood vessels determine the availability of drugs throughout the body and within individual tissues. However, heterogeneous microvascular function as present within tumors can compromise delivery and undermine the effects of therapeutic agents (14). Enhanced permeability and retention (EPR) in leaky vessels has facilitated the targeting of macromolecular therapies (15-19). Yet, the asymmetric distributions of oxygen or drugs within a tumor provide a conducive landscape for the evolution of resistance within heterogeneous populations of cancer cells (20). Although vascular structure and function largely regulate the spatiotemporal distribution of drug, interstitial space can also affect transport rates (21). In particular, excessive ECM deposition due to fibrotic remodeling (also termed desmoplasia) physically hinders diffusion of large anti-tumor molecules through the interstitium (21).

Despite the well-established physical principles governing biological transport phenomena, the opportunity to leverage these principles to improve therapeutic outcomes is limited. Conventionally, new anti-cancer compounds are first tested in 2D tissue culture, which provide homogeneous access to drug and neglect the 3D microenvironmental properties inherent to tumors. Additionally, even positive results from animal studies do not always translate to efficacy in humans due to species-dependent discrepancies in signaling and physiology (22, 23). The development of tissue-engineered model systems that accurately recapitulate human tumor with increasing physiological complexity may help to understand and test microenvironmental parameters affecting tumor response. Here, we review current understanding of the biological

characteristics underlying tumor-associated changes of the vasculature and ECM properties, examine the consequences of these parameters for mass transport and drug delivery, and present emerging *in vitro* strategies that may provide new insights for improved anti-cancer therapies (24-26).

Tumor vasculature: biophysical changes and their relevance to drug delivery

Biological characteristics of tumor microvasculature

Since Judah Folkman's seminal observations in 1971 that tumorigenesis is associated with the ingrowth of abnormal blood vessels (27, 28), vascular dysfunction has become an enduring theme in cancer biology and anti-cancer therapy. When compared to healthy vasculature, tumor vessels are leaky, fenestrated, tortuous, and dilated, with chaotic branching patterns including shunts and loops, as well as irregular hierarchy of vessels (29-34) (Figure 1). The tumor vasculature comprises at least six types of vascular structures with distinct properties, including mother vessels (MVs) and several varieties of daughter vessels (capillaries, glomeruloid microvascular proliferations, vascular malformations) (35, 36). MVs are enlarged sinusoids resulting from pericyte detachment, basal membrane (BM) degradation, and endothelial thinning (36). Despite this distension, MVs do not increase blood flow, possibly due to their hyper-permeable membrane function (35). Meanwhile, immature daughter vessels are fenestrated and lack functional perfusion. Vascular leakage, coupled to dysfunctional lymphatic drainage, results in an accumulation of interstitial fluid, which compromises the hydrostatic and osmotic pressure gradients that drive transvascular convection (37). Collectively, this heterogeneous network of aberrant blood vessels yields erratic perfusion of diseased tissue, with important consequences for pathogenesis and therapy.

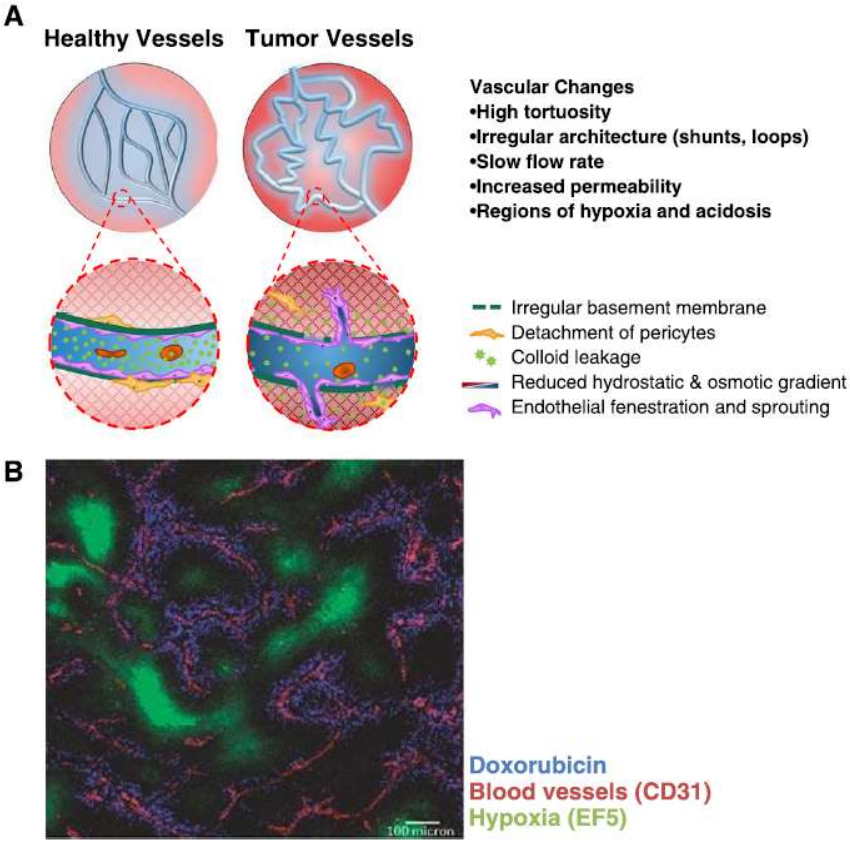

Fig. 1. Biophysical changes of tumor vasculature. A) Schematic illustration of the structural and functional changes in tumor vasculature, in duding tortuous vessels, chaotic branching, disrupted barrier function, and compromised hydrostatic and osmotic gradients. B) Aberrant vasculature undermines transport processes within diseased tissue, resulting in asymmetric distributions of oxygen and drugs to the tumor. This micrograph illustrates the penetration depth of doxorubicin and highlights the large, hypoxic regions of the tumor unaffected by therapy (154). Reproduced with permission from Nature Publishing Group.

Hypoxia and acidosis are the most prominent consequences of deregulated vascular function. Compromised vessel characteristics lead to poor supply of oxygen and clearance of metabolic wastes, mediating sustained hypoxia (<1% O_2) and acidosis (as low as pH ~6.6-6.8 in some areas) (38-40). These microenvironmental conditions directly promote tumor progression and new vessel formation by activating a variety of transcriptional programs (41-44). In particular, stabilization of the alpha subunit of the hypoxia inducible factor 1 (HIF-1) transcription factor in low-oxygen conditions leads to an orchestrated program of hypoxic response (42, 45-47) that includes the up-regulation of pro-angiogenic morphogens (including vascular endothelial growth factor [VEGF] and basic fibroblast growth factor [bFGF]). However, rather than promoting the formation of healthy blood vessels that could normalize tissue O_2 levels and pH, excess pro-angiogenic signaling activates a vicious cycle that undermines vascular stability by impairing vessel organization and permeability thus exacerbating these pathological conditions (48-50).

In addition to metabolic transport, impaired vascular function also compromises the homogeneous delivery of therapeutic agents, resulting in poor distribution of drugs throughout the tumor (51). Low vascular function at the tumor interior prevents therapeutic access to large regions of tissue (31). Homogeneous delivery is further undermined by the absence of hydrostatic and osmotic pressure gradients, which are necessary for interstitial convection to distribute large therapeutic agents (52, 53). In some cases, enhanced vascular permeability and retention (EPR) has been coopted as a mechanism for tumor targeting of large particles such as antibodies and micelles (15). However, although high molecular weight drugs and drug carriers easily traverse the endothelial membrane of the tumor, they have poor penetration depth and achieve little benefit in regions distal to blood vessels (51, 54, 55). Therefore, vascular normalization is an emerging theme for improving therapeutic delivery (56-58).

Whereas most vascular therapies emphasize the destruction of blood vessels to stunt tumor growth, some researchers hope to re-appropriate angiogenic drugs as adjuvant therapy in order to improve drug distribution (59). By increasing perfusion in the tumor, this method may overcome major disadvantages of chemotherapy such as short half-life and small therapeutic index (range of concentration between efficacy and toxicity) (60). In the past decade, numerous clinical trials have revealed the benefits of anti-angiogenic therapy as an adjuvant to chemotherapy or radiation therapy (60-62). However, the dearth of pre-clinical models to recapitulate vascular transport remains a challenge for the development of new strategies for vascular normalization.

Effects of microvascular dysfunction on transport physics

Whereas conventional pharmacokinetic metrics (e.g. distribution volume, half-life, clearance rate) characterize the average availability of drug in tissues, these measurements only poorly approximate the effective distribution of agents within tumors. In fact, large regions of tumors lack adequate vascular perfusion and thus, can remain unaffected by treatment, even at high doses. This is particularly true of large molecules (>10 kDa), which are not able to freely diffuse across the endothelium and through the tissue. Instead, convective forces govern the exchange of large compounds from the circulation (Box 1). In healthy tissues, these forces balance the influx and outflux at the arterioles and post-capillary venules to provide adequate perfusion. In the case of a tumor, however, vascular leakiness reduces hydrostatic pressure in the vessel while increasing osmotic pressure in the interstitium (approximately 29 +/- 3 mmHg in breast tumor, compared to -0.3 +/- 0.1 mmHg in healthy breast tissue) (63, 64). Together, these changes significantly diminish the bioavailability of drugs by reducing transcapillary hydrostatic gradients necessary for fluid exchange (65).

Box 1. Forces governing transvascular transport.

The Kedem–Katchalsky equation describes solute flux (J_s) as a combination of convective and diffusive forces across the endothelial membrane:

$$J_s = J_v\left(1-\sigma_f\right)\overline{C}_s + PS\Delta C$$

where σ_f is the filtration reflection coefficient, $\overline{C}_s$ is the average molar concentration in the membrane, P is the permeability coefficient, S is the surface area, and ΔC is the change in concentration across the endothelium. The fluid flux (J_v) is derived from Starling's Law, which describes the contributions of hydrostatic (p) and osmotic (π) pressure gradients:

$$J_v = L_p S(\Delta p - \sigma_s \Delta\pi)$$

where L_p is hydraulic conductivity, S is surface area, and σ_s is the osmotic reflection coefficient, which ranges from 0 to 1 based on the membrane permeability to solutes. Based on these equations, transvascular solute transport is governed by four physiological constants describing solute and membrane characteristics:

$$\text{Hydraulic conductivity}: \quad L_p = \frac{J_v/S}{\Delta p} = \frac{\textit{fluid flux}}{\textit{hydrostatic pressure difference}}$$

$$\text{Permeability coefficient}: \quad P = \frac{J_s/S}{\Delta C} = \frac{\textit{solute flux}}{\textit{concentration difference}}$$

$$\text{Osmotic reflection coefficient}: \quad \sigma_s = \frac{\Delta p}{\Delta\pi} = \frac{\textit{hydrostatic pressure difference}}{\textit{osmotic pressure difference}}$$

$$\text{Filtration reflection coefficient}: \quad \sigma_f = 1 - \frac{J_s}{J_v C_0} = 1 - \frac{\textit{solute flux in membrane}}{\textit{solute flux insolution}}.$$

Measurements for these parameters in healthy and tumor tissue are provided by [52]. These factors are affected by solute (size, charge, polarity) and membrane (pore size, pore density) properties [66].

In addition to simple mass transport equations, a variety of tools have been developed to quantitatively evaluate the effectiveness of mass transport in tissues. Dimensionless numbers are particularly useful to identify transport limitations (66). For example, the Biot number compares the relative resistance attributed to the endothelial membrane versus the interstitial matrix. Likewise, the effectiveness factor describes the rate of transport compared to the rate of reaction. Both of these parameters can help identify limitations to drug penetration and efficacy. For example, in cases where transvascular transport limits therapeutic efficiency, combinations with permeabilizing agents may improve delivery, while other therapies limited by interstitial diffusion may benefit from stroma-targeted treatments. A modified effectiveness factor can incorporate the Biot number to identify the relative resistance due to vascular versus interstitial transport (67, 68).

Similarly, the "observable modulus" evaluates penetration distance based on transport and reaction considerations (67). This parameter defines a "dimensionless reaction rate" (the effectiveness factor * thiele modulus), and is defined as a function of the distance from the nearest vessel. This parameter allows the calculation of a penetration depth, or the distance at which the concentration drops below an effective dose. A low modulus indicates deeper penetration, and high modulus indicates poor distribution away from the capillary. The observable modulus has been used to determine the Krogh distance, or the range for diffusion-limited oxygen transport before reaching anoxia and necrosis (67). In the case of therapy, the same parameter can describe the effective therapeutic range of a drug and thus characterize and inform angiogenic therapy or EPR designs.

By evaluating the specific physical contributions to therapeutic resistance by transport or reaction kinetics, these quantitative methods may help identify major barriers of delivery and enable the rational design of dosing strategies, including in combination with drugs that target the

vasculature or the stroma to optimize therapeutic efficacy. Nevertheless, many of these quantitative approaches are frequently neglected. This may be due in part to the inaccessibility of the various coefficients needed to determine the dimensionless parameters. Conventional methods to test vascular permeability, such as Evan's blue staining, provide little chance for rigorous quantification. Meanwhile, *in vitro* methods to measure endothelial permeability or tissue diffusivity, such as multilayer or spheroid cultures, may not accurately reflect *in vivo* parameters (55). Therefore, new methods to accurately determine the parameters affecting vascular and interstitial mass transport will provide a valuable resource for the design of therapeutic strategies that target the tumor microenvironment (66).

Recapitulating tumor-associated vascular transport through in vitro models

Organotypic 3D culture models present an emerging opportunity to create controlled experimental conditions that faithfully reproduce aspects of the physiological environment. However, as sufficient mass transport within cell-laden biomaterials remains a significant limitation of 3D cultures, these approaches are typically performed in a microscale format and lack the recapitulation of tumor-inherent transport physics. New *in vitro* platforms that integrate functional vascular structures can help to overcome this limitation (69). Biomimetic microvascular networks provide controlled experimental platforms to evaluate specific interactions between endothelial cells and tumor environment, improve the design of therapies targeting the vasculature, and assess the efficacy of new drugs or drug delivery strategies (70, 71).

Two categories of microfluidic vascular models have been introduced. The first design, pioneered by the groups of Roger Kamm and Lance Munn, employs microfabricated silicone molds to confine biological hydrogels between parallel microfluidic channels (Figure 2A). Endothelial cells cultured on the surface of these confined gels are able to sprout into the matrix

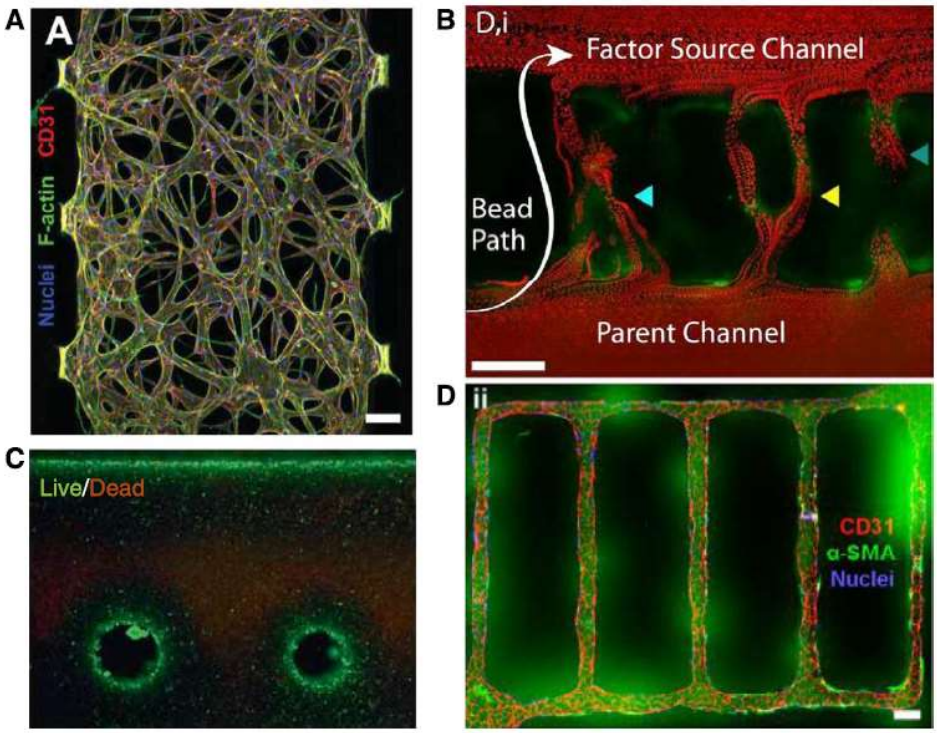

Fig. 2. Examples of microengineered vascular structures. A) Vascular structures created by culturing endothelial cells in confined gels within a microfluidic platform are useful for evaluating endothelial cell response to angiogenic gradients, shear stresses, or paracrine interactions (73). B) Anastomosis between parallel vessels enables the autonomous formation of capillary-scale networks fully embedded within 3D biological matrices. The original vessel structures were fabricated by the pull-through method (75). C) Live/dead staining illustrates dependence of cell viability on spatial differences in oxygen and nutrient supply caused by diffusion-limited transport from perfused vascular channels. Vessels were produced by molding a hydrogel against a bioprinted sacrificial scaffold (77). D) Vascular networks enabling control over endothelial cell (CD31) interactions with pericytes (α-SMA) and membrane permeability (fluorescein leakage) permit complex studies of vascular biology in healthy and disease conditions. Networks were generated in hydrogels by soft lithography (81). Images were reproduced with permission from the Royal Society of Chemistry (A) and the National Academy of Sciences, USA (B-D).

and recapitulate aspects of angiogenic invasion, including sensitivity to shear stress, interstitial flow, and various angiogenic gradients (72-74). These assays have been used to facilitate co-culture with stromal or tumor cells and evaluate paracrine effects in angiogenesis (74). However, these models are confined by thin geometries (~100 μm) and are therefore sensitive to boundary effects due to cell and molecular interactions with the device surface. In addition, the endothelial cells initially form a monolayer against the gel region, rather than a fully-mimetic lumen structure. Therefore, more advanced models of microvascular structure and function have recently been developed.

This second type of platform comprises bona fide vascular structures fully embedded within 3D ECM. Such structures can be developed by molding biomaterials against a thin needle to define a vessel lumen and subsequently seeded with endothelial cells (75, 76) (Figure 2B). These vessels allow high throughput and facile fabrication, but they are restricted to simple linear geometries and are limited by the resolution of the needle. More complex channel configurations can be fabricated by patterning of a sacrificial resist that dissolves after gel crosslinking (77, 78) (Figure 2C), or by replica molding and soft lithography methods, originally developed by George Whitesides group in silicone plastics (79, 80). Recently, advances in this technique allowed patterning of cell-laden biological materials (81, 82) and the perfusion of scaffolds with endothelialized microvascular channels (77, 78, 82, 83) (Figure 2D). Although lithographic techniques are limited to planar configurations, the bioprinted sacrificial molds were capable of generating a lattice of interconnected vessels (78). Finally, modular assembly of cell-laden beads permits the formation of contiguous endothelial architectures, although the geometries of these networks are less defined than the other approaches (84, 85). Together, these platforms enable unprecedented access to questions in vascular biology and vascularized tissue function (86).

In vitro microvascular platforms are particularly suited to quantify physiological parameters governing mass transport and drug delivery (76, 82). For example, microfabricated vascular structures permit measuring endothelial permeability in authentic lumenized channels as a function of pericyte coverage, and in response to biochemical factors known to interfere with endothelial cell signaling (82). Furthermore, microvascular platforms offer exquisite opportunity to measure cell viability as a function of Krogh distance and metabolic consumption at specific cell densities (78, 81) and to monitor transvascular and interstitial transport of therapeutic agents. Finally, they provide increasingly accurate models of the tumor environment, allowing tumor-stromal cell cross talk in the assessment of efficacy (74, 87-90). Taken together, engineering models of vascular transport facilitate pre-clinical studies of drug delivery with human cells within a biomimetic tissue environment.

Tumor desmoplasia and ECM remodeling: biophysical changes and their relevance to drug delivery

Biology of tumor desmoplasia and ECM remodeling

As tumors progress from a benign to malignant stage, they recruit cancer-associated fibroblasts (CAFs) that can modulate drug response through altering ECM physicochemical properties (Figure 3). CAFs, which include myofibroblasts, deposit abundant amounts of fibrillar ECM molecules including collagen I and fibronectin (91). These ECM compositional changes entail structural and mechanical alterations of the ECM (92-94). For example, CAFs mediate the partial unfolding of fibronectin, which increases both the stiffness of individual fibronectin fibers (95, 96) and their ability to bind other ECM molecules such as glycosaminoglycans (GAGs) and collagen (97). Along with elevated collagen crosslinking (e.g., by lysyl oxidase, non-enzymatic glycation, or transglutamination (98, 99)) and GAG concentration (93), these pronounced changes

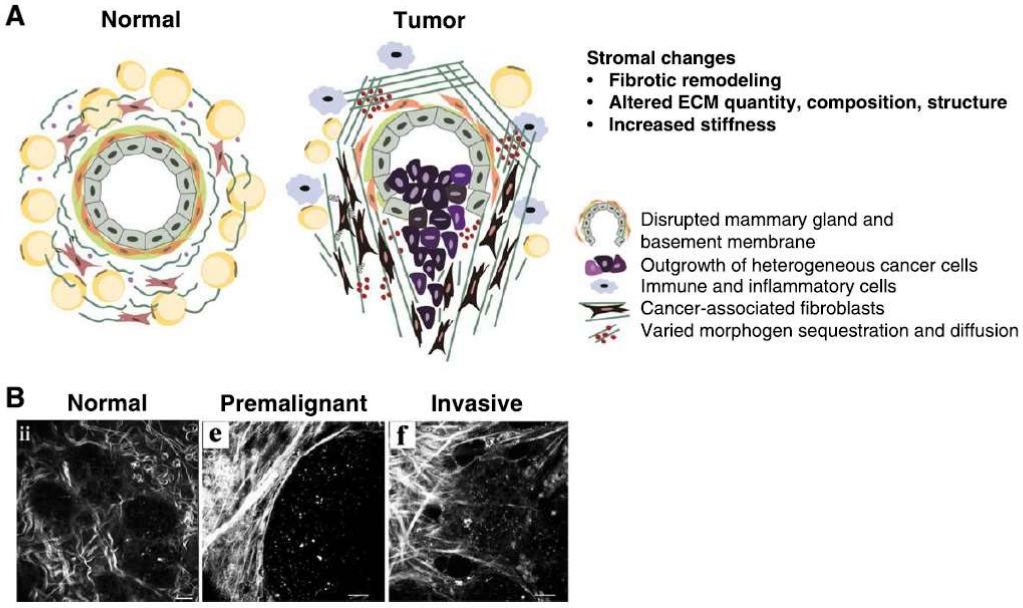

Fig. 3. Biophysical changes of mammary tumor stroma. A) Schematic illustration of the structural and functional changes in tumor-associated mammary stroma. Tumor-derived cytokines not only promote recruitment of inflammatory cells, but also cancer-activated fibroblasts, which stiffen tumors by thickening, linearizing and aligning fibrillar ECM components. These changes alter the transport of growth factors and cytokines, but also of therapeutic compounds with consequences on cancer cell drug resistance. B) Visualization of collagen structure in mammary tissue of normal and tumor-bearing mice via second harmonic generation imaging. Coiled and disorganized collagen fibers are present in normal mammary tissue. Upon tumorigenesis, thicker and linearized collagen fibers develop, which are tangentially and radially oriented along the boundary of premalignant and invasive mammary tumors, respectively (148). Reproduced with permission from Biomed Central.

in ECM density and intermolecular interactions globally enhance tumor stiffness with direct consequences for tumor progression.

Despite this overall increase in matrix deposition and cross-linking, tumor cells simultaneously mediate the degradation of the ECM, in part by secreting enzymes such as matrix metalloproteinases (MMPs). In addition to generating tumorigenic ECM fragments (100), elevated MMP activity affects the local (microscale) physical properties of the tumor ECM. For example, MMPs can govern degradation and reorganization of fibrillar collagen, while enhancing interactions with other ECM components through exposure of cryptic binding sites (101-103). Nevertheless, it has to be kept in mind that non-proteolytic functions of MMPs may be similarly important. For example, MMP-9 has been associated with smooth muscle cell adhesion, migration, and cell-mediated collagen contraction, independent of it's proteolytic function (103, 104). The diverse roles of MMPs in tumorigenesis have previously been reviewed by Egeblad (105) and Page-McCaw (106).

Alterations of ECM composition, structure, and mechanics stimulate malignancy and drug resistance by inducing manifold changes in cell signaling (107-110). In general, cell-ECM interactions facilitate the clustering of integrin adhesion receptors leading to cytoskeletal reorganization and cell contractility (108, 111). These changes activate signaling cascades that play critical roles in cell fate decisions, tumor progression, and drug resistance (e.g., Rho/Rock, ERK/MAPK, and PI3K) (112-115). For example, integrin signaling alters the co-activation of certain growth factor receptors (e.g., epidermal growth factor receptor [EGFR]) (116) which can impact targeted therapies designed to interfere with the related signaling cascades (e.g., cetuximab and panitumumab targeting EGFR, PLX4720 and PLX403 interfering with BRAF kinase activity) (117, 118). Changes in ECM composition and exposure of cryptic binding domains

partially modulate these signaling cascades by affecting integrin selectivity (119, 120). Likewise, increased stiffness-mediated integrin signaling plays a major role in promoting cell contractility, which directly stimulates malignancy by fueling tumor cell proliferation and migration (121). Moreover, matrix stiffness alters the behavior of tumor-associated stromal cells to drive disease progression. For example, increased stiffness promotes the pro-tumorigenic capability of mesenchymal stem cells (114, 122), compromises endothelial barrier functions (123, 124), and alters macrophage functions (125). Finally, stiffness-dependent changes in cell contractility are critical to the myofibroblastic differentiation of stromal fibroblasts (97), thus, providing a positive feedback mechanism that further stimulates desmoplastic remodeling. For these reasons, stromal markers have the potential to serve as important indices that can help to assess and predict patient diagnostics and outcomes (126-133).

In addition to the direct mechano-biological effects, physicochemical changes in the ECM can impact soluble factor signaling (134). Specifically, the increase of ECM components with growth factor-binding domains affects the bioavailability of these molecules. However, this process is complicated by the reciprocal interplay between multiple ECM molecules. For example, interactions with GAG (e.g. heparin) modulate fibronectin conformation and expose cryptic binding sites involved in growth factor sequestration (135). Likewise, changes in cell contractility can expose these latent binding sites and thereby cause the release of morphogens from their ECM depots (e.g. post-translational activation of latent transforming growth factor β [TGF-β]) (136).

Effects of tumor-associated ECM on transport physics

Transport of therapeutic molecules through interstitial tissue is dependent on convection and diffusion (21). However, the combination of leaky vasculature and dense ECM increases interstitial fluid pressure (IFP) (137, 138) and inhibits convection-mediated transport.

Consequently, drug-delivery within tumor stroma primarily depends on diffusion (21). However, dense cellular and matrix components represent diffusion barriers that hinder transport through the interstitium (139, 140). Specific parameters that regulate diffusion efficiency through the stroma include 1) diffusion distance, 2) available volume fraction of pores (accessible space where molecules can pass through), 3) tortuosity of pathway, 4) hydrodynamic resistance, and 5) ECM affinity of the molecule of interest (67) (BOX2). All of these parameters are affected by tumor stroma remodeling. For example, desmoplasia-mediated enhancement of ECM density and structural changes decrease the available volume fraction of pores and increase the tortuosity of the void space, both of which reduce the rate of diffusion through the stroma (141, 142). Therefore, properties of both the drug (e.g. size, charge, configuration, etc.) (143) and the ECM (e.g., composition, viscoelasticity, geometrical arrangement, and/or electrostatic properties) should be considered when approximating an agent's bioavailability (139, 141, 144-146).

The specific structure of ECM components also modulates diffusion fluxes of therapeutic molecules. Analysis of collagen fiber orientation via second harmonic generation imaging (SHG) revealed that increased malignancy is associated with collagen fiber re-orientation. While collagen in initiating tumors is characterized by isotropic orientation, progression leads to tangential and ultimately radial alignment in expanded and invading tumors, respectively (147, 148) (Figure 3B). These changes in ECM fiber network orientation can promote diffusion anisotropy without affecting the overall diffusion coefficient of the drug (149). For example, fibers tangentially aligned to the tumor boundary could redirect drug diffusion away from the tumor and, therefore, impair therapy efficacy during initial stage of tumorigenesis. Theoretically, radially aligned fibers should mediate the opposite effect; however, at this stage tumor cells may have developed resistance phenomena rendering them unresponsive to therapy.

Box 2. Forces governing interstitial transport.

Solute transport through interstitial space results from the sum of convective (J_C) and diffusive (J_D) fluxes:

$$J_s = J_D + J_C = -D\nabla C + v_f f C$$

where D is the effective diffusion coefficient, C is the solute concentration, f is the retardation coefficient, and v_f is the interstitial fluid velocity, determined by the solution to the Brinkman equation for flow through porous media:

$$\mu\nabla^2 v_f - \frac{1}{K} v_f - \nabla p = 0$$

where μ is the fluid viscosity, K is the hydraulic conductivity, and p is the hydrostatic pressure difference between the vascular and lymphatic vessels. In most cases, K, D, and f are approximately equivalent to the hydraulic conductivity (L_p), permeability (P), and 1 minus the filtration reflection coefficient ($1 - \sigma_f$) for membrane transport (see Box 1). Parameter values can be found in [11,66].

Finally, changes in ECM composition can affect delivery by altering hydrodynamic and electrostatic interactions of the drug with the ECM. Generally, tumor-mediated elevation of ECM viscosity increases the hydrodynamic resistance of molecules and hence slows down their movement through the interstitial space (67, 139, 142, 144, 150). These differences are aggravated by changes in ECM charge distribution (e.g. due to increased association with negatively charged sulfated GAGs including heparan sulfate (134, 144). More specifically, electrostatic repulsion or attraction of charged particles can reduce the available volume fraction of pores and/or cause local sequestration of the drug. Furthermore, electrostatic interaction may not only be relevant to ECM-drug interactions per se, but can also alter the conformation of ECM molecules (e.g. as outlined above for fibronectin-heparin interactions (151)). These variations, in turn, can impact their ability to bind morphogens ultimately exaggerating asymmetric drug distribution within tumors.

The potential opportunity for enhancing drug transport by modifying tumor matrix was demonstrated in a mouse model of pancreatic cancer, where gemcitabine delivery was improved through depletion of desmoplastic stroma by inhibition of hedgehog signaling (152). However, Infinity Pharmaceuticals' phase II clinical trials for saridegib (IPI-926) in combination with gemcitabine were halted last year due to increased mortality, suggesting that this strategy may require improved understanding of tumor-stromal interactions in human patients. Consequently, tumor-associated ECM remodeling critically impacts diffusive transport, yet, most drug testing approaches neglect the contribution of the above-described parameters. Physiologically relevant 3D tumor models recapitulating the physicochemical properties of the ECM that interfere with diffusion fluxes offer promise to selectively define coefficients modulating drug transport dynamics in tumors.

In vitro models recapitulating ECM-mediated changes in tumor transport

Natural biomaterials can be employed to assess tumorigenesis as a function of altered ECM characteristics. Matrigel®, a basement membrane mixture isolated from murine Engelbreth-Holm-Swarm sarcoma, is currently most widely used. However, inherent batch-to-batch variability, incomplete controllability of physicochemical parameters (e.g. narrow range of stiffness), and lack of covalent crosslinks critical to the basement membrane barrier function (95, 153-155) represent limitations of this material. Collagen type I is a defined biological scaffold that can be synthetically modified to provide a wider range of physicochemical properties. For example, collagen stiffness can be adjusted through covalent crosslinking by non-enzymatic glycation (156). However, this procedure can impact cell behavior by preventing enzymatic degradation of the matrix and by accumulating advanced glycation end products, both of which affect biochemical signaling. (157).

Synthetic biomaterials have emerged as attractive alternatives to modulate stiffness in a more controlled manner. ECM-coated polyacrylamide (PA) gels allow adjustment of stiffness independent of ligand concentration. This platform has been critical to the identification of mechanoregulatory signaling mechanisms of tumorigenesis (121). However, PA gels cannot be remodeled by cells, and the fabrication method further limits their use to 2D studies which may affect critical cell functions (110, 158). Moreover, altering crosslinking density can affect the surface porosity of PA gels, which may cause conformational changes of the ECM coating that modulate cell behavior (159).

Poly(ethylene glycol) (PEG)-based materials can address some of these challenges. For example, remodelable PEG-based hydrogels have been developed to study the independent effects of stiffness and peptide ligand density on lung cancer cells in a 3D context (Figure 4A) (160). Moreover, photodegradable or photoreversible crosslinks may be introduced to enable temporal

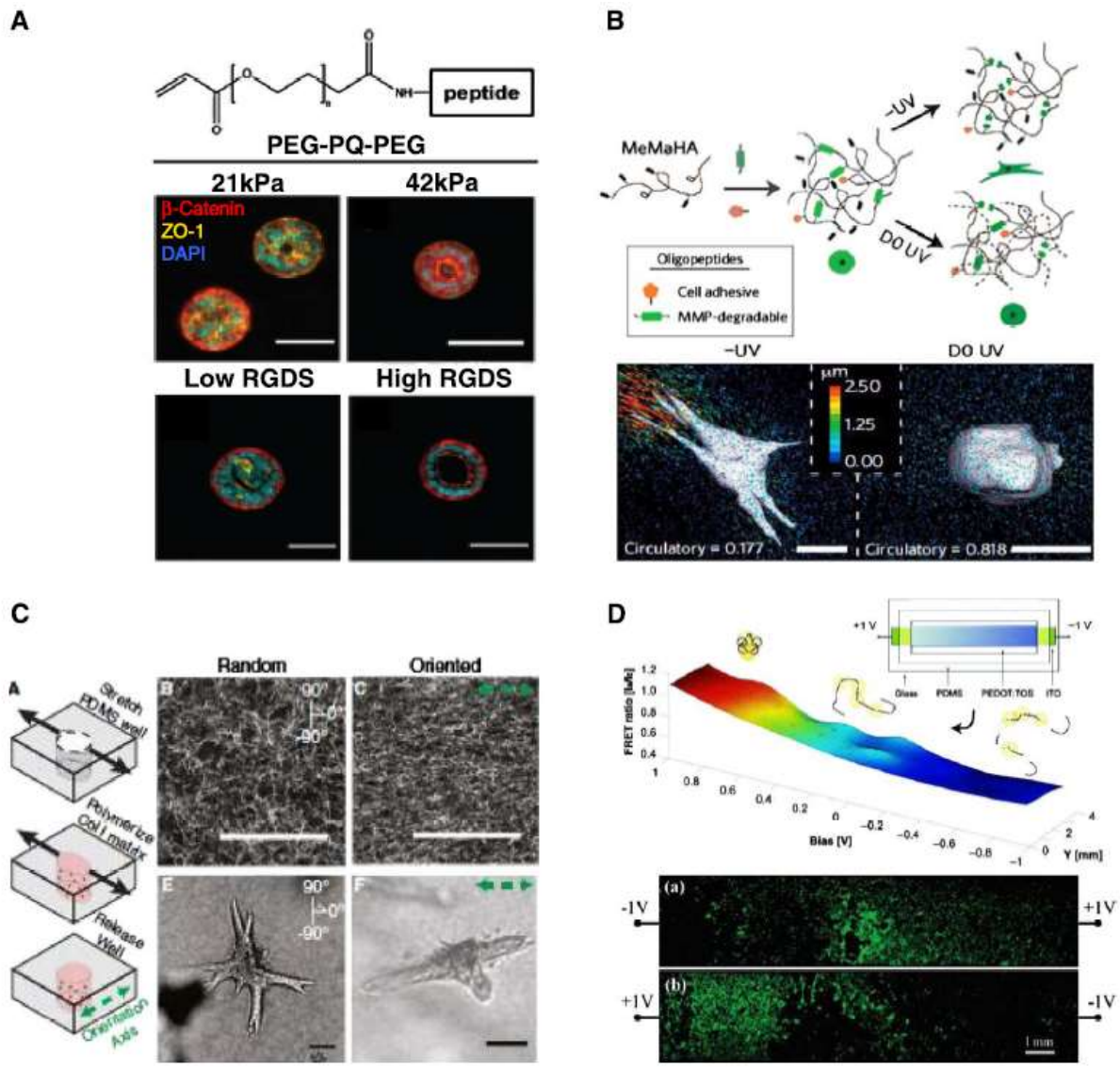

Fig. 4. Examples of engineering approaches to recapitulate tumor-associated ECM characteristics. A) Covalently cross-linked PEG-based hydrogels with controlled stiffness and ligand concentration have been used to investigate the impact of these parameters on lung cancer cells (159). B) Tunable hyaluronic acid-based 3D hydrogels containing proteolytically cleavable crosslinks revealed a role of ECM degradation-mediated cellular traction in cell fate decisions (162). C) Studies with stretchable PDMS molds containing fibrillar collagen gels revealed that axially oriented collagen fibers promote epithelial co-orientation, which is prevented by randomly oriented collagen fibers (167). D) Tumor-mediated changes in fibronectin conformation can be simulated with conducting polymers. Applying an appropriate potential to the cytocompatible conducting polymer poly (3,4-ethylenedioxythiophene) doped with p-toluenesulfonate (PEDOT:TOS) yields conformation gradients of adsorbed fibronectin that can be confirmed by FRET analysis and that influence cellular adhesion (green calcein staining) (150,175). Images were reproduced with permission from American Association for Cancer Research (A), Nature Publishing Group (B), Cell Press (C), Wiley Online Library and Royal Society of Chemistry (D).

control of substrate stiffness *in situ* (161, 162). By allowing dynamic physicochemical changes in the ECM, such platforms can provide important new insights to tumor development. For example, studying proteolysis-mediated variations of cellular traction could reveal the temporal effects of substrate stiffness on cell fate decisions (as recently shown with hyaluronic acid-based degradable materials (Figure 4B) (163). Furthermore, integration of growth factor binding sites could mimic the effects of matrix-binding on morphogen or drug distribution (164).

While the above approaches rely on changing the material chemistry, ECM structural changes can also be introduced by varying the scaffold fabrication conditions. One relatively simple approach to modify collagen fibril characteristics is by adjusting the gelation temperature, pH, and/or material concentration (165). Additionally, the collagen isolation technique is a critical consideration, as fibers from acid-solubilized collagen may mimic *in vivo* microarchitecture, but these gels also contain telopeptides that may compromise biocompatibility relative to pepsin-digested collagen (166, 167). Furthermore, the random orientation of spontaneously formed collagen fibrils does not recapitulate fiber alignment in tumors. One method to orient collagen fibers is by casting collagen gels into PDMS molds and exposing them to tensile stress axially (168) (Figure 4C). However, this loading method may also modulate the behavior of the embedded cells, and interpretation of results is complicated by non-linear cellular response to combinations of mechanical forces and ECM properties (169). Electrospinning of artificial ECM scaffolds may help to overcome some of these challenges and allow the selective manipulation of ECM structural features at relevant length scales (170-173).

Fibronectin represents an important tumor-associated ECM component whose conformation can be quantified and recapitulated using biomaterials-based approaches. FRET-based analysis as established by the Vogel lab has provided quantitative insights into tumor-

mediated fibronectin unfolding (96, 174). This unfolding impacts integrin selectivity by altering the spatial separation between the RGD adhesion and PHSRN synergy sequence. One elegant approach to study the consequences of protein conformation is to modify synthetic, otherwise nonadhesive, hydrogels with RGD and PHSRN peptides either alone or in combination (175). Alternatively, conducting polymer substrates have been employed to unfold native fibronectin. Applying differential voltages to poly (3,4-ethylenedioxythiophene) doped with *p*-toluenesulfonate (PEDOT:TOS) permits selective manipulation of the conformation of adsorbed fibronectin (Figure 4D) (151). Such systems have been used to elucidate that fibronectin conformational changes influence cell adhesion and secretory patterns for both stromal and tumor cells (176, 177). Yet, fibronectin does not occur in isolation, but is part of complex ECM scaffolds, which can be partially mimicked with fibroblast-derived 3D ECMs. These matrices are generated by detergent-based decellularization and recapitulate various physicochemical aspects of native ECMs including fiber alignment, composition, and density (115, 178). Furthermore, they allow the delineation of effects mediated by healthy and tumor-associated ECMs and have revealed differential cell morphology, orientation, and migration, as well as drug response in healthy versus disease conditions (179).

In order to be useful in drug discovery and screening, the *in vitro* platforms described above must support high-throughput testing of complex libraries of bio-chemical-physical cues. Recently, sophisticated high throughput methods were introduced to screen for combinational effects of ECM physicochemical parameters on cells incorporated in 3D hydrogels (180). These high throughput microarrays, combined with topographically-controllable biomaterial-based scaffolds, afford a more comprehensive understanding of the integrated effects of the tumor microenvironment on drug delivery and efficacy.

Future directions

Artificial cell culture platforms have traditionally benefited from the ability to isolate individual biological parameters in a controlled experimental environment, but many challenges exist when moving toward increasingly realistic models for replicating tumor pathology and therapy. Specifically, such biomimetic cultures are confined by boundaries of space, time, and complexity. Addressing these limitations will help to accurately study cancer biology and translate the findings to clinical practice.

Spatial resolution is a critical parameter of engineered tissues. Although microfabrication technologies afford unprecedented access to cell-scale precision, integrating this resolution into meaningful tissue or organ-level organization is nontrivial. For example, artificial tumors grown in confined structures may undergo differential morphogenesis relative to human disease. In addition, most microfluidic geometries present boundary artifacts, including mechanical and chemical interactions along the walls of the device that may contribute to this end (181-183). Moreover, engineered tumors are often isolated systems that lack an organism-level context. Recent integration of multiple organ compartments into body-on-a-chip devices has started to simulate aspects of organism physiology, including drug metabolism and toxicity of anti-cancer drugs (184, 185). These *in vitro* models provide a first glimpse at holistic consequences of tumor growth or therapy; however, they still neglect critical physiological characteristics, including cellular transport through the blood contributing to tumor progression or metastatic homing. For example, the molecular communication between breast cancer cells and bone marrow-derived progenitor cells may contribute to pre-metastatic niche formation in the target organ (186). Systemic *in vitro* models that connect diverse organ compartments through engineered vascular

systems may facilitate a more comprehensive understanding of the mechanisms underlying metastasis and define future treatment strategies (187, 188).

The temporal scale of *in vitro* models introduces a second experimental obstacle. Culture conditions of days to weeks must simulate emergent phenomena of months and years. This challenge is especially relevant in the evolution of drug resistance, where population drift relies on many generations of cell division (189, 190). *In vitro* platforms may approximate these effects of tumor heterogeneity by cell sourcing from primary tumors or by seeding mixed cell populations representing different stages of tumor development (191). In addition to drug resistance, morphological changes in tissue stroma, including vascular and ECM remodeling, often require longer durations than conventional experimental techniques. This motivates the use of artificial factors such as phorbol 12-myristate 13-acetate (PMA) to rapidly stimulate cellular response (192, 193), or the use of low density matrices to accelerate remodeling and migration (194, 195). Although useful experimental tools, these artifices may compromise the integrity of the *in vitro* system. Computational models of tumorigenesis offer an alternative strategy for recapitulating the time-scale of pathogenesis (196). For example, multiscale computational models of the tumor microenvironment can be used to predict changes in tumor malignancy as a function of stroma-dependent selective pressure (20). However, in order to mimic physiological growth rates, these models rely on the accurate measurement of cell kinetics. By providing controlled platforms to measure these critical coefficients, *in vitro* tumor models may inform the development of accurate *in silico* models of progression and response.

Physiological complexity, including matrix composition, cellular components, or spatiotemporal presentation of soluble factors, introduces additional compromises for *in vitro* tissue culture. Notably, increasing complexity often undermines the controllability of the system.

For example, although *in vitro* tumor models enable human-specific drug screening, tumor cells have a broad spectrum of characteristics depending on originating organ, stage or malignancy, and patients' genetic background, additional health complications, and life style. Therefore, short-term culture of cell lines may not cover organ-, patient-, and stage-specific features of tumors. Furthermore, genomic and epigenomic instability leads to diverse clonal populations within a single tumor that cross-communicate (197, 198), and this signaling is lost given the uniformity of conventional cell culture lines. Advances in personalized medicine have begun to appreciate the unique molecular signature of individual patients. Integration of patient-derived biopsies within engineered models may allow personalized drug screening prior to treatment. The advantages of closely approximating physiological complexity is an asset of engineered tumor models, but remembering these limitations will help guide the interpretation and translation of data collected with these systems.

Conclusions

By integrating cancer biology and engineering approaches, realistic tumor models may be developed that have the potential to advance current anti-cancer therapies. More specifically, this approach will help to better define qualitative and quantitative parameters currently complicating drug transport in tumor-associated blood vessels and stroma. In the future, however, further improvements are needed to enhance the relevance of these models. For example, integration with organ-on-a-chip devices may not only help to recapitulate systemic aspects of the disease, but also to better define the spatiotemporal relationships and patient-inherent complexity complicating drug transport in the clinic. Together with current advances in cancer (epi)-genomics and computational modeling engineered tumor models offer promise to bridge the gap between bench to bedside research and help translate new therapeutic approaches to the clinic.

References

1. Hodis E, *et al.* (2012) A Landscape of Driver Mutations in Melanoma. *Cell* 150(2):251-263.

2. Paraiso KHT, *et al.* (2010) Recovery of phospho-ERK activity allows melanoma cells to escape from BRAF inhibitor therapy. *British Journal of Cancer* 102(12):1724-1730.

3. Chin L, Andersen JN, & Futreal PA (2011) Cancer genomics: from discovery science to personalized medicine. *Nature Medicine* 17(3):297-303.

4. Guoren Deng YL, Galina Zlotnikov, Ann D. Thor, Helene S. Smith (1996) Loss of Heterozygosity in Normal Tissue Adjacent to Breast Carcinomas. *Science* 274(5295):2057-2059.

5. Bissell MJ & Radisky D (2001) Putting tumours in context. *Nat. Rev. Cancer* 1(1):46-54.

6. Caino MC, *et al.* (2013) Metabolic stress regulates cytoskeletal dynamics and metastasis of cancer cells. *The Journal of clinical investigation* 123(7):2907-2920.

7. Pollard JW (2004) Tumour-educated macrophages promote tumour progression and metastasis. *Nat. Rev. Cancer* 4:71-78.

8. Park J, Euhus DM, & Scherer PE (2011) Paracrine and endocrine effects of adipose tissue on cancer development and progression. *Endocrine reviews* 32(4):550-570.

9. Khandekar MJ, Cohen P, & Spiegelman BM (2011) Molecular mechanisms of cancer development in obesity. *Nature reviews. Cancer* 11(12):886-895.

10. Ravid Straussman TM, Kevin Shee, Michal Barzily-Rokni, Zhi Rong Qian, Jinyan Du, Ashli Davis, Margaret M. Mongare, Joshua Gould, Dennie T. Frederick, Zachary A. Cooper, Paul B. Chapman, David B. Solit, Antoni Ribas, Roger S. Lo, Keith T. Flaherty, Shuji Ogino, Jennifer A. Wargo & Todd R. Golub (2012) Tumour micro-environment elicits innate resistance to RAF inhibitors through HGF secretion. *Nature Letter* 487(7408):500-504.

11. McMillin DW, Negri JM, & Mitsiades CS (2013) The role of tumour-stromal interactions in modifying drug response: challenges and opportunities. *Nature reviews. Drug discovery* 12(3):217-228.

12. Jain RK (1987) Transport of molecules in the tumor interstitium- a review. *Cancer Research* 47(12):3039-3051.

13. Jain RK (1999) Transport of molecules, particles, and cells in solid tumors. *Annual review of biomedical engineering* 1:241-263.

14. Jain RK (1994) Barriers to drug-delivery in solid tumors. *Scientific American* 271(1):58-65.

15. Iyer AK, Khaled G, Fang J, & Maeda H (2006) Exploiting the enhanced permeability and retention effect for tumor targeting. *Drug Discov Today* 11(17-18):812-818.

16. Maeda H, Wu J, Sawa T, Matsumura Y, & Hori K (2000) Tumor vascular permeability and the EPR effect in macromolecular therapeutics: a review. *J Control Release* 65(1-2):271-284.

17. Fang J, Nakamura H, & Maeda H (2011) The EPR effect: Unique features of tumor blood vessels for drug delivery, factors involved, and limitations and augmentation of the effect. *Advanced drug delivery reviews* 63(3):136-151.

18. Torchilin V (2011) Tumor delivery of macromolecular drugs based on the EPR effect. *Advanced drug delivery reviews* 63(3):131-135.

19. Davis ME, Chen Z, & Shin DM (2008) Nanoparticle therapeutics: an emerging treatment modality for cancer. *Nature Reviews Drug Discovery* 7(9):771-782.

20. Anderson AR, Weaver AM, Cummings PT, & Quaranta V (2006) Tumor morphology and phenotypic evolution driven by selective pressure from the microenvironment. *Cell* 127(5):905-915.

21. Jain RK & Stylianopoulos T (2010) Delivering nanomedicine to solid tumors. *Nature Reviews Clinical Oncology* 7(11):653-664.

22. Singh M & Ferrara N (2012) Modeling and predicting clinical efficacy for drugs targeting the tumor milieu. *Nature biotechnology* 30(7):648-657.

23. Richert L, *et al.* (2008) Species differences in the response of liver drug-metabolizing enzymes to (S)-4-O-tolylsulfanyl-2-(4-trifluormethyl-phenoxy)-butyric acid (EMD 392949) in vivo and in vitro. *Drug metabolism and disposition: the biological fate of chemicals* 36(4):702-714.

24. Mueller MM & Fusenig NE (2004) Friends or foes - bipolar effects of the tumour stroma in cancer. *Nature reviews. Cancer* 4(11):839-849.

25. Primeau AJ, Rendon A, Hedley D, Lilge L, & Tannock IF (2005) The distribution of the anticancer drug Doxorubicin in relation to blood vessels in solid tumors. *Clinical cancer research : an official journal of the American Association for Cancer Research* 11(24 Pt 1):8782-8788.

26. Saggar JK, Yu M, Tan Q, & Tannock IF (2013) The tumor microenvironment and strategies to improve drug distribution. *Frontiers in oncology* 3:154.

27. Folkman J (1985) Tumor angiogenesis. *Advances in Cancer Research* 43:175-203.

28. Folkman J, *et al.* (1971) Tumor angiogenesis- therapeutic implications. *New England Journal of Medicine* 285:1182-&.

29. Hashizume H, *et al.* (2000) Openings between defective endothelial cells explain tumor vessel leakiness. *American Journal of Pathology* 156:1363-1380.

30. Hobbs SK, *et al.* (1998) Regulation of transport pathways in tumor vessels: Role of tumor type and microenvironment. *Proceedings of the National Academy of Sciences of the United States of America* 95:4607-4612.

31. Dvorak HF, Nagy JA, Dvorak JT, & Dvorak AM (1988) Identification and characterization of the blood-vessels of solid tumors that are leaky to circulating macromolecules. *American Journal of Pathology* 133:95-109.

32. Dvorak HF, Brown LF, Detmar M, & Dvorak AM (1995) Vascular-permeability factor/vascular endothelial growth-factor, microvascular hyperpermeability, and angiogenesis. *American Journal of Pathology* 146:1029-1039.

33. Roberts WG & Palade GE (1997) Neovasculature induced by vascular endothelial growth factor is fenestrated. *Cancer Research* 57:765-772.

34. Jain RK (1988) Determinants of tumor blood-flow - a review. *Cancer Research* 48:2641-2658.

35. Nagy JA, Benjamin L, Zeng H, Dvorak AM, & Dvorak HF (2008) Vascular permeability, vascular hyperpermeability and angiogenesis. *Angiogenesis* 11:109-119.

36. Nagy JA, Chang S-H, Shih S-C, Dvorak AM, & Dvorak HF (2010) Heterogeneity of the Tumor Vasculature. *Seminars in Thrombosis and Hemostasis* 36(3):321-331.

37. Jain RK (1987) Transport of molecules across tumor vasculature. *Cancer and Metastasis Reviews* 6:559-593.

38. Harris AL (2002) Hypoxia - A key regulatory factor in tumour growth. *Nat. Rev. Cancer* 2:38-47.

39. Hockel M & Vaupel P (2001) Tumor hypoxia: Definitions and current clinical, biologic, and molecular aspects. *Journal of the National Cancer Institute* 93:266-276.

40. Helmlinger G, Yuan F, Dellian M, & Jain RK (1997) Interstitial pH and pO(2) gradients in solid tumors in vivo: High-resolution measurements reveal a lack of correlation. *Nature medicine* 3:177-182.

41. Gatenby RA & Gillies RJ (2004) Why do cancers have high aerobic glycolysis? *Nat. Rev. Cancer* 4:891-899.

42. Semenza GL (2003) Targeting HIF-1 for cancer therapy. *Nat. Rev. Cancer* 3:721-732.

43. Fukumura D, *et al.* (2001) Hypoxia and acidosis independently up-regulate vascular endothelial growth factor transcription in brain tumors in vivo. *Cancer Research* 61:6020-6024.

44. Forsythe JA, *et al.* (1996) Activation of vascular endothelial growth factor gene transcription by hypoxia-inducible factor 1. *Molecular and Cellular Biology* 16(9):4604-4613.

45. Majmundar AJ, Wong WJ, & Simon MC (2010) Hypoxia-Inducible Factors and the Response to Hypoxic Stress. *Molecular Cell* 40:294-309.

46. Huang LE, Gu J, Schau M, & Bunn HF (1998) Regulation of hypoxia-inducible factor 1 alpha is mediated by an O-2-dependent degradation domain via the ubiquitin-proteasome pathway. *Proceedings of the National Academy of Sciences of the United States of America* 95(14):7987-7992.

47. Maxwell PH, *et al.* (1999) The tumour suppressor protein VHL targets hypoxia-inducible factors for oxygen-dependent proteolysis. *Nature* 399(6733):271-275.

48. Veikkola T, Karkkainen M, Claesson-Welsh L, & Alitalo K (2000) Regulation of angiogenesis via vascular endothelial growth factor receptors. *Cancer Research* 60:203-212.

49. Ferrara N, Gerber HP, & LeCouter J (2003) The biology of VEGF and its receptors. *Nature medicine* 9:669-676.

50. Bergers G & Benjamin LE (2003) Tumorigenesis and the angiogenic switch. *Nature reviews. Cancer* 3(6):401-410.

51. Saggar JK, Fung AS, Patel KJ, & Tannock IF (2013) Use of Molecular Biomarkers to Quantify the Spatial Distribution of Effects of Anticancer Drugs in Solid Tumors. *Molecular Cancer Therapeutics* 12(4):542-552.

52. Jain RK (1987) Transport of molecules in the tumor interstitium- a review. *Cancer Research* 47:3039-3051.

53. Baxter LT & Jain RK (1989) Transport of fluid and macromolecules in tumors 1. Role of interstitial pressure and convection. *Microvascular research* 37:77-104.

54. Primeau AJ, Rendon A, Hedley D, Lilge L, & Tannock IF (2005) The distribution of the anticancer drug Doxorubicin in relation to blood vessels in solid tumors. *Clinical cancer research : an official journal of the American Association for Cancer Research* 11(24 Pt 1):8782-8788.

55. Minchinton AI & Tannock IF (2006) Drug penetration in solid tumours. *Nature reviews. Cancer* 6(8):583-592.

56. Jain RK (2001) Normalizing tumor vasculature with anti-angiogenic therapy: A new paradigm for combination therapy. *Nature medicine* 7:987-989.

57. Jain RK (2005) Normalization of tumor vasculature: An emerging concept in antiangiogenic therapy. *Science* 307(5706):58-62.

58. Fukumura D & Jain RK (2007) Tumor microvasculature and microenvironment: Targets for anti-angiogenesis and normalization. *Microvascular Research* 74:72-84.

59. Carmeliet P & Jain RK (2011) Principles and mechanisms of vessel normalization for cancer and other angiogenic diseases. *Nature Reviews Drug Discovery* 10:417-427.

60. Goel S, *et al.* (2011) Normalization of the vasculature for treatment of cancer and other diseases. *Physiological Reviews* 91:1071-1121.

61. Ellis LM & Hicklin DJ (2008) VEGF-targeted therapy: mechanisms of anti-tumour activity. *Nat. Rev. Cancer* 8(8):579-591.

62. Hurwitz H, *et al.* (2004) Bevacizumab plus irinotecan, fluorouracil, and leucovorin for metastatic colorectal cancer. *New England Journal of Medicine* 350(23):2335-2342.

63. Nathanson SD & Nelson L (1994) Interstitial Fluid Pressure in Breast-Cancer, Benign Breast Conditions, and Breast Parenchyma. *Ann Surg Oncol* 1(4):333-338.

64. Less JR, *et al.* (1992) Interstitial Hypertension in Human Tumors .4. Interstitial Hypertension in Human Breast and Colorectal Tumors. *Cancer Research* 52(22):6371-6374.

65. Heldin CH, Rubin K, Pietras K, & Ostman A (2004) High interstitial fluid pressure - An obstacle in cancer therapy. *Nat. Rev. Cancer* 4:806-813.

66. Griffith LG & Swartz MA (2006) Capturing complex 3D tissue physiology in vitro. *Nature Reviews Molecular Cell Biology* 7:211-224.

67. G. A. Truskey FY, D. F. Katz, Pearson Prentice Hall (2004) Transport phenomena in biological systems.

68. Thurber GM, Schmidt MM, & Wittrup KD (2008) Factors determining antibody distribution in tumors. *Trends in Pharmacological Sciences* 29:57-61.

69. Gauvin R, Guillemette M, Dokmeci M, & Khademhosseini A (2011) Application of microtechnologies for the vascularization of engineered tissues. *Vascular cell* 3(1):24-24.

70. Young EWK (2013) Cells, tissues, and organs on chips: challenges and opportunities for the cancer tumor microenvironment. *Integrative Biology* 5:1096-1109.

71. Stroock AD & Fischbach C (2010) Microfluidic Culture Models of Tumor Angiogenesis. *Tissue Engineering Part A* 16:2143-2146.

72. Song JW & Munn LL (2011) Fluid forces control endothelial sprouting. *Proceedings of the National Academy of Sciences of the United States of America* 108:15342-15347.

73. Shin Y, *et al.* (2012) Microfluidic assay for simultaneous culture of multiple cell types on surfaces or within hydrogels. *Nature protocols* 7(7):1247-1259.

74. Kim S, Lee H, Chung M, & Jeon NL (2013) Engineering of functional, perfusable 3D microvascular networks on a chip. *Lab on a chip* 13:1489-1500.

75. Chrobak KM, Potter DR, & Tien J (2006) Formation of perfused, functional microvascular tubes in vitro. *Microvascular Research* 71:185-196.

76. Nguyen D-HT, *et al.* (2013) Biomimetic model to reconstitute angiogenic sprouting morphogenesis in vitro. *Proceedings of the National Academy of Sciences of the United States of America* 110:6712-6717.

77. Golden AP & Tien J (2007) Fabrication of microfluidic hydrogels using molded gelatin as a sacrificial element. *Lab on a Chip* 7:720-725.

78. Miller JS, *et al.* (2012) Rapid casting of patterned vascular networks for perfusable engineered three-dimensional tissues. *Nature materials* 11(9):768-774.

79. Whitesides GM, Ostuni E, Takayama S, Jiang XY, & Ingber DE (2001) Soft lithography in biology and biochemistry. *Annual review of biomedical engineering* 3:335-373.

80. Borenstein JT, *et al.* (2002) Microfabrication technology for vascularized tissue engineering. *Biomedical microdevices* 4(3):167-175.

81. Choi NW, *et al.* (2007) Microfluidic scaffolds for tissue engineering. *Nature Materials* 6:908-915.

82. Zheng Y, *et al.* (2012) In vitro microvessels for the study of angiogenesis and thrombosis. *Proceedings of the National Academy of Sciences of the United States of America* 109:9342-9347.

83. Verbridge SS, *et al.* (2013) Physicochemical regulation of endothelial sprouting in a 3D microfluidic angiogenesis model. *Journal of Biomedical Materials Research Part A* 10(10):2948-2956.

84. McGuigan AP & Sefton MV (2006) Vascularized organoid engineered by modular assembly enables blood perfusion. *Proceedings of the National Academy of Sciences of the United States of America* 103:11461-11466.

85. Du Y, *et al.* (2011) Sequential assembly of cell-laden hydrogel constructs to engineer vascular-like microchannels. *Biotechnology and bioengineering* 108(7):1693-1703.

86. Wong KHK, Chan JM, Kamm RD, & Tien J (2012) Microfluidic Models of Vascular Functions. *Annual Review of Biomedical Engineering, Vol 14* 14:205-230.

87. Huang CP, *et al.* (2009) Engineering microscale cellular niches for three-dimensional multicellular co-cultures. *Lab on a chip* 9(12):1740-1748.

88. Sung KE, *et al.* (2011) Transition to invasion in breast cancer: a microfluidic in vitro model enables examination of spatial and temporal effects. *Integrative Biology* 3(4):439-450.

89. Moya M, Tran D, & George S (2013) An integrated in vitro model of perfused tumor and cardiac tissue. *Stem Cell Research and Therapy* 4(Suppl 1).

90. Sung KE, *et al.* (2013) Understanding the impact of 2D and 3D fibroblast cultures on in vitro breast cancer models. *PloS one* 8(10).

91. De Wever O, Demetter P, Mareel M, & Bracke M (2008) Stromal myofibroblasts are drivers of invasive cancer growth. *International journal of cancer. Journal international du cancer* 123(10):2229-2238.

92. Egeblad M, Rasch MG, & Weaver VM (2010) Dynamic interplay between the collagen scaffold and tumor evolution. *Current opinion in cell biology* 22(5):697-706.

93. Cox TR & Erler JT (2011) Remodeling and homeostasis of the extracellular matrix: implications for fibrotic diseases and cancer. *Dis Model Mech* 4(2):165-178.

94. Butcher DT, Alliston T, & Weaver VM (2009) A tense situation: forcing tumour progression. *Nature reviews. Cancer* 9(2):108-122.

95. Baneyx G, Baugh L, & Vogel V (2002) Fibronectin extension and unfolding within cell matrix fibrils controlled by cytoskeletal tension. *Proc Natl Acad Sci U S A* 99(8):5139-5143.

96. Chandler EM, Saunders MP, Yoon CJ, Gourdon D, & Fischbach C (2011) Adipose progenitor cells increase fibronectin matrix strain and unfolding in breast tumors. *Physical biology* 8(1):015008.

97. Tomasek JJ, Gabbiani G, Hinz B, Chaponnier C, & Brown RA (2002) Myofibroblasts and mechano-regulation of connective tissue remodelling. *Nat Rev Mol Cell Biol* 3(5):349-363.

98. Levental KR, *et al.* (2009) Matrix crosslinking forces tumor progression by enhancing integrin signaling. *Cell* 139(5):891-906.

99. Erler JT & Weaver VM (2009) Three-dimensional context regulation of metastasis. *Clinical & experimental metastasis* 26(1):35-49.

100. Kessenbrock K, Plaks V, & Werb Z (2010) Matrix metalloproteinases: regulators of the tumor microenvironment. *Cell* 141(1):52-67.

101. George E. Davis KJB, Michael J. Davis, Gerald A. Meininger (2000) Regulation of Tissue Injury Responses by the Exposure of Matricryptic Sites within Extracellular Matrix Molecules. *American Journal of Pathology* 156(5):1489-1498.

102. Wolf K, *et al.* (2007) Multi-step pericellular proteolysis controls the transition from individual to collective cancer cell invasion. *Nature cell biology* 9(8):893-904.

103. Johnson C & Galis ZS (2004) Matrix metalloproteinase-2 and -9 differentially regulate smooth muscle cell migration and cell-mediated collagen organization. *Arterioscler Thromb Vasc Biol* 24(1):54-60.

104. Defawe OD, *et al.* (2005) MMP-9 regulates both positively and negatively collagen gel contraction - A nonproteolytic function of MMP-9. *Cardiovasc Res* 66(2):402-409.

105. Egeblad M & Werb Z (2002) New functions for the matrix metalloproteinases in cancer progression. *Nat. Rev. Cancer* 2(3):161-174.

106. Page-McCaw A, Ewald AJ, & Werb Z (2007) Matrix metalloproteinases and the regulation of tissue remodelling. *Nature Reviews Molecular Cell Biology* 8(3):221-233.

107. Provenzano PP, Inman DR, Eliceiri KW, & Keely PJ (2009) Matrix density-induced mechanoregulation of breast cell phenotype, signaling and gene expression through a FAK-ERK linkage. *Oncogene* 28(49):4326-4343.

108. Vogel V & Sheetz M (2006) Local force and geometry sensing regulate cell functions. *Nat Rev Mol Cell Biol* 7(4):265-275.

109. Guo W & Giancotti FG (2004) Integrin signalling during tumour progression. *Nat Rev Mol Cell Biol* 5(10):816-826.

110. Fischbach C, *et al.* (2009) Cancer cell angiogenic capability is regulated by 3D culture and integrin engagement. *Proc Natl Acad Sci U S A* 106(2):399-404.

111. Geiger B, Spatz JP, & Bershadsky AD (2009) Environmental sensing through focal adhesions. *Nat Rev Mol Cell Biol* 10(1):21-33.

112. Engler AJ, Sen S, Sweeney HL, & Discher DE (2006) Matrix elasticity directs stem cell lineage specification. *Cell* 126(4):677-689.

113. Schrader J, *et al.* (2011) Matrix stiffness modulates proliferation, chemotherapeutic response, and dormancy in hepatocellular carcinoma cells. *Hepatology* 53(4):1192-1205.

114. Chandler EM, *et al.* (2012) Implanted adipose progenitor cells as physicochemical regulators of breast cancer. *Proc Natl Acad Sci U S A* 109(25):9786-9791.

115. Castello-Cros R, Khan DR, Simons J, Valianou M, & Cukierman E (2009) Staged stromal extracellular 3D matrices differentially regulate breast cancer cell responses through PI3K and beta1-integrins. *BMC cancer* 9:94.

116. DuFort CC, Paszek MJ, & Weaver VM (2011) Balancing forces: architectural control of mechanotransduction. *Nat Rev Mol Cell Biol* 12(5):308-319.

117. Dienstmann R, De Dosso S, Felip E, & Tabernero J (2012) Drug development to overcome resistance to EGFR inhibitors in lung and colorectal cancer. *Molecular oncology* 6(1):15-26.

118. Paraiso KH, *et al.* (2011) PTEN loss confers BRAF inhibitor resistance to melanoma cells through the suppression of BIM expression. *Cancer Res* 71(7):2750-2760.

119. Sottile J (2004) Regulation of angiogenesis by extracellular matrix. *Biochimica et biophysica acta* 1654(1):13-22.

120. Huebsch N, *et al.* (2010) Harnessing traction-mediated manipulation of the cell/matrix interface to control stem-cell fate. *Nat Mater* 9(6):518-526.

121. Paszek MJ, *et al.* (2005) Tensional homeostasis and the malignant phenotype. *Cancer cell* 8(3):241-254.

122. Spaeth EL, *et al.* (2009) Mesenchymal stem cell transition to tumor-associated fibroblasts contributes to fibrovascular network expansion and tumor progression. *PloS one* 4(4):e4992.

123. Mammoto A, *et al.* (2013) Control of lung vascular permeability and endotoxin-induced pulmonary oedema by changes in extracellular matrix mechanics. *Nature communications* 4:1759.

124. Huynh J, *et al.* (2011) Age-related intimal stiffening enhances endothelial permeability and leukocyte transmigration. *Science translational medicine* 3(112):112ra122.

125. Naimish R. Patel MB, Cheng Chen, Charles C. Hardin, Alvin T. Kho, Justin Mih, Linhong Deng, James Butler, Daniel Tschumperlin, Jeffrey J. Fredberg, Ramaswamy Krishnan, Henry Koziel (2012) Cell Elasticity Determines Macrophage Function. *PloS one* 7(9).

126. Finak G, *et al.* (2008) Stromal gene expression predicts clinical outcome in breast cancer. *Nature medicine* 14(5):518-527.

127. Kellermann MG, *et al.* (2007) Myofibroblasts in the stroma of oral squamous cell carcinoma are associated with poor prognosis. *Histopathology* 51(6):849-853.

128. Caporale A, *et al.* (2010) Quantitative Investigation of Desmoplasia as a Prognostic Indicator in Colorectal Cancer. *J Invest Surg* 23(2):105-109.

129. Hasebe T, *et al.* (1996) Fibrotic focus in invasive ductal carcinoma: An indicator of high tumor aggressiveness. *Jpn J Cancer Res* 87(4):385-394.

130. Van den Eynden GG, *et al.* (2007) A fibrotic focus is a prognostic factor and a surrogate marker for hypoxia and (lymph)angiogenesis in breast cancer: review of the literature and proposal on the criteria of evaluation. *Histopathology* 51(4):440-451.

131. Halvorsen TB & Seim E (1989) Association between Invasiveness, Inflammatory Reaction, Desmoplasia and Survival in Colorectal-Cancer. *J Clin Pathol* 42(2):162-166.

132. Karagiannis GS, *et al.* (2012) Proteomic Signatures of the Desmoplastic Invasion Front Reveal Collagen Type XII as a Marker of Myofibroblastic Differentiation During Colorectal Cancer Metastasis. *Oncotarget* 3(3):267-285.

133. Okada KI, *et al.* (2010) Stromal thrombospondin-1 expression is a prognostic indicator and a new marker of invasiveness in intraductal papillary-mucinous neoplasm of the pancreas. *Biomed Res-Tokyo* 31(1):13-19.

134. Griffith LG & Swartz MA (2006) Capturing complex 3D tissue physiology in vitro. *Nature reviews. Molecular cell biology* 7(3):211-224.

135. Mitsi M, Hong Z, Costello CE, & Nugent MA (2006) Heparin-mediated conformational changes in fibronectin expose Vascular Endothelial Growth Factor binding sites. *Biochemistry* 45(34):10319-10328.

136. Mott JD & Werb Z (2004) Regulation of matrix biology by matrix metalloproteinases. *Current opinion in cell biology* 16(5):558-564.

137. Bouzin C & Feron O (2007) Targeting tumor stroma and exploiting mature tumor vasculature to improve anti-cancer drug delivery. *Drug resistance updates : reviews and commentaries in antimicrobial and anticancer chemotherapy* 10(3):109-120.

138. Heldin CH, Rubin K, Pietras K, & Ostman A (2004) High interstitial fluid pressure - an obstacle in cancer therapy. *Nature reviews. Cancer* 4(10):806-813.

139. Pluen A, *et al.* (2001) Role of tumor-host interactions in interstitial diffusion of macromolecules: cranial vs. subcutaneous tumors. *Proc Natl Acad Sci U S A* 98(8):4628-4633.

140. Chauhan VP, *et al.* (2009) Multiscale measurements distinguish cellular and interstitial hindrances to diffusion in vivo. *Biophysical journal* 97(1):330-336.

141. Ramanujan S, *et al.* (2002) Diffusion and convection in collagen gels: implications for transport in the tumor interstitium. *Biophysical journal* 83(3):1650-1660.

142. Netti PA, Berk DA, Swartz MA, Grodzinsky AJ, & Jain RK (2000) Role of Extracellular Matrix Assembly in Interstitial Transport in Solid Tumors. *Cancer Res* 60:2497-2503.

143. Choi HS, *et al.* (2010) Design considerations for tumour-targeted nanoparticles. *Nature Nanotechnology* 5(1):42-47.

144. Stylianopoulos T, *et al.* (2010a) Diffusion of particles in the extracellular matrix: the effect of repulsive electrostatic interactions. *Biophysical journal* 99(5):1342-1349.

145. Yuan F, Krol A, & Tong S (2001) Available Space and Extracellular Transport of Macromolecules: Effects of Pore Size and Connectedness. *Annals of Biomedical Engineering* 29(12):1150-1158.

146. Choi J, Credit, K., Henderson, K., Deverkadra, R., He, Z., Wiig, H., Vanpelt, H., Flessner, M. F. (2006) Intraperitoneal immunotherapy for metastatic ovarian carcinoma: Resistance of intratumoral collagen to antibody penetration. *Clinical cancer research : an official journal of the American Association for Cancer Research* 12(6):1906-1912.

147. Provenzano PP, *et al.* (2006) Collagen reorganization at the tumor-stromal interface facilitates local invasion. *BMC medicine* 4(1):38.

148. Provenzano PP, *et al.* (2008) Collagen density promotes mammary tumor initiation and progression. *BMC medicine* 6.

149. Stylianopoulos T, Diop-Frimpong B, Munn LL, & Jain RK (2010b) Diffusion anisotropy in collagen gels and tumors: the effect of fiber network orientation. *Biophysical journal* 99(10):3119-3128.

150. Lieleg O, Baumgartel RM, & Bausch AR (2009) Selective filtering of particles by the extracellular matrix: an electrostatic bandpass. *Biophysical journal* 97(6):1569-1577.

151. Wan AM, *et al.* (2012) Electrical control of protein conformation. *Advanced materials* 24(18):2501-2505.

152. Olive KP, *et al.* (2009) Inhibition of Hedgehog Signaling Enhances Delivery of Chemotherapy in a Mouse Model of Pancreatic Cancer. *Science* 324:1457-1461.

153. Kleinman HK & Martin GR (2005) Matrigel: basement membrane matrix with biological activity. *Semin Cancer Biol* 15(5):378-386.

154. Clarke KC, Douglas AM, Brown AC, Barker TH, & Lyon LA (2013) Colloid-matrix assemblies in regenerative medicine. *Current Opinion in Colloid & Interface Science* 18(5):393-405.

155. Sodek KL, Brown TJ, & Ringuette MJ (2008) Collagen I but not Matrigel matrices provide an MMP-dependent barrier to ovarian cancer cell penetration. *BMC cancer* 8:223.

156. Girton TS, Oegema TR, & Tranquillo RT (1999) Exploiting glycation to stiffen and strengthen tissue equivalents for tissue engineering. *Journal of Biomedical Materials Research* 46(1):87-92.

157. Goldin A, Beckman JA, Schmidt AM, & Creager MA (2006) Advanced glycation end products: sparking the development of diabetic vascular injury. *Circulation* 114(6):597-605.

158. Fraley SI, *et al.* (2010) A distinctive role for focal adhesion proteins in three-dimensional cell motility. *Nature cell biology* 12(6):598-604.

159. Trappmann B, *et al.* (2012) Extracellular-matrix tethering regulates stem-cell fate. *Nat Mater* 11(7):642-649.

160. Gill BJ, *et al.* (2012) A synthetic matrix with independently tunable biochemistry and mechanical properties to study epithelial morphogenesis and EMT in a lung adenocarcinoma model. *Cancer Res* 72(22):6013-6023.

161. Kloxin AM, Kasko AM, Salinas CN, & Anseth KS (2009) Photodegradable hydrogels for dynamic tuning of physical and chemical properties. *Science* 324(5923):59-63.

162. DeForest CA & Anseth KS (2012) Photoreversible patterning of biomolecules within click-based hydrogels. *Angewandte Chemie* 51(8):1816-1819.

163. Khetan S, *et al.* (2013) Degradation-mediated cellular traction directs stem cell fate in covalently crosslinked three-dimensional hydrogels. *Nat Mater* 12(5):458-465.

164. Lutolf MP & Hubbell JA (2005) Synthetic biomaterials as instructive extracellular microenvironments for morphogenesis in tissue engineering. *Nature biotechnology* 23(1):47-55.

165. Achilli M & Mantovani D (2010) Tailoring Mechanical Properties of Collagen-Based Scaffolds for Vascular Tissue Engineering: The Effects of pH, Temperature and Ionic Strength on Gelation. *Polymers* 2(4):664-680.

166. Zeugolis DI, Paul RG, & Attenburrow G (2008) Factors influencing the properties of reconstituted collagen fibers prior to self-assembly: animal species and collagen extraction method. *Journal of biomedical materials research. Part A* 86(4):892-904.

167. Friess W (1998) Collagen-biomaterial for drug delivery. *European Journal of Pharmaceutics and Biopharmaceutics* 45(2):113-136.

168. Brownfield DG, *et al.* (2013) Patterned collagen fibers orient branching mammary epithelium through distinct signaling modules. *Current biology : CB* 23(8):703-709.

169. Moraes C, Sun Y, & Simmons CA (2011) (Micro)managing the mechanical microenvironment. *Integrative biology : quantitative biosciences from nano to macro* 3(10):959-971.

170. Matthews JA WG, Simpson DG, Bowlin GL. (2002) Electrospinning of collagen nanofibers. *Biomacromolecules* 3(2):232-238.

171. Kim TG & Park TG (2006) Biomimicking Extracellular Matrix: Cell Adhesive RGD Peptide Modified Electrospun Poly(D,L-lactic-co-glycolic acid) Nanofiber Mesh. *Tissue Engineering* 12(2):221-233.

172. Jang JH, Castano O, & Kim HW (2009) Electrospun materials as potential platforms for bone tissue engineering. *Advanced drug delivery reviews* 61(12):1065-1083.

173. Hasan A, *et al.* (2013) Electrospun scaffolds for tissue engineering of vascular grafts. *Acta biomaterialia*.

174. Smith ML, *et al.* (2007) Force-induced unfolding of fibronectin in the extracellular matrix of living cells. *PLoS biology* 5(10):e268.

175. Brown AC, Rowe JA, & Barker TH (2011) Guiding epithelial cell phenotypes with engineered integrin-specific recombinant fibronectin fragments. *Tissue engineering. Part A* 17(1-2):139-150.

176. Wan AM, Brooks DJ, Gumus A, Fischbach C, & Malliaras GG (2009) Electrical control of cell density gradients on a conducting polymer surface. *Chemical communications* (35):5278-5280.

177. Wan AM, *et al.* (2013) Fibronectin conformation regulates the proangiogenic capability of tumor-associated adipogenic stromal cells. *Biochimica et biophysica acta* 1830(9):4314-4320.

178. Amatangelo MD, Bassi DE, Klein-Szanto AJP, & Cukierman E (2005) Stroma-derived three-dimensional matrices are necessary and sufficient to promote desmoplastic differentiation of normal fibroblasts. *American Journal of Pathology* 167(2):475-488.

179. Serebriiskii I, Castello-Cros R, Lamb A, Golemis EA, & Cukierman E (2008) Fibroblast-derived 3D matrix differentially regulates the growth and drug-responsiveness of human cancer cells. *Matrix Biol* 27(6):573-585.

180. Gobaa S, *et al.* (2011) Artificial niche microarrays for probing single stem cell fate in high throughput. *Nature methods* 8(11):949-955.

181. Paguirigan AL & Beebe DJ (2009) From the cellular perspective: exploring differences in the cellular baseline in macroscale and microfluidic cultures. *Integrative Biology* 1:182-195.

182. Regehr KJ, *et al.* (2009) Biological implications of polydimethylsiloxane-based microfluidic cell culture. *Lab on a Chip* 9:2132-2139.

183. Toepke MW & Beebe DJ (2006) PDMS absorption of small molecules and consequences in microfluidic applications. *Lab on a chip* 6:1484-1486.

184. Sung JH & Shuler ML (2009) A micro cell culture analog (mu CCA) with 3-D hydrogel culture of multiple cell lines to assess metabolism-dependent cytotoxicity of anti-cancer drugs. *Lab on a chip* 9:1385-1394.

185. Sung JH, Kam C, & Shuler ML (2010) A microfluidic device for a pharmacokinetic-pharmacodynamic (PK-PD) model on a chip. *Lab on a chip* 10:446-455.

186. Kaplan RN, Rafii S, & Lyden D (2006) Preparing the "Soil": The premetastatic niche. *Cancer Research* 66:11089-11093.

187. Esch MB, King TL, & Shuler ML (2011) The Role of Body-on-a-Chip Devices in Drug and Toxicity Studies. *Annual Review of Biomedical Engineering, Vol 13* 13:55-72.

188. DelNero P, Song YH, & Fischbach C (2013) Microengineered tumor models: insights and opportunities from a physical sciences-oncology perspective. (Biomedical Microdevices), pp 583-593.

189. Gerlinger M & Swanton C (2010) How Darwinian models inform therapeutic failure initiated by clonal heterogeneity in cancer medicine. *British journal of cancer* 103:1139-1143.

190. Gerlinger M, *et al.* (2012) Intratumor Heterogeneity and Branched Evolution Revealed by Multiregion Sequencing. *New England Journal of Medicine* 366:883-892.

191. Carey SP, Starchenko A, McGregor AL, & Reinhart-King CA (2013) Leading malignant cells initiate collective epithelial cell invasion in a three-dimensional heterotypic tumor spheroid model. *Clinical & experimental metastasis* 30:615-630.

192. Yang S, Graham J, Kahn JW, Schwartz EA, & Gerritsen ME (1999) Functional roles for PECAM-1 (CD31) and VE-cadherin (CD144) in tube assembly and lumen formation in three-dimensional collagen gels. *American Journal of Pathology* 155:887-895.

193. Sieminski AL, Hebbel RP, & Gooch KJ (2005) Improved microvascular network in vitro by human blood outgrowth endothelial cells relative to vessel-derived endothelial cells. *Tissue Engineering* 11:1332-1345.

194. Ramanujan S, *et al.* (2002) Diffusion and convection in collagen gels: Implications for transport in the tumor interstitium. *Biophysical Journal* 83:1650-1660.

195. Cross VL, *et al.* (2010) Dense type I collagen matrices that support cellular remodeling and microfabrication for studies of tumor angiogenesis and vasculogenesis in vitro. *Biomaterials* 31:8596-8607.

196. Anderson ARA & Quaranta V (2008) Integrative mathematical oncology. *Nat. Rev. Cancer* 8:227-234.

197. Navin N, *et al.* (2011) Tumour evolution inferred by single-cell sequencing. *Nature* 472:90-U119.

198. Campbell PJ, *et al.* (2008) Subclonal phylogenetic structures in cancer revealed by ultra-deep sequencing. *Proceedings of the National Academy of Sciences of the United States of America* 105:13081-13086.

CHAPTER 3

3D CULTURE REGULATES TUMOR HYPOXIA RESPONSE AND ANGIOGENESIS VIA PRO-INFLAMMATORY PATHWAYS

Peter DelNero, Maureen Lane, Scott Verbridge, Brian Kwee, Pouneh Kermani, Barbara Hempstead, Abraham Stroock, and Claudia Fischbach. (2015). 3D culture broadly regulates tumor cell hypoxia response and angiogenesis via pro-inflammatory pathways. *Biomaterials* 55(1):110–118.

Abstract

Oxygen status and tissue dimensionality are critical determinants of tumor angiogenesis, a hallmark of cancer and an enduring target for therapeutic intervention. However, it is unclear how these microenvironmental conditions interact to promote neovascularization, due in part to a lack of tumor models that allow independent control of oxygen levels within three-dimensional (3D) culture. Here, we integrated biomaterials and microfabrication technologies to generate oxygen-controlled 3D tumor models, which permit evaluating the interdependence of culture context and the hypoxia response. A comprehensive microarray gene expression analysis of cells cultured in 2D versus 3D under ambient or hypoxic conditions revealed strong coupling between culture dimensionality and hypoxia response, which was mediated in part by inflammatory signaling pathways. In particular, interleukin-8 (IL-8) emerged as a major player in the microenvironmental regulation of the hypoxia program. Notably, this interaction between dimensionality and oxygen status via IL-8 increased angiogenic sprouting in a 3D endothelial invasion assay. Taken together, our data suggest that inflammatory pathways are critical regulators of tumor hypoxia response within 3D environments that ultimately impact tumor angiogenesis, potentially providing important therapeutic targets. Furthermore, these results highlight the importance of pathologically

relevant tissue culture models to study the complex physical and chemical processes by which the cancer microenvironment mediates new vessel formation.

Introduction

Hypoxia, and subsequent angiogenic signaling, is conventionally attributed to increased oxygen consumption in a proliferating, 3D tumor mass (1). Spatiotemporal depletion of oxygen due to absent or dysfunctional vasculature activates a hypoxia response program largely controlled by the stabilization of transcription factor hypoxia inducible factor-1 (HIF-1) (2). As a consequence of HIF signaling, the up-regulation of pro-angiogenic morphogens including vascular endothelial growth factor (VEGF), basic fibroblast growth factor (bFGF), and interleukin-8 (IL-8) activates the 'angiogenic switch' necessary for new vessel growth (3, 4). However, microenvironmental conditions other than hypoxia may also modulate the pro-angiogenic capability of tumors (5-7). For example, changes in tissue dimensionality and integrin engagement can activate nuclear factor-κB (NF-κB) and activator protein-1 (AP-1) transcription factors, which regulate the expression of IL-8 and VEGF (8, 9). Nevertheless, how the interactions between hypoxia and tissue dimensionality may contribute to tumor vascularization is poorly understood, due in part to the lack of culture systems that allow independent control of oxygen levels in 3D scaffolds.

Due to diffusion-limited oxygen transport, hypoxic gradients inevitably accompany 3D tumor growth (10, 11). However, in addition to transport limitations, the 3D context also introduces myriad changes in matrix architecture, adhesion receptor signaling, cell morphology and polarity, and substrate mechanics (12). These changes have profound consequences for cell behavior (13-15). When tumor cell hypoxia response and angiogenic capability is typically studied

in 2D monolayer culture, 3D microenvironmental conditions are absent and accordingly, these alternate phenotypic characteristics are also lost. For example, hypoxia and the resulting oxidative stress is necessary to stimulate IL-8/NF-κB signaling in 2D culture, whereas this signaling axis is constitutively active in 3D (16). Accordingly, we have previously shown that hypoxia upregulates secretion of IL-8 in 2D, while causing an opposite effect in 3D culture (16). Hence, pathologically relevant culture conditions may provide new insights regarding the role of tissue dimensionality in guiding hypoxia-related tumor cell responses. Insights gained from such studies will be critical to advance our understanding of tumor angiogenesis and to identify routes toward more effective therapy.

Biomaterials-based in vitro models are increasingly employed to study the role of tissue dimensionality in tumorigenesis and angiogenesis (17-27). We recently developed an oxygen-controlled, 3D culture system with which we circumvented the challenges of diffusion-limited mass transport to control oxygen concentrations (28). Fabrication of thin (200 μm) hydrogel-based scaffolds relieved interior oxygen depletion, allowing us to create homogeneous O_2 levels within the 3D matrix (28, 29). Here, we used this model to distinguish the independent and co-dependent effects of dimensionality and oxygen tension in regulating the tumor hypoxia response and angiogenesis. More specifically, we determined gene expression profiles of tumor cells cultured in 2D and 3D under uniform hypoxic or normoxic conditions using a comprehensive microarray analysis. We validated the results for molecules of interest by RT-PCR and ELISA, and we confirmed their relevance across multiple tumor cell lines. Finally, using a 3D model of endothelial cell invasion, we evaluated the functional consequences of 3D culture and oxygen conditions on sprouting angiogenesis.

Materials and Methods

Cell Culture

Cell lines used in this study included human oral squamous cell carcinoma (OSCC)-3 (gift from Peter Polverini, University of Michigan), A549 lung carcinoma, KATO-III gastric signet ring carcinoma, and MDA-MB231 breast cancer cells (all from ATCC). Tumor cells were cultured in Dulbecco's modified eagle medium (DMEM, Gibco), supplemented with 10% fetal bovine serum (20% for KATO-III), and 1% penicillin-streptomycin (P/S). In addition, human umbilical vein endothelial cells (HUVEC, Lonza) at low passage ($p < 6$) were cultured in Bio-Whittaker medium 199 (M199, Lonza), supplemented with endothelial cell growth supplement (ECGS, Millipore, Billerica, MA), 20% FBS, 1% P/S, 2 mM Glutamax, and 5 U/mL heparin.

Preparation of Alginate Discs

Microfabricated alginate hydrogels (4% wt/vol) were used for 3D tumor cell culture, as previously described (16). Briefly, cells were suspended in alginate (Protanal LF, FMC Biopolymer, Philadelphia, PA) at 20 x 10^6 cells/mL. The cell-laden gel was cast in a Plexiglass mold (4 mm diameter, 200 µm deep to ensure uniform O_2 concentration) and cross-linked with 60 mM calcium chloride ($CaCl_2$) solution for 15 minutes. Alginate disks were cultured in 24-well plates (one disk per well) on an orbital shaker for 6 days in the appropriate media at 37^o C and 5% CO_2. Oxygen levels were set to either hypoxic (1%) or ambient (17 %) O_2 in a controlled atmosphere incubator (ThermoFisher Scientific, Inc., Waltham, MA). Media was changed every 48 hours.

Endothelial Invasion Assays

Collagen-based microwell invasion assays were fabricated as previously described (30). Briefly, PDMS microwells (200 µm deep, 4 mm diameter; Dow Corning, Midland, MI) were

fabricated by soft-lithography against an SU-8 mold. The PDMS surface was pre-treated with 1% poly(ethyleneimine) (PEI; Aldrich Chemical, St. Leouis, MO) and 0.1% glutaraldehyde (GA; Fischer Scientific, Fair Lawn, NJ) for 10 minutes and 20 minutes, respectively, and washed thoroughly with sterile water. Stock solutions of 1.5% (wt/vol) type I rat tail collagen in 0.1% acetic acid were osmotically balanced (9:1) with 10x M199 media, neutralized with 1N sodium hydroxide (NaOH), and diluted to 0.8% (wt/vol) for mono-culture assays. For co-culture invasion assays, tumor cells were suspended in 0.068% collagen gel at a density of 10 million cells/mL. The collagen gel was then cast onto the PDMS microwell mold and cross-linked at 4^{o} C for 15 minutes, followed by 37^{o} C for 15 minutes. HUVECs were seeded at 300 cells/mm^2 on the collagen surface and cultured in HUVEC invasion media at ambient O_2, 5% CO_2, and 37^{o} C. Invasion media was HUVEC growth media spiked with 1% [v/v] L-ascorbic acid (50 µg/mL; Acros Organics, Morris Plains, NJ), and 0.16% [v/v] tetradecanoyl phorbol acetate (TPA; 50 ng/mL; Cell Signaling Technology Inc., Danvers, MA) to sensitize endothelial cells. In mono-culture experiments, recombinant human IL-8 (GenScript, Piscataway, NJ) and VEGF (R&D Systems, Minneapolis, MN) was added at 40 ng/mL, and their respective inhibitors were added at 200 ng/mL in co-culture experiments (both from R&D Systems). Co-culture invasion assay media also contained 40 ng/mL bFGF (Invitrogen, Carlsbad, CA). After three days, gels were fixed in 10% formalin and stained with 4',6-diamidino-2-phenylindole (DAPI), phalloidin (Alexa Fluor 568; Introgen), and a combination of mouse anti-human CD31 (BD Biosciences, San Jose, CA) with goat anti-mouse IgG (Alexafluor 488, Invitrogen). Imaging was performed by confocal microscopy (Zeiss 710, Carl Zeiss, Inc., Thornwood, NY) at 250x magnification for a 0.46 mm^2 area and z-slices up to 40 µm depth. Images were analyzed using ImageJ software by counting the number of CD31$^+$ cell invasions extending beyond 12 µm (~3 slices) from the surface.

Microarray Processing

Total RNA from cells was isolated by using Trizol (Invitrogen) according to manufacturer's instructions. A one-round in vitro transcription (IVT) RNA Amplification Kit (Life Technologies, Grand Island, NY) was used to amplify 1.5 micrograms of total RNA. The cDNA was synthesized with a primer containing oligo (dT) and T7 RNA polymerase promoter sequences. Double-stranded cDNA was then purified and used as a template to generate biotinylated cRNA. The quantity and quality of the amplified cRNA was assessed using NanoDrop ND-1000 Spectrophotometer (Thermo Scientific, Wilmington, DE) and Agilent Bioanalyzer (Santa Clara, CA). The biotin labeled cRNA was fragmented and hybridized to the Affymetrix ChIP kit (Genechip Human Genome U133 plus 2.0) (Santa Clara, CA) for analysis of over 39,000 transcripts on a single array. After Hybridization, GeneChip arrays were washed, stained, and scanned by GeneChip Scanner 3000 7G according to the Affymetrix Expression Analysis Technical Manual.

Affymetrix GeneChip Operating Software was used for image acquisition. The target signal intensity from each chip was scaled to 500. The data normalization, statistical analysis, and pattern study were performed with GeneSpring GX 12.6.1 software. Pathway and functional analyses were generated through the use of IPA (Ingenuity® Systems, www.ingenuity.com).

Confirmation of Microarray Results by ELISA and qRT-PCR

Secreted protein levels were measured by ELISA (R&D Systems) following 24 hours of culture in serum-free media, according to the manufacturer instructions. Cells were released by dissolving alginate disks with ethylenediaminetetraacetic acid (EDTA) and lysed in Caron's buffer. DNA content of cell lysates was fluormetrically measured with Quant-iT PicoGreen

dsDNA reagent (Invitrogen) and used to normalize secretion levels. To determine changes at the transcriptional level, total RNA was harvested from isolated cells using TRIzol (Invitrogen). Reverse-transcription of 1 μg to cDNA (qScript cDNA supermix, Quanta BioSciences, Gaithersburg, MD) was performed with random hexamer and IL-8 specific oligo(dt) primers, followed by qRT-PCR using SYBR green detection (Quanta Biosciences) and an Applied Biosystems 7500 system. Quantification was normalized relative to β-actin using the $\Delta\Delta C_t$ method.

Statistical Analysis

Chip data raw intensity files (.cel) that were processed using the RMA algorithm were imported into the GeneSpring GX 12.6.1 program (Agilent Technologies, Foster City, CA). Signal values <0.01 were set to 0.01, arrays were normalized to the 20th percentile, and individual genes normalized to the median. A one-way analysis of variance (ANOVA) with a corrected asymptotic p-value of <0.05 for significant differential gene expression and a p-value of < 0.0001 for pathway analysis was performed comparing OSCC3 cells grown under the following conditions: 3D matrix in 1% oxygen, 2D matrix in1% oxygen, 3D matrix in 17% oxygen, and 2D matrix in 17% oxygen. Multiple Testing Correction (Benamini-Hochberg) was performed and a filter for greater or less than 2.0-fold differences was applied to determine potential differential expression. A post-hoc test using the Student-Newman Keuls (SNK) method was also applied. Data were imported into Ingenuity Pathway Analysis software (Ingenuity Systems, Redwood City, CA) for molecular pathway analysis using a 2.5 fold change filter. ELISA, RT-PCR, and invasion assays were compared using Fisher's T-test. All experiments were performed in triplicate (N=3). Results are presented as mean +/- the standard deviation.

Results

Dimensionality and oxygen status interdependently regulate tumor cell gene expression

In order to determine the interdependent effect of hypoxia and dimensionality on gene expression, microarray analysis of 46803 gene transcripts was performed on OSCC3 cells cultured in a 2D monolayer on conventional tissue culture polystyrene or encapsulated within microfabricated alginate discs after 6 days. OSCC-3 cells were chosen as representative of an aggressive tumor whose highly vascular nature may result from a latent relationship between oxygen depletion and dimensionality. The 3D discs were microfabricated at 200 μm thickness (Fig. 1A), allowing uniform control of intrascaffold oxygen concentration by incubation at either hypoxic (1% O_2) or ambient (normoxic, 17% O_2) conditions. Homogeneous oxygen transport was previously predicted by finite element models incorporating oxygen diffusion and cellular consumption and confirmed by histological analysis (16). Principle component analysis of gene expression assays performed on 2D and 3D samples from normoxic or hypoxic cultures (Fig. 1B) showed a consistent clustering of samples within each treatment, as well as maximum disparity between groups along each axis (Fig 2A). This data distribution affirms that cells in each condition exhibited a unique and reproducible expression profile.

In total, 29866 genes satisfied the corrected p-value criteria ($p < 0.05$), and 8637 genes were identified based on a response to hypoxia and/or dimensionality by a relative fold-change greater than 2. The populations of genes associated with each comparison are provided in the Venn diagram in Fig 2B. We begin by noting that interaction between oxygen status and dimension played a role in the transcription of 77% of genes (6653 genes, denoted “a”). One fifth of oxygen-sensitive genes were independent of dimensionality: the expression of 19% of the genes (1592), denoted “b”, occupy the intersection of the blue (1% vs. 17% in 3D) and green (1% vs. 17% in

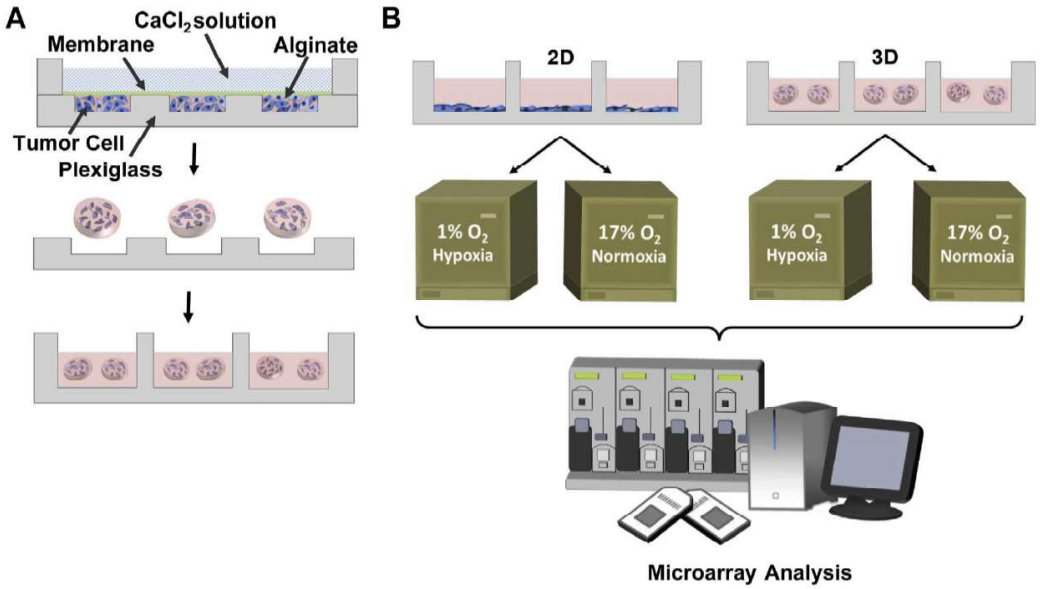

Fig. 1. Experimental design to compare 2D versus 3D hypoxic response. A) Schematic illustrating the fabrication of microscale alginate scaffolds. Cells were suspended within algmate and cast onto an array of 200 µm-deep x 4 mm-diameter wells. $CaCl_2$ solution was applied through a filtration membrane to crosslink the gels. Scaffolds were removed from the mold and cultured in suspension. B) Experimental design comprised culturing OSCC-3 cells on conventional tissue culture polystyrene (2D) or embedded within microfabricated alginate discs (3D) inside ambient (17% 0_2) or hypoxic (1% 0_2) incubators for 6 days. Subsequently, total RNA was isolated and transcriptional changes analyzed by Affymetrix GeneChip microarray.

2D) ovals, but were unaffected by changes in dimensionality at either hypoxic (brown oval) or normoxic (orange oval) conditions. Furthermore, merely 5.6% (392 genes, denoted "c", intersection of brown and orange ovals) of dimension-associated genes were not also affected by oxygen concentration. Surprisingly, the majority (66%, 4558 genes, denoted "x") of hypoxia-associated genes were unique to either 2D or 3D culture; only 34% (2316 genes, denoted "y") were similarly regulated by hypoxia in both substrate conditions. Likewise, only 19% (838 genes, denoted "z") of genes regulated by substrate dimension were shared in both low- and high-oxygen conditions. Notably, dimensionality affected a larger number of genes in hypoxia (3093 genes, sum of red oval) than in normoxia (2230 genes, sum of orange oval), suggesting that the hypoxia response depended strongly on whether cells were cultured under 2D or 3D conditions. Specifically, hypoxia may have sensitized cells to respond to changes in dimensionality, or conversely, changes in dimensionality may have sensitized cells to hypoxia. Altogether, this data suggests a strong interdependence between oxygen status and dimensionality at the gene expression level.

Although the Venn diagram identified populations of genes that respond to 3D context and oxygen concentration, the direction and magnitude of regulation are also important. In order to more clearly define these parameters, we generated a scatter plot of the relative fold-change expression levels in response to hypoxia in 2D and 3D culture (Fig 2C). Changes in gene expression were ranked by the magnitude of the residual (3D FC/2D FC), and a total of 2563 genes were identified that exhibited a differential response to hypoxia greater than 2-fold in 2D versus 3D culture (blue data points). Of the genes that responded differently in 2D versus 3D hypoxia, 12% (317 genes, purple quadrants) exhibited an inversion of expression, 28% (714 genes, yellow quadrants) produced an exaggerated up or down regulation, and the remaining 60% (1536 genes,

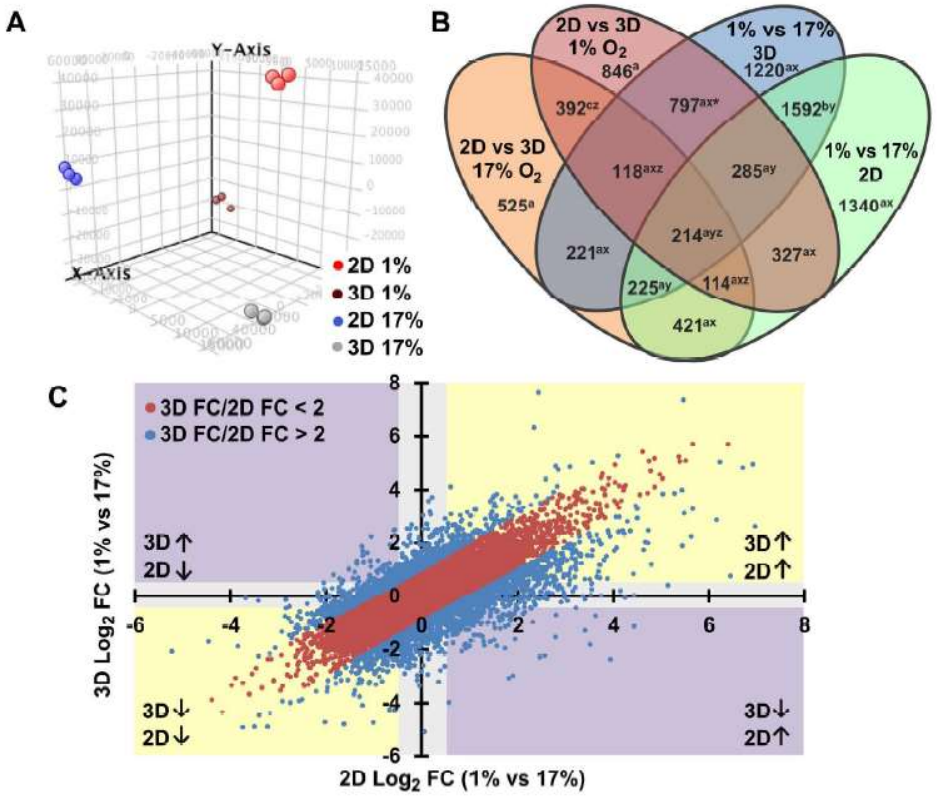

Fig. 2. Global changes in gene expression induced by hypoxia or dimensionality. A) Principal component analysis of the microarray data was performed using GeneSpring GX 12.6.1 software. Clustering of each substrate and oxygen level indicated the reliability of each treatment to generate independent and self-consistent gene expression profiles. B) The Venn diagram displays genes that were associated with changes in dimensionality and/or oxygen status. Intersections between various groups indicate populations of genes that are significantly altered (fold-change > 2, corrected p-value < 0.05) in multiple comparisons of oxygen treatment or substrate dimension. Most of the changes in expression were linked with both dimensionality and oxygen status (sum of regions denoted "a"), indicating an intimate interdependence in gene regulation associated with these conditions. C) The scatterplot of the 3D hypoxia vs normoxia (y-axis) and 2D hypoxia vs normoxia (x-axis) shows the magnitude (FC: fold change) and direction (↑ and ↓ : up- and down-regulation, respectively) of gene expression changes. This plot depicts a large cluster of genes (2563 genes, blue) for which the hypoxic response is differentially regulated (greater than 2-fold change) depending on substrate dimension.

grey background) were regulated by hypoxia in one context but not the other. The subset of genes displaying a differential regulation of hypoxia response based on 2D or 3D substrate became the subject of subsequent analysis in the link between hypoxia and dimensionality.

Interactions between hypoxia and dimensionality regulate inflammatory response pathways

Ingenuity Pathways Analysis (Ingenuity Systems) software was used to identify signaling networks and biofunctions that were associated with the differential changes in gene expression for the 3D versus 2D hypoxia response. Data for this analysis used a gene list of 11,828 entities satisfying a p-value of < 0.0001 and a FC cut- off of 2.0; data was further filter in IPA to a fold change cut-off of 2.5. Top ranked networks from the individual comparisons are listed in Supplementary Table 1. Not surprisingly, top categories included cancer-associated cell and tissue functions, including cell cycle, cellular development and growth, metabolic processes, and tissue-specific disorders. In most cases, these networks were significant in all four comparisons (2D 1% vs 17%; 3D 1% vs 17%; 1% 2D vs 3D; 17% 2D vs 3D; data not shown). In order to identify divergence between the 2D and 3D hypoxia response, we performed an analysis of the changes in gene expression in response to both oxygen status and substrate dimension. Again, top networks were associated with traditional cancer motifs which are known to depend on hypoxia and 3D, including cell cycle, DNA replication, cell death and survival, cell signaling, cell growth and proliferation, and cancer (Fig 3A). Interestingly, the inflammatory response was highly ranked in this meta-comparison, and also emerged among the top biofunctions in the 3D 17% vs 2D 17% and the 3D 1% vs 3D 17% comparisons (Supplementary Table 1). This result suggests that inflammatory signaling is one of the top functions linked to both substrate dimension and oxygen status.

Next, we identified the top signaling pathways associated with each treatment by comparing the expression profiles to canonical responses; several metabolic and cell cycle signaling cascades emerged as prominent features of this analysis (Supplementary Table 2). Looking at the divergence between the 2D and 3D hypoxia response, we observed that leukocyte trafficking signaling, as well as interferon signaling and pattern recognition receptor (PRR) activity, were strongly co-regulated by dimension and hypoxia (Fig 3B). The differential regulation of these inflammatory pathways is consistent with the biofunctions analysis described above.

Finally, we investigated the integrated effects of culture dimensionality and hypoxia on the transcription of individual genes (Fig 3C, Supplementary Tables 3-4). In accord with the network and pathways analyses, we observed that several of the top regulated genes (PLAT, IL-8, CXCL1, and TFAIP6) were associated with inflammatory signaling (Fig 3C, red boxes). Taken together, this analysis suggests that the differential regulation of hypoxic signaling in 2D versus 3D culture has significant consequences for inflammatory signaling at the network, pathway, and molecular level.

Validation of IL-8 expression and secretion confirms regulation of inflammatory signaling in 3D

Because IL-8 was prominently regulated by the integrated effects of hypoxia and dimensionality at both the individual gene (Fig. 3C) and canonical pathway level (Fig. 3B), and because IL-8 has pleiotropic effects on inflammation and angiogenesis (31-33), we chose to pursue this molecule as a representative candidate for further investigation. Interestingly, IL-8 was one of 214 genes affected by all four combinations of oxygen status and dimensionality, and also one of 351 genes that exhibited an inverted hypoxia response depending on culture dimension.

A

Rank	Network (Biofunction)	Score
1	Cell Cycle, Cellular Assembly & Organization, DNA Replication, Recombination, & Repair	43
2	Cell Death & Survival, Cell-To-Cell Signaling & Interaction, Cellular Movement	38
3	Cell Death & Survival, Cellular Development, Cellular Growth & Proliferation	32
4	Dermatological Diseases & Conditions, Antimicrobial Response, Inflammatory Response	32
5	Tissue Development, Cellular Growth & Proliferation, Cancer	30

B

Rank	Canonical Pathway	P-value	Ratio
1	Hepatic Fibrosis / Hepatic Stellate Cell Activation	1.3E-8	0.15
2	Granulocyte Adhesion & Diapedesis	2.82E-6	0.14
3	Agranulocyte Adhesion & Diapedesis	7.69E-6	0.13
4	Interferon Signaling	6.64E-4	0.21
5	Pattern Recognition Receptor Signaling	8.22E-4	0.20
6	GADD45 Signaling	1.23E-3	0.26
7	IL-8 Signaling	1.51E-3	0.10

C

Rank	Gene	Fold-Change
1	LAMP3	-79.8
2	PLAT	-51.8
3	IL8	-46.9
4	CXCL1	-40.7
5	TNFAIP6	-40.3
6	MMP1	+32.5
7	CGA	-30.3
8	ANPEP	-26.3
9	LCN2	-26.2
10	IGFBP1	-26.1

Fig. 3. Inflammatory signaling may underlie the differential hypoxic response in 3D. A) Ingenuity's Global Functional Analysis was used to evaluate functional networks from the gene expression data. Top ranked networks were identified based on the connectivity of focus genes in the Global Molecular Network in the Ingenuity Pathways Knowledge Base, and the score, calculated as the $-\log_{10}$(p-value) of the network emerging by chance, indicates the statistical improbability of a false positive result. B) Ingenuity's Global Canonical Pathways tool was used to associate changes in gene expression with known signaling processes. The p-value was calculated based on the number of focus genes compared to a reference set for each pathway, and the ratio represents the fraction of focus genes identified in each pathway. Top ranked canonical pathways were largely linked to inflammatory processes, suggesting these pathways are differentially regulated by the culture environment. C) When ranked by fold change in expression, five of the top ten genes were associated with inflammatory signaling (outlined in red). The fold-change value represents the difference in the hypoxia-induced expression in 3D versus 2D.

Specifically, IL-8 expression was increased in 2D hypoxia but reduced in 3D hypoxia, compared to the respective expression under ambient conditions. Moreover, IL-8 was the most strongly up-regulated molecule in 3D culture compared to 2D culture at 17% O_2 (Supplementary Table 3). Indeed, the changes in IL-8 transcription detected via microarray analysis were relevant as quantitative RT-PCR and ELISA analysis similarly confirmed the direction and magnitude of regulation of IL-8 in response to hypoxia in 2D and 3D culture (Fig 4A-B). Most importantly, IL-8 was expressed and secreted at significantly higher levels in 3D vs. 2D culture independent of oxygen concentration. These changes were not specific to the OSCC-3 cell line used for the initial investigations, but also applied to three additional human epithelial tumor cell lines: A549 alveolar basal adenocarcinoma, KATO-III gastric carcinoma, and MDA-MB231 breast carcinoma. Each of these cell lines similarly demonstrated a robust up-regulation of IL-8 in normoxic 3D versus 2D culture (Fig 5A-B). These results support the broad applicability of the microarray results, and specifically reaffirm that 3D microenvironmental conditions can regulate IL-8.

Pro-inflammatory signals in the 3D environment may promote angiogenesis via IL-8 and VEGF interaction

Next, we examined the relevance of microenvironmentally-induced IL-8 on tumor angiogenesis. To this end, we used a microwell invasion assay to evaluate the direct interactions between tumor and endothelial cells within a 3D culture environment. The microwell assay comprised remodelable type I collagen molded to the same dimensions as the alginate discs, but confined within a PDMS template to prevent gel contraction (Fig 6A). We had previously confirmed that culturing OSCC-3 in 3D collagen disks similarly upregulated IL-8 (16), but the assay used here additionally allowed the seeding of HUVECs on the surface of the scaffold, and the quantification of endothelial cell invasions into the collagen under mono- or co-culture

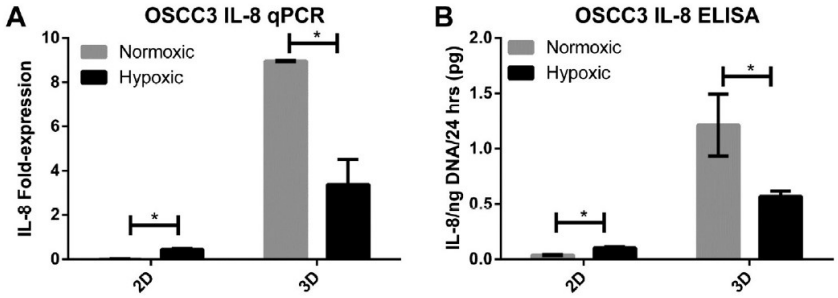

Fig. 4. Microenvironmental control of lL-8 signaling confirmed by qPCR and ELISA. A-B) Fold-change in mRNA transcription and protein secretion of lL-8 by qPCR (A) and ELISA (B) between normoxia (17% 0_2) and hypoxia (1% 0_2) for 2D and 3D cultures. Interaction between hypoxia- and dimensionality-associated changes in IL-8 gene expression were validated at the mRNA transcription and protein secretion levels by qPCR (A) and ELISA (B), respectively. IL-8 expression was constitutively increased in 3D environments compared to 2D monolayers, but hypoxia produced an inverted effect on IL-8 activity depending on substrate dimension.

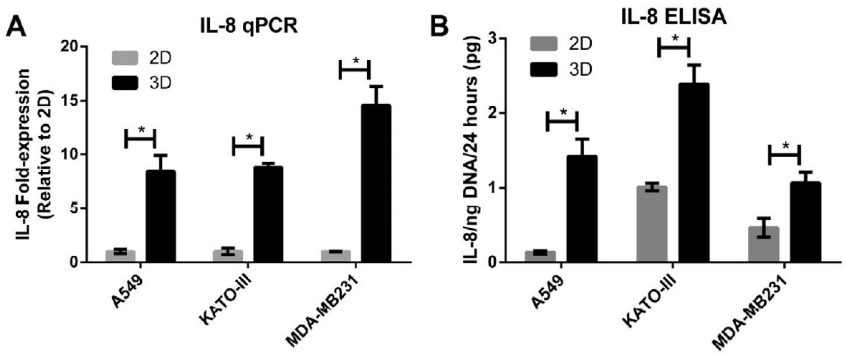

Fig. 5. Relevance of 3D up-regulation of IL-8 across additional epithelial tumor cell lines. A-B) Fold-change in mRNA transcription and protein secretion levels of IL-8 was measured by qPCR (A) and ELISA (B), respectively, for 2D and 3D cultures of three cell lines (A549 lung carcinoma, KATO-Ill gastric carcinoma, and MDA-MB231 mammary gland/breast adenocarcinoma). 3D up-regulation of IL-8 was consistent across 3 additional tumor cell lines under normoxic conditions.

conditions (Fig 6B). In the mono-culture assay, IL-8 and VEGF were added exogenously to the media, either alone or in combination. While IL-8 has previously been reported to exert direct pro-angiogenic effects (34, 35), our results suggest that exogenous IL-8 alone exhibits no effect on endothelial cell invasion. However, in the presence of VEGF, IL-8 synergistically enhances sprouting, suggesting that interactions with VEGF are necessary for IL-8 to modulate endothelial cell behavior (Fig 6C). Likewise, inhibition of either IL-8 or VEGF in the co-culture assay showed significant reduction in sprouting; combined inhibition of both molecules showed no additional benefits (Fig 6D). These results indicate a direct functional consequence of the 3D culture environment in regulating tumor hypoxia response and neovascularization as a function of increased IL-8 levels.

Discussion

Microenvironmental conditions are critical determinants of tumor angiogenic capability; however, due to a lack of culture systems capable of delineating the effects of tissue dimensionality and oxygen status, it is unclear how these conditions interact to regulate neovascularization (36, 37). In order to evaluate the interdependence between tissue culture environment and the hypoxia response, we used custom biomaterials-based assays to control oxygen concentrations within 3D cell-laden scaffolds. A comprehensive microarray analysis revealed profound coupling between culture dimensionality and hypoxia response, which was mediated in part by inflammatory signaling pathways. In particular, IL-8 emerged as a major component of the microenvironmental regulation of the hypoxic program with important functional consequences on endothelial sprouting in a 3D invasion assay. Taken together, our results highlight the importance of pathologically relevant tissue culture models to study complex biological processes such as hypoxia-related cell responses and tumor angiogenesis.

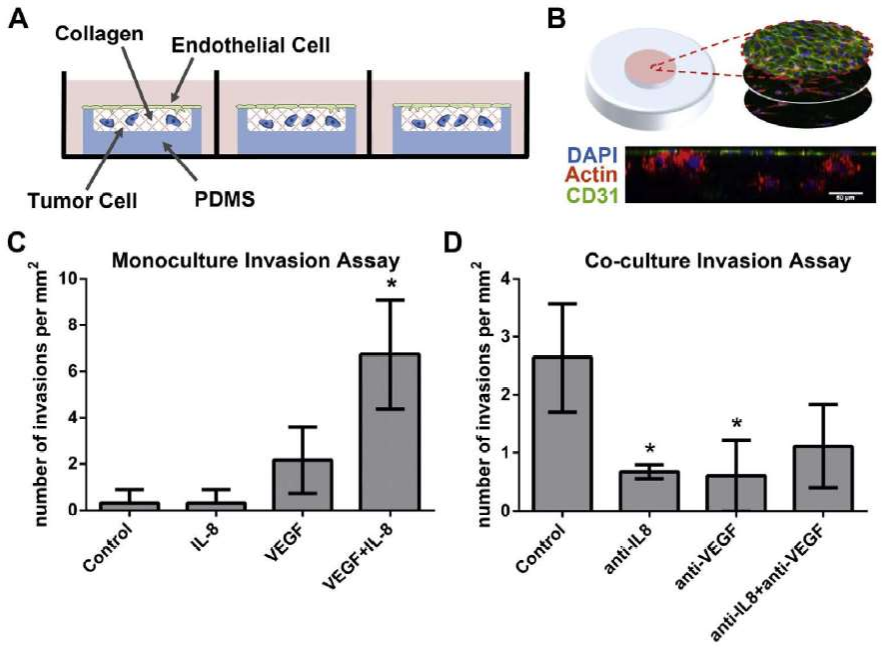

Fig. 6. Synergistic IL-8 and VEGF interactions promoted endothelial cell sprouting. A) A custom, 3D microwell invasion assay used to evaluate endothelial cell invasion into collagen gels in mono- or co-culture with tumor cells. Schematic illustrates the microwell design, in which HUVECs were seeded on the gel surface and tumor cells were embedded within the matrix. A PDMS mold confined the gel to prevent contraction. B) Representative micrographs of a co-culture invasion assay showing a series of z-slices and the xz cross-section. Cells were labeled with DAPI (nuclear, blue), phalloidin (actin, red), and CD31 (endothelial-specific marker, green). Scale bar = 50 µm. C-D) Endothelial cell sprouting was evaluated by counting the number of $CD31^{+}$ invasions extending beyond 12 µm from the gel surface. Results from the mono-culture invasion assay show no induction of sprouting with the addition of exogenous IL-8 or VEGF alone, but the combination of both factors exhibited synergistically enhanced number of invasions (C). Likewise, co-culture invasion assays containing OSCC-3 cells within the collagen bulk demonstrated sprout inhibition through function-blocking antibodies for either IL-8 (anti-lL-8) or VEGF (anti-VEGF), possibly by preventing this interaction (D).

We maintained homogeneous oxygen-concentration by fabricating 200 μm alginate discs, which alleviated the depletion of oxygen typically found beyond 150 μm from the surface. Although we cannot exclude that subcellular level oxygen variations may exist in this model, it has demonstrated stable, uniform conditions throughout the culture period at the cellular scale (16). We used this platform to conduct a comprehensive microarray analysis of gene expression for cells cultured in 2D, or in 3D alginate discs, subjected to hypoxic (1% O_2) or normoxic (17% O_2) conditions.

Results from the microarray analysis revealed a striking interdependence between oxygen status and culture dimensionality. Of the 8637 genes that responded to dimension or oxygen conditions by greater than 2-fold change, 77% were co-regulated rather than independent. Similarly, we found that changes in gene expression induced by hypoxia varied greatly based on its 2D or 3D substrate, and genes regulated by dimensionality also depended on oxygen status. In total, 2563 genes were found to be differentially expressed by greater than 2-fold change. These results support the conclusion that the change in dimensionality had a strong effect on cells' biological response to low oxygen conditions, and vice versa. Therefore, the intimate coupling of mass transport and 3D culture is both a physically and biologically relevant problem.

Our results are consistent with previous efforts to characterize the effects of oxygen deprivation in 3D using spheroid models and biomaterials-based approaches. For example, the rate of osteogenic differentiation of adipose stem cells in response to low oxygen conditions has been reported to change in 3D poly(lactide-co-glycolide) (PLG) scaffolds compared to 2D polystyrene (38). Likewise, we previously reported that secretion of VEGF and IL-8 depends on both 3D environment and oxygen status (16). On the other hand, our results contrast with a recent proteomic

study comparing 11 different tumor cell lines cultured in 2D monolayers and 3D spheroids under ambient or hypoxic conditions (39), in which the authors concluded that changes due to oxygenation in 2D are predominantly similar in 3D. This disparity may be due to the method of acquiring and analyzing data. Whereas the previous study was designed to identify the top similarities between various treatments and across multiple cell lines at the protein level, our study specifically examined top differences in each condition at the gene expression level. In both cases, careful validation for individual molecules of interest should be performed when interpreting high-throughput data.

Our next task was to identify which genes were most affected by dimensionality and hypoxia. Not surprisingly, Ingenuity pathway analysis revealed significant regulation of cell cycle, cancer, cell growth and proliferation, and cell death and survival in all four comparisons. These are known consequences of both hypoxic and 3D culture conditions (40). Divergence in the 3D versus 2D hypoxia response was associated with an inflammatory phenotype at the network, pathway, and molecular levels, suggesting that this process is equally sensitive to the culture environment. Together, this supports the conclusion that inflammatory signals are closely linked to the differential regulation of hypoxic signaling in 2D and 3D culture. These results are consistent with a recent study focusing on IL-6/pSTAT signaling, which similarly suggested that the 3D tissue context can regulate inflammatory potential (41). Collectively, these data imply an important role of the environment in regulating inflammatory processes.

The interdependence between hypoxia and dimensionality was particularly striking in the regulation of IL-8. In the microarray analysis, IL-8 was one of 214 genes affected by all four combinations of oxygen status and dimensionality, and also one of 351 genes that exhibited an

inverted hypoxia response depending on culture dimension. IL-8 was strongly up-regulated in 3D culture compared to 2D culture in both 1% and 17% O_2. On the other hand, IL-8 levels were increased in 2D hypoxia but reduced in 3D hypoxia, compared to the respective ambient expression. This observation supports previous reports of microenvironmental regulation of IL-8 (16). Furthermore, we confirmed the 3D-mediated up-regulation of this cytokine in a panel of three additional tumor cell lines derived from lung, breast, and gastric epithelial tissue, demonstrating relevance of microenvironmentally-regulated IL-8 signaling in multiple disease types. These results suggest that IL-8 may play a critical role in coordinating the interactions between hypoxia and dimensionality in the tumor microenvironment.

Tumor angiogenesis is one of the clinically important consequences of hypoxic signaling (4). Because the tumor hypoxia response was clearly regulated by culture dimensionality, we explored the functional consequences of these changes on tumor vascularization using an endothelial invasion assay. Results from both the mono-culture and co-culture inhibition studies suggest a synergistic relationship between IL-8 and VEGF signaling pathways contributing to sprouting angiogenesis. Because conventional 2D angiogenesis assays typically supplement the culture media with VEGF, this interaction has not been previously reported. This result suggests that the 3D culture environment does indeed impact the efficacy of angiogenic signaling pathways. Compensatory IL-8 signaling has been implicated in the underwhelming clinical performance of targeted anti-angiogenic therapies (33, 42). In addition, our results motivate further study of specific interactions between inflammatory and hypoxia response pathways that may provide novel avenues for intervention.

The study and treatment of cancer requires the development of controlled experimental platforms that faithfully explore tissue phenomena in vitro. These systems, such as the alginate-based disc assay described here, provide a unique opportunity to recreate critical features of the physiological environment. Furthermore, such platforms help delineate the individual and combined effects of various tissue-level conditions, including dimensionality, hypoxia, or inflammation. However, despite the advantages of simple and realistic tumor models, these systems remain only approximations of the true disease. As with any in vitro assay, these models neglect numerous features of *in vivo* tissue and provide a simplified representation of cancer pathology. However, by selective integration of salient microenvironment characteristics, tissue engineering approaches provide the opportunity for "designed complexity," thus allowing the definition of specific microenvironmental conditions to examine their independent and co-dependent effects. In this case, exploring the interactions between hypoxia and dimensionality helped distinguish their relative contributions to tumor angiogenesis.

Taken together, these results present several ramifications. First, the distinct behaviors in various regions of a tumor or spheroid, particularly regarding the proximity to functional vasculature, may be linked to the differential response to these physiological stimuli. Second, these results suggest that the conventional hypoxia response observed in 2D culture may not accurately represent the pathophysiological hypoxic program. Finally, investigation of therapeutic agents that target hypoxia, matrix, or inflammatory signaling should consider the potential confounding interactions between low-oxygen and 3D that may interfere with or potentially facilitate the desired intervention. The rational design of therapeutic strategies that address this interdependence may enhance the efficacy of existing pharmaceutical regimens.

Conclusion

Using biomaterials-based models of tumor hypoxia response and tumor angiogenesis with isolated control of oxygen distribution and culture dimensionality, we have demonstrated a differential response to hypoxic stress in 2D versus 3D culture, with direct consequences for tumor angiogenesis. Specifically, we found that the inflammatory response pathway, notably through IL-8 signaling, represents a critical link between oxygen status and dimensionality. This observation proved functionally relevant through the synergistic enhancement of VEGF-dependent endothelial sprouting in a 3D microwell invasion assay. Because tumor hypoxia response and angiogenic capability are products of complex microenvironmental interactions, therapeutic strategies that target matrix structure, hypoxia, angiogenesis, or inflammation may benefit from an improved understanding the interdependence between of these processes.

Supplementary information

Supplementary information is available in the online version of the paper.

References

1. Carmeliet P & Jain RK (2000) Angiogenesis in cancer and other diseases. *Nature* 407(6801):249-257.

2. Semenza GL (2000) HIF-1: mediator of physiological and pathophysiological responses to hypoxia. *Journal of Applied Physiology* 88(4):1474-1480.

3. Semenza GL (1999) Regulation of mammalian O-2 homeostasis by hypoxia- inducible factor 1. *Annual Review of Cell and Developmental Biology* 15:551-578.

4. Bergers G & Benjamin LE (2003) Tumorigenesis and the angiogenic switch. *Nature Reviews Cancer* 3(6):401-410.

5. Dery MAC, Michaud MD, & Richard DE (2005) Hypoxia-inducible factor 1: regulation by hypoxic and non-hypoxic activators. *International Journal of Biochemistry & Cell Biology* 37(3):535-540.

6. Semenza GL (2010) Defining the role of hypoxia-inducible factor 1 in cancer biology and therapeutics. *Oncogene* 29(5):625-634.

7. Aung KZ, Pereira BP, Tan PHS, Han HC, & Nathan SS (2012) Interstitial fluid pressure as an alternate regulator of angiogenesis independent of hypoxia driven HIF-1a in solid tumors. *Journal of Orthopaedic Research* 30(12):2038-2045.

8. Xu L, Xie KP, Mukaida N, Matsushima K, & Fidler IJ (1999) Hypoxia-induced elevation in interleukin-8 expression by human ovarian carcinoma cells. *Cancer Res* 59(22):5822-5829.

9. Bianchi E, *et al.* (2000) Integrin LFA-1 interacts with the transcriptional co-activator JAB1 to modulate AP-1 activity. *Nature* 404(6778):617-+.

10. Braun RD & Beatty AL (2007) Modeling of oxygen transport across tumor multicellular layers. *Microvascular Research* 73(2):113-123.

11. Grimes DR, Kelly C, Bloch K, & Partridge M (2014) A method for estimating the oxygen consumption rate in multicellular tumour spheroids. *Journal of the Royal Society Interface* 11(92).

12. Lu PF, Weaver VM, & Werb Z (2012) The extracellular matrix: A dynamic niche in cancer progression. *Journal of Cell Biology* 196(4):395-406.

13. Bissell MJ, Radisky DC, Rizki A, Weaver VM, & Petersen OW (2002) The organizing principle: microenvironmental influences in the normal and malignant breast. *Differentiation* 70(9-10):537-546.

14. Yamada KM & Cukierman E (2007) Modeling tissue morphogenesis and cancer in 3D. *Cell* 130(4):601-610.

15. Griffith LG & Swartz MA (2006) Capturing complex 3D tissue physiology in vitro. *Nat Rev Mol Cell Bio* 7(3):211-224.

16. Verbridge SS, *et al.* (2010) Oxygen-Controlled Three-Dimensional Cultures to Analyze Tumor Angiogenesis. *Tissue Eng Pt A* 16(7):2133-2141.

17. Bin Kim J, Stein R, & O'Hare MJ (2004) Three-dimensional in vitro tissue culture models of breast cancer - a review. *Breast Cancer Research and Treatment* 85(3):281-291.

18. Debnath J & Brugge JS (2005) Modelling glandular epithelial cancers in three-dimensional cultures. *Nature Reviews Cancer* 5(9):675-688.

19. Elliott NT & Yuan F (2011) A Review of Three-Dimensional In Vitro Tissue Models for Drug Discovery and Transport Studies. *Journal of Pharmaceutical Sciences* 100(1):59-74.

20. Kim JB (2005) Three-dimensional tissue culture models in cancer biology. *Seminars in Cancer Biology* 15(5):365-377.

21. Nelson CM & Bissell MJ (2005) Modeling dynamic reciprocity: Engineering three-dimensional culture models of breast architecture, function, and neoplastic transformation. *Seminars in Cancer Biology* 15(5):342-352.

22. Fischbach C, *et al.* (2007) Engineering tumors with 3D scaffolds. *Nat Methods* 4(10):855-860.

23. Seo BR, DelNero P, & Fischbach C (2014) In vitro models of tumor vessels and matrix: engineering approaches to investigate transport limitations and drug delivery in cancer. *Advanced Drug Delivery Reviews*.

24. DelNero P, Song YH, & Fischbach C (2013) Microengineered tumor models: insights & opportunities from a physical sciences-oncology perspective. *Biomedical Microdevices* 15(4):583-593.

25. Song H-HG, Park KM, & Gerecht S (2014) Hydrogels to model 3D in vitro microenvironment of tumor vascularization. *Advanced Drug Delivery Reviews* In Press.

26. Huang CP, *et al.* (2009) Engineering microscale cellular niches for three-dimensional multicellular co-cultures. *Lab Chip* 9(12):1740-1748.

27. Ghajar CM, *et al.* (2008) The effect of matrix density on the regulation of 3-D capillary morphogenesis. *Biophys J* 94(5):1930-1941.

28. Verbridge SS, *et al.* (2013) Physicochemical regulation of endothelial sprouting in a 3D microfluidic angiogenesis model. *Journal of Biomedical Materials Research Part A* 101(10):2948-2956.

29. Ehsan SM & George SC (2013) Nonsteady State Oxygen Transport in Engineered Tissue: Implications for Design. *Tissue Eng Pt A* 19(11-12):1433-1442.

30. Cross VL, *et al.* (2010) Dense type I collagen matrices that support cellular remodeling and microfabrication for studies of tumor angiogenesis and vasculogenesis in vitro. *Biomaterials* 31(33):8596-8607.

31. Li AH, Dubey S, Varney ML, Dave BJ, & Singh RK (2003) IL-8 directly enhanced endothelial cell survival, proliferation, and matrix metalloproteinases production and regulated angiogenesis. *Journal of Immunology* 170(6):3369-3376.

32. Waugh DJJ & Wilson C (2008) The Interleukin-8 Pathway in Cancer. *Clinical Cancer Research* 14(21):6735-6741.

33. Gyanchandani R, *et al.* (2013) Interleukin-8 as a modulator of response to bevacizumab in preclinical models of head and neck squamous cell carcinoma. *Oral Oncology* 49(8):761-770.

34. Masuya D, *et al.* (2001) The intratumoral expression of vascular endothelial growth factor and interleukin-8 associated with angiogenesis in nonsmall cell lung carcinoma patients. *Cancer* 92(10):2628-2638.

35. Heidemann J, *et al.* (2003) Angiogenic effects of interleukin 8 (CXCL8) in human intestinal microvascular endothelial cells are mediated by CXCR2. *Journal of Biological Chemistry* 278(10):8508-8515.

36. Shen YI, *et al.* (2014) Hyaluronic acid hydrogel stiffness and oxygen tension affect cancer cell fate and endothelial sprouting. *Biomater Sci-Uk* 2(5):655-665.

37. Hielscher AC & Gerecht S (2012) Engineering Approaches for Investigating Tumor Angiogenesis: Exploiting the Role of the Extracellular Matrix. *Cancer Res* 72(23):6089-6096.

38. He JW, Genetos DC, Yellowley CE, & Leach JK (2010) Oxygen Tension Differentially Influences Osteogenic Differentiation of Human Adipose Stem Cells in 2D and 3D Cultures. *J Cell Biochem* 110(1):87-96.

39. Levin VA, Panchabhai S, Shen L, & Baggerly KA (2012) Protein and phosphoprotein levels in glioma and adenocarcinoma cell lines grown in normoxia and hypoxia in monolayer and three-dimensional cultures. *Proteome Science* 10.

40. Rak J, Yu JL, Klement G, & Kerbel RS (2000) Oncogenes and angiogenesis: Signaling three-dimensional tumor growth. *Journal of Investigative Dermatology Symposium Proceedings* 5(1):24-33.

41. Leslie K, *et al.* (2010) Differential interleukin-6/Stat3 signaling as a function of cellular context mediates Ras-induced transformation. *Breast Cancer Research* 12(5).

42. Huang D, *et al.* (2010) Interleukin-8 Mediates Resistance to Antiangiogenic Agent Sunitinib in Renal Cell Carcinoma. *Cancer Res* 70(3):1063-1071.

CHAPTER 4

FORMATION OF MICROVASCULAR NETWORKS IN VITRO

John Morgan*, Peter DelNero*, Ying Zheng, Scott Verbridge, Junmei Chen, Michael Craven, Nak Won Choi, Anthony Diaz-Santana, Pouneh Kermani, Barbara Hempstead, José López, Thomas Corso, Claudia Fischbach, and Abraham Stroock. (2013) Formation of microvascular networks in vitro. *Nat Protoc* 8(9):1820–1836.

**Authors contributed equally.*

Abstract

This protocol describes how to form a 3D cell culture with explicit, endothelialized microvessels. The approach leads to fully enclosed, perfusable vessels in a bioremodelable hydrogel (type I collagen). The protocol uses microfabrication to enable user-defined geometries of the vascular network and microfluidic perfusion to control mass transfer and hemodynamic forces. These microvascular networks (mVNs) allow for multiweek cultures of endothelial cells or cocultures with parenchymal or tissue cells in the extra-lumen space. The platform enables real-time fluorescence imaging of living engineered tissues, *in situ* confocal fluorescence of fixed cultures, and transmission electron microscopy (TEM) imaging of histological sections. This protocol enables studies of basic vascular and blood biology, provides a model for diseases such as tumor angiogenesis or thrombosis, and serves as a starting point for constructing prevascularized tissues for regenerative medicine. After one-time microfabrication steps, the system can be assembled in less than 1 d and experiments can run for weeks.

Introduction

The microvasculature is a pervasive organ system that mediates the transfer of solutes (for example, metabolites, waste products, and signals) and cells (for example, leukocytes) throughout the body. These living pipes have a central role in the regulation of metabolic activity,

development, healing, immune response, and the progression of many diseases. This diversity of function places stringent constraints on the physical (network architecture) and biological (cellular composition) properties of the microvasculature. These constraints limit the size, complexity, and physiological relevance of tissues grown *in vitro* for applications in regenerative medicine, pharmaco-toxicological studies, and basic research. The development of methods to incorporate appropriate microvascular infrastructure into scaffolds for tissue engineering is indispensable for the progression of the field. Microfluidic control of mass transfer within biological scaffolds provides one solution to this crucial challenge in tissue engineering.

This protocol describes a platform (Fig. 1) that recapitulates the structure and function of microvascular vessels to serve in studies of basic vascular and blood biology, as models of diseases such as tumor angiogenesis or thrombosis, and as a starting point for engineering prevascularized tissues for regenerative medicine (1-5). In contrast to other uses of microfluidic endothelial cell cultures by confined gels or 2D models (6-9), our approach (1-5) leads to fully enclosed vessels in a bioremodelable hydrogel, suitable for biological questions that require a fully 3D extracellular environment with a contiguous parenchymal or stromal space. Our model represents a complementary extension of simpler, 3D assays of vasculogenesis and invasion angiogenesis (10); this extension is necessary where explicit vessel structure and perfusion of lumens have important roles in the study or application of interest.

Development of the protocol

Tissue engineers have long appreciated the need to incorporate vascular functionality in the design and fabrication of biological scaffolds (11-14). Diverse efforts have been made toward the incorporation of endothelial cells (15-17) and explicit vessel structures (18-21) within 3D biomaterials. The approach presented in this protocol builds on work over the past decade to bring

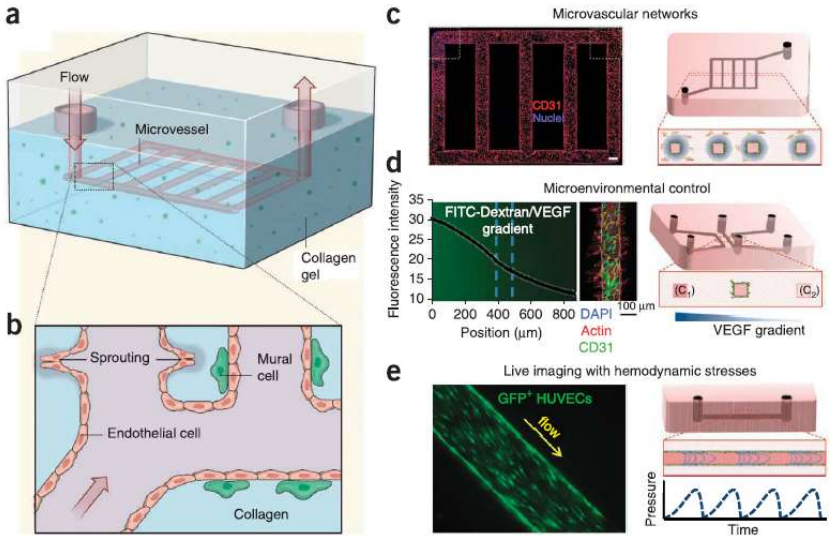

Fig. 1. Examples of vessel configuration. (a-e) Diverse vessel configurations have been adapted for various applications, including μVNs (a-c), steady-state morphogen gradients (d), and live imaging under controlled flow regimes (e). (a,b) Illustration of an endothelial cell-coated microfluidic network in a cell-laden collagen construct; inset highlights the endothelial confluence, pericyte-endothelial cell interactions, and angiogenic sprouting from the vessel. (c) Appropriate endothelial cell health, integrity, and confluence are demonstrated by uniform CD31 (also known as PECAM-1) (red) staining of cell-cell junctions in a quiescent vascular network; such networks provide nutrient and waste transport to sustain cells within the contiguous biological matrix. Scale bar, 100 μm. (d) The incorporation of parallel source (C1) and sink (C2) channels generates a stable biochemical gradient to mimic the heterogeneous distribution of potent morphogens, such as VEGF, and to stimulate endothelial cell sprouting in the study of invasion angiogenesis. (e) μVNs are used to study responsiveness of vessels to hemodynamic forces with live imaging of GFP-expressing endothelial cells. Under physiological shear stress and flow, the endothelial cells align in the direction of the flow. Diagrams in a,b are reproduced with permission from Franco and Gerhardt (47). Micrograph in c is adapted with permission from Zheng *et al.* (2).

microfluidic structure—sub-millimeter channels formed by microfabrication—into biomaterial scaffolds. The design and fabrication of micropatterned biomaterials was pioneered by Whitesides and colleagues (22, 23) with the development of replica molding of soft polymer microfluidic systems, also known as soft lithography. These techniques were later adapted to the molding of hydrogel scaffolds (24, 25). Alternatives to soft lithography such as bioprinting, sacrificial elements (21, 26) or modular assembly (27) have emerged; Gauvin et al. (28) have reviewed the distinct advantages and limitations of these methods. Soft lithography was first exploited to form vascular-like structure by Borenstein and colleagues (29-31) within poly(lactic-co-glycolic acid) films, poly(glycerol-sebacate), and silk fibroin; however, such materials prohibit cell encapsulation during the fabrication process. Building on this work, our group and others used micropatterning of natural hydrogels to provide convective transport to cells embedded within the bulk of physiologically relevant biological scaffolds (1, 19, 32). The Tien laboratory was the first to generate perfusable, endothelialized microvascular tubes and networks in such materials using lithographic methods and sacrificial elements (20, 33, 34). Our current protocol extends this progress with the incorporation of cells in the perivascular space, perfusion with whole blood, and functional angiogenic and thrombotic response to appropriate biochemical stimulation (2). Here we present the methods for the design, fabrication, and application of such μVNs.

Application of the method

In our first report, confocal fluorescence and TEM of the *in vitro* μVNs demonstrated the formation of a confluent, functional endothelium on the walls of the microfluidic channels and the viability of cells within the collagen bulk (Fig. 1c; ref. (2)) . In addition, we demonstrated appropriate morphology, barrier function, angiogenic remodeling, and appropriate cell-cell junctions. We further examined pericyte-endothelial cell interactions in defining barrier function

and angiogenesis, as well as blood-endothelium interactions, including thrombosis. We have also exploited the microfluidic control of flows to study angiogenesis in the presence of well-defined gradients of vascular endothelial growth factor (VEGF) and doses of anti-VEGF (Avastin) (3).

Moving forward, this assay presents opportunities to address questions in vascular biology that are inaccessible in planar cultures, such as the effects of geometry, hydrodynamic stresses, and convective mass transfer on vessel stability, angiogenesis, and development (35). μVNs also provide a basis for *in vitro* models of clinical conditions that implicate the vasculature in tissue-scale processes, such as wound healing, solid tumor cancers, and diabetes. Within such models, the explicit vasculature and perivascular space could, for example, allow for the study of mechanisms of intra- and extravasation (4, 5), the capture and incorporation of circulating endothelial progenitor cells (36), and the interplay of stroma, matrix, and endothelium in defining health and disease (37). In technological contexts, the ability to form vascularized scaffolds *in vitro* also opens new possibilities. For example, scaffolds with functional vasculature will have a central role in the engineering of any macroscopic and highly metabolically active tissue (38); tissue models with explicit vasculature could markedly improve the effectiveness of *in vitro* screens of drugs and of strategies of drug delivery (39). Further examples of the use of μVNs in models of solid tumors are reviewed in Stroock et al. (4). Wong et al. (40) present a comprehensive review of the opportunities for microfluidic models of vascular physiology.

Experimental design

This protocol describes a vascularization strategy to sustain 3D cell-laden biological scaffolds by convective mass transfer through endothelialized microfluidic networks. By combining a simple biomaterial and replica molding, artificial μVNs fully enclosed within cell-remodelable hydrogel constructs can be constructed. Our protocol includes photolithography

(Steps 1–11), biomaterial-based soft lithography (Steps 12–47), 3D microfluidic culture (Steps 48–54), live fluorescence imaging (Step 55A), *in situ* immunofluorescence staining and confocal imaging and analysis (Step 55B), and TEM imaging (Step 55C), as well as assays for the characterization of endothelium diffusivity and permeability (Box 1) and interactions with whole blood (Box 2). For a detailed overview of lithographic processes (Steps 1–6), see reference (23). Alternately, Steps 1–6 can be contracted to a custom third-party service, such as http://www.creatvmicrotech.com/intromicro.html, http://www.micralyne.com/novel-material-processing, or http://www.nilt.com/default.asp?Action=Details&Item=500. Videos are provided that show detailed assembly of the microfluidic culture device (Supplementary Video 1); seeding of cells into the channels of the microfludic culture device, including both successful (Supplementary Video 2) and unsuccessful (Supplementary Videos 3 and 4) examples; and live fluorescence imaging (Supplementary Video 5).

Limitations

Because this assay emphasizes physiological accuracy over simplicity, it introduces challenges with regard to throughput and multiplexing. This μVN assay is most appropriate for applications that require explicit vessel structures and network architectures and the ability to control perfusion of lumens. In some cases, simpler angiogenesis assays (10) may be more appropriate, such as to perform screens of cell types, reagents, and biomaterials (41). These simpler platforms can be used to establish parameters for the μVN assay presented here. In our experience, the soft lithographic manipulation of native collagen used in our protocol fails to provide good fidelity of channel structures for lateral dimensions below 50 μm. In addition, microfabrication by SU-8 soft lithography described here necessarily generates unphysiological rectangular channel cross-sections, although remodeling of the matrix by endothelial cells yields a rounded vessel

Box 1 | Characterization of the permeability of matrix and endothelium

● TIMING 30 min

To evaluate the permeability of the endothelium, it is convenient to first measure the diffusivity of the fluorescent solute within the matrix. This diffusivity should be measured in a microfluidic scaffold without an endothelium (steps 1–3). This diffusivity is used in the measurement of the permeability of the endothelium (steps 4 and 5).

Diffusivity within matrix

1. To measure the diffusivity of small and large molecules in matrix, prepare a microfluidic scaffold with no endothelial cells seeded on the walls of the channels (Steps 12–48 of the main PROCEDURE). Deliver solutions of fluorescein (10 μmol l^{-1} in PBS) and 70-kDa FITC-dextran (10 μmol l^{-1} in PBS) into the scaffold via microchannels. Stop the flow as soon as microchannels are filled uniformly with the fluorescent solution. The flow rate for delivery should be sufficiently high that minimal diffusion into matrix occurs during filling of channels. See Choi *et al.*[1] for more details.
2. Take fluorescence images sequentially for 3–30 min with an inverted microscope (e.g., Olympus, IX81) using a CCD camera (e.g., Hamamatsu, Orca-ER).
3. Analyze the images using appropriate software (e.g., Slidebook Olympus, ImageJ or MATLAB) to estimate the diffusivity of fluorescent molecules in the collagen gels, as described in detail by Choi *et al.*[1].

Permeability of the endothelium

4. To determine the permeability of the endothelium, transient delivery experiments can be carried out in the μVNs (Steps 49–53 of the main PROCEDURE). The flow rate should be sufficiently high that minimal depletion of the fluorescent solute occurs in the fluid during complete passage along the channel. See Zheng *et al.*[1,2] for more details.
5. Analyze the images using appropriate software (e.g., Slidebook Olympus, ImageJ or MATLAB) to estimate the permeability of the endothelium to fluorescent species given known diffusivity in the surrounding matrix (see steps 1–3). Details of the analysis are presented in Zheng *et al.*[1,2].

Box 2 | Characterization of blood-endothelial interactions ● TIMING 1 h

Tracking platelet interactions with the endothelium using whole blood

1. Draw 10 ml of blood from a consenting donor into a citrate-containing syringe, and store it in a 15-ml conical tube (3.8% (wt/vol) sodium citrate in the final volume).

! CAUTION Informed consent must be obtained from the blood donor. Experiments must conform to all relevant governmental and institutional regulations.

2. Separate whole blood into its components, including platelet-rich plasma (PRP), buffy coat and red blood cells by centrifugation. Transfer 95% of the PRP to a sterile conical tube and calculate the volume ratio.
3. Transfer 200 µl of the PRP to a microcentrifuge tube and label the platelets via incubation with fluorophore-conjugated antibodies (CD41a-APC) for 30 min.
4. Reconstitute 1 ml of whole blood by adding a proportional amount of the remaining red blood cells and buffy coat mixture to the labeled PRP tube (800 µl in this example).
5. Transfer the reconstituted whole blood to a 1-ml syringe connected with the microvessel inlet through sterile tubing. Connect the outlet to tubing filled with PBS buffer. Set the height difference between the syringe and outlet tubing to satisfy the target flow rate.
6. Monitor the perfusion process on a microscope stage with both bright-field and fluorescence microscopes.

vWF secretion and blood-endothelial interactions

7. To study vWF secretion and blood interactions with the stimulated microvessels, activate the vessels with PMA (50 ng ml^{-1} in GM) for 20 min at a shear stress of ~1 dyne cm^{-2}.
8. Wash the microvessels with PBS buffer and perfuse them with an FITC-conjugated vWF antibody (Abcam, 100 µg ml^{-1} in GM) or whole blood with labeled platelets.

morphology after about 2 d. Alternatively, fabrication of molds with isotropic etching could produce hemispherical cross-sections without altering the rest of the protocol. We have not attempted to create μVNs with multiple layers of channels; such extensions of the microfluidic approach have been shown in other materials (42). Chemical adhesion of the matrix to the boundaries of the jig and the use of higher densities of collagen mitigate contraction of microvessels as the density of cells embedded within the collagen bulk increases, as we have demonstrated in previous publications (5, 41). To date, human umbilical vein endothelial cells (HUVECs) are the only endothelial cells that have been cultured in this system; however, we believe that the assay will be broadly applicable to diverse endothelial cell types that have been successfully cultured on collagen substrates for angiogenesis and vasculogenesis assays, if used with the appropriate culture medium (20, 43).

Materials

Reagents

- Photoresist SU-8 2000 series (Permanent epoxy resist for photolithography, Microchem)

  ! CAUTION Wear protective goggles and gloves and suitable protective clothing.
- Silicon wafers for master mold (100-mm SSP silicon wafers, 500 μm in thickness, undoped; University Wafer)
- Photoresist developer (Microchem)
- Silane for passivation of master mold: tridecafluoro-1,1,2,2-tetrahydrooctyl-1-trichlorosilane (Gelest, cat. no. SIT8174.0)
- Isopropyl alcohol (for photolithography; Sigma-Aldrich)
- Sylgard 184 silicone elastomer base and curing agent (for soft lithography, Dow Corning)
- (poly)-dimethylsiloxane (PDMS) (Sylgard 184, Dow Corning)

- Sterile 1× PBS, pH 7.4 (Invitrogen, cat. no. 10010-023)
- Ethanol, 70% (vol/vol) in sterile deionized water (VWR, cat. no. BDH1162-4LP)
- Poly(ethyleneimine) (PEI, see Reagent Setup; Fluka Analytical, cat. no. P3143-500ML)
- Glutaraldehyde (GA, see Reagent Setup; Fluka Chemika, cat. no. 49629)

  ! CAUTION Use GA in a chemical hood and wear protective goggles and gloves and suitable protective clothing.
- Lyophilized type I collagen isolated from rat tails (Pel-Freez, cat. no. 5654-1) according to the procedures described by Bornstein (44) or Rajan et al. (45)
- HEPES buffer (Cambrex, cat. no. CC-5024)
- Sodium hydroxide (NaOH) solution, 2N (BDH, cat. no. 3223-1)

  ! CAUTION Wear protective goggles and gloves and suitable protective clothing.
- Cells of interest, e.g., human umbilical vein endothelial cells (HUVECs, Lonza, cat. no. CC-2519) or human brain perivascular cells (ScienCell, cat. no. 1200)
- DMSO (Sigma Life Science, cat. no. D8418-100ML)
- Medium appropriate for the cells being cultured, e.g., HUVEC culture medium EGM-2 (Lonza Clonetics, cat. no. CC-4176) or Lonza M199 (Lonza, cat. no. 12-117F)
- Endothelial cell growth factor (Millipore, cat. no. 02-102)
- FBS (Tissue Culture Biologicals, cat. no. 101)
- Penicillin-streptomycin (Lonza, cat. no. 17-602F)
- Heparin sodium (Acros, cat. no. 41121-0010, 9041-08-1)
- Trypsin-EDTA, 0.025% (wt/vol) (Invitrogen, cat. no. R-001-100)
- l-Glutamine (Cambrex, cat. no. 17-605C)

- l(+)-Ascorbic acid, reagent ACS (Acros Organics, Code 401471000, cat. no. CAS:50-81-7, EC:200-066-2)
- Human vascular endothelial growth factor (VEGF; Millipore, cat. no. 01-185, GF315)
- Human basic fibroblast growth factor (bFGF-2; Millipore, cat. no. 01-106)
- Phorbol 12-myristate 13-acetate (PMA) also known as 12-*O*-tetradecanoylphorbol-13-acetate (Sigma-Aldrich, product no. P 1585)

  ! CAUTION Wear protective goggles and gloves and suitable protective clothing.
- BSA (Calbiochem, cat. no. 126609)
- Rabbit polyclonal antibody (Rb pAb) to CD31, also known as platelet endothelial cell adhesion molecule (PECAM-1) (Abcam, cat. no. ab28364)
- Rabbit polyclonal antibody (Rb pAb) to vascular endothelial (VE)-cadherin (Abcam, cat. no. ab33168)
- Mouse monoclonal antibody to α-smooth muscle actin (α-SMA; Abcam, cat. no. ab54723)
- Anti-von Willebrand factor antibody conjugated with fluorescein isothiocyanate (FITC) (Abcam, cat. no. ab8822)
- APC anti-human CD41a (BD Pharmingen)
- PE anti-human CD45 (BD Pharmingen)
- Goat anti-rabbit IgG conjugated with Alexa Fluor 568 or Alexa Fluor 647 (Invitrogen and Molecular Probes, cat. nos. A11011 and A21244, respectively)
- Goat anti-mouse IgG conjugated with Alexa Fluor 488, Alexa Fluor 568 or Alexa Fluor 647 (Invitrogen and Molecular Probes, cat. nos. A11001, A21124 and A21240, respectively)
- DAPI, dilactate (Invitrogen, cat. no. D3571)

- Alexa Fluor phalloidin 488 (Invitrogen and Molecular Probes, cat. nos. A12379 and 1023568 300U, respectively)
- Formaldehyde, 16% (wt/vol) methanol-free, ultrapure electron microscopy grade (Polysciences, cat. no. 18814)
- Triton X-100 solution (see Reagent Setup; MP Biomedicals, cat. no. 807426)
- FITC protein label (Invitrogen, cat. no. F6434)
- Fluorescein (Sigma-Aldrich)
- TEM epoxy (Sigma-Aldrich)
- Cacodylate buffer ($Na(CH_3)_2AsO_2 \cdot 3H_2O$; 0.1M)
- Ruthenium red (0.05%, wt/vol)

  ! CAUTION Use this reagent in a chemical hood; wear protective goggles, gloves and other suitable protective clothing.
- Osmium tetroxide (OsO_4, 1.0% wt/vol)

  ! CAUTION Use this reagent in a chemical hood; wear protective goggles, gloves and other suitable protective clothing.
- Uranyl acetate ($UO_2(CH_3COO)_2 \cdot 2H_2O$; 2%, wt/vol)

  ! CAUTION Use this reagent in a chemical hood; wear protective goggles, gloves and other suitable protective clothing.
- Acetone
- Bleach

Equipment

- Plasma cleaner (for surface modification, Harrick, PDC-001, 115V)
- Disposable biopsy punches (4 mm and 1 mm diameter, Miltex)

- Autoclave (Market Force Industries, Sterilmatic)
- Incubator at 37 °C, 5% CO_2, (Thermo Electron Forma Series II waterjacketed CO_2 incubator HEPA Class100, (also NAPCO series 8000WJ))
- Water bath at 37 °C (VWR International, Sheldon Manufacturing, model no. 1212)
- Inverted microscope (for imaging cells, Nikon Eclipse TS100)
- Confocal microscope (for imaging cells, Zeiss 710)
- Transmission electron microscope (Technai F20)
- ImageJ software (or similar)
- Microtome (Leica Ultracut UCT ultramicrotome)
- Sterile syringe filters (PALL, Acrodisc 13-mm syringe filter with 0.2-μm HT Tufryn membrane, cat. no. PN 4454)
- Filter system, 500 ml, 0.22 μm (Fisher Scientific, cat. no. 09-761-102)
- Flask, 25 cm^2 with membrane cap (Fisher Scientific, cat. no. 10-126-28)
- Flask, 75 cm^2 with membrane cap (Fisher Scientific, cat. no. 10-126-37)
- Petri dish, small, 100 × 15 mm, 500/CS (Fisher Scientific, cat. no. 08-757-11Z)
- Petri dish, large, 150 × 15 mm, 100/CS (Fisher Scientific, cat. no. 08-757-14)
- Aluminum foil
- Syringe, 1 ml (VWR, BD Syringe, cat. no. BD329650)
- Syringe, 3 ml (VWR, BD Syringe, cat. no. BD09656)
- Pipette tips, 1,000 μl (VWR, cat. no. BD329650)
- Stainless steel machine screws, Phillips head, 4–40 (thread size) for microfluidic culture device
- Machine screws for aluminum casting jig

- Stainless steel dowel pins, 1 inch, 16-gauge diameter (Small Parts, cat. no. B001OBPJY6)
- PDMS flat slabs (30 mm × 30 mm; 3–5 mm in thickness)
- Self-standing, sterile conical tubes, 50 ml and 30 ml (VWR, cat. nos. 21008-777, 89012-778)
- Sterile conical vial, 15 ml (Fisher Scientific, cat. no. 14-959-49B)
- Tweezers
- Scalpel handle and blades
- Spatula
- Phillips head screwdriver
- Glass crystallizing dish and cover (125 × 65 mm) (Corning, cat no. 3140-125)
- Paper towels
- Autoclavable, medical-grade tubing (CorSolutions)
- Pump (CorSolutions) and pump connections (CorSolutions)

Reagent setup

! CAUTION Be sure to consult the relevant MSDS for safety information and use appropriate protective equipment when handling reagents.

PEI solution Dilute PEI to 1.0% (wt/vol) with sterile deionized water. Filter-sterilize the solution with a 0.22-μm sterile syringe filter. It can be stored for up to 6 months if it is sealed and refrigerated.

GA solution Dilute GA to 0.1% (wt/vol) with sterile deionized water. Filter-sterilize the solution with a 0.22-μm sterile syringe filter. It can be stored for up to 6 months if it is sealed and refrigerated at 4 °C.

Triton X-100 solution Dilute Triton X-100 to 1.0% (vol/vol) Triton X-100 in sterile deionized water and store it at room temperature (~20–25 °C). It can be stored for up to 6 months if it is sealed and refrigerated at 4 °C.

Formaldehyde solution Dilute formaldehyde to 3.7% (wt/vol) formaldehyde in PBS and store it at room temperature in the dark. It can be stored for up to 1 year if it is sealed.

Endothelial cell growth medium (GM) GM is a rich medium for expanding cells. To conduct rigorous biochemistry experiments, use a defined medium, such as EGM-2 (Lonza; see Reagents). To make GM, mix the components given in the following table:

Components	**Supplier and cat. no.**	**Volume**
Growth serum M199	Lonza, cat. no. 12-117F	500 ml
L-Glutamine (for a 2-mM working concentration)	Cambrex, cat. no. 17-605C	6.5 ml
Endothelial cell growth supplement (for a working concentration of 20 μg ml^{-1})	Millipore, cat. no. 02-102	15 mg (one vial)
Heparin (10,000 U ml^{-1} stock solution)	Acros, cat. no. 41121-0010, 9041-08-1	250 μl
FBS (for a working concentration of 18% (vol/vol))	Tissue Culture Biologicals, cat. no. 101	100 ml
Penicillin-streptomycin (for a working concentration of 150 U $ml^{-1)}$	BioWhittaker, 10,000 U ml^{-1}	7.5 ml

Cap and mix the contents gently without creating bubbles (the FBS enhances bubble formation). Connect a filter system (see Equipment) and attach it to a vacuum pump. Filter-sterilize the solution. It may be stored for up to 1 month if refrigerated at 4 °C.

Vasculogenesis medium (VM) VM is a rich medium used to activate endothelial cells to spontaneously form lumens and tubes in bulk collagen and undergo sprouting angiogenesis by invading from a monolayer. Determine the volume of VM needed (typically VM is only prepared as needed) on the basis of the volume of the channels, the flow rate, and the duration of the experiment. Calculate the volumes to be added into the base GM to form the VM, and mix these reagents (below) into GM that has been preheated to 37 °C. The following quantities should be added per the final volume of the VM: PMA at 50 ng ml^{-1}; VEGF165 at 40 ng ml^{-1} (keep on ice while handling it); bFGF at 40 ng ml^{-1} (keep on ice while handling it), and ascorbic acid at 50 μg ml^{-1}.

The difference between the added volumes of these substances and the final VM volume desired is the volume of GM to add. For example, 1 ml of VM, 2 μl of VEGF (from a 20 μg ml^{-1} stock), 1.6 μl of bFGF (from a 25 μg ml^{-1} stock), 1.6 μl of PMA (from a 50 μM stock), and 10 μl of ascorbic acid (from a 5,000 μg ml^{-1} stock) would be added to 985 μl of GM.

! CRITICAL Owing to protein degradation, keep VEGF165 and bFGF on ice while handling them, and only prepare VM as needed, typically 5 ml per day for gravity-driven flow or 10 ml for pump setup. The exact volume depends on device configuration and flow rates.

Collagen stock Collagen stock takes ~2 d to prepare. Resuspend lyophilized type I rat tail collagen in 0.1% (vol/vol) acetic acid to 1.5 mg ml^{-1} in a conical tube, to create a working stock solution. Shake the conical tube vigorously once a day to mix the contents, and keep it refrigerated at 4 °C. The collagen will dissolve over an ~2-d period. When it has dissolved, centrifuge the mixture at 1,950*g* for 5 min at 4 °C to remove air bubbles. The stock collagen can be maintained refrigerated at 4 °C for up to 3 months.

Procedure

Fabrication of a master mold ● TIMING 3 h

1| Design channel network geometry with appropriate computer-aided design (CAD) software, for example, AutoCAD, L-edit or Illustrator. Store it as a digital file (see Supplementary Data for an AutoCAD file of our system).

! CRITICAL STEP When you design the device, ensure that the inlet and outlet ports of the microfluidic network will align with the reservoir ports in the top piece of the microfluidic culture device (v in Fig. 2a).

2| Use the digital CAD file of the network channel geometry to create a photographic plate (the 'mask') by using appropriate technology, e.g., a high-resolution laser printer on a transparency sheet (if no microfabrication laboratory is available) or a dedicated photo pattern generator (such as the Heidelberg Mask Writer DWL2000 or the GCA 3600F Pattern Generator) on a glass plate coated with chromium and photoresist. Develop and etch the chrome mask.

! CRITICAL STEP The channel features should be transparent regions on the mask to allow for exposure of the SU-8 photoresist in the next step.

3| Spin-coat SU-8 photoresist onto a clean silicon wafer to a thickness that corresponds to the desired channel height; follow the spin curves and prebake temperatures and times from the supplier (http://microchem.com/pdf/SU-82000DataSheet2025thru2075Ver4.pdf).

4| Expose the wafer to UV light (365 nm), postbake it and develop it according to the supplier's instructions (http://microchem.com/pdf/SU-82000DataSheet2025thru2075Ver4.pdf).

5| Cut the wafer to fit into a molding jig (this is manufactured in Step 7; Fig. 2b).

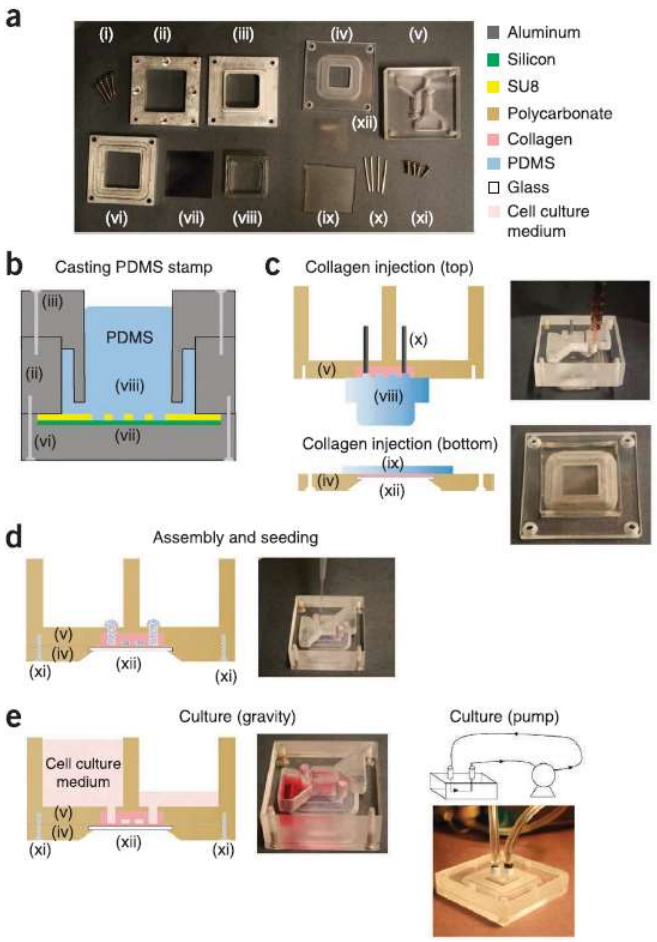

Fig. 2. Summary of microfluidic device fabrication (Steps 1-54), assembly (Steps 24-48), seeding (Steps 49-53), and culture (Steps 54A and 54B) processes. (a) Photograph of all the components for casting the PDMS stamp and assembling the microfluidic culture device. (a-e) Individual components are cross-referenced between the photograph in a and the diagrams in b-e using Roman numerals. (i) Machine screws for the aluminum casting jig; (ii, iii) top and middle pieces, respectively of the aluminum casting jig; (iv, v) bottom and top pieces, respectively, of the microfluidic culture device; (vi) bottom piece of the aluminum casting jig; (vii) lithographically-patterned silicon wafer master mold; (viii) PDMS stamp; (ix) flat PDMS slab; (x) stainless steel dowel pins; (xi) stainless steel machine screws (4-40 thread size) for microfluidic culture device; (xii) glass microscope coverslip. Technical drawings for the aluminum casting jig and microfluidic culture device can be found in Supplementary Figures 1 and 2, respectively. (b) Schematic of the aluminum jig assembly for casting the PDMS stamp using the lithographically-patterned silicon wafer master mold. (c) (Top) 3D micropatterned vessels are formed by injection molding of native collagen gel against the PDMS stamp through the injection ports on the top piece of the microfluidic culture device. Stainless steel dowel pins are used to preserve the connection between the cell culture medium reservoirs and the microfluidic channels. (Bottom) Collagen is injected onto the glass coverslip in the bottom piece of the microfluidic culture device and molded into a thin layer by sealing the gel cavity with a flat slab (~3 mm thick) of PDMS. (d) After the collagen gels, the top and bottom pieces of the microfluidic culture device are assembled to form the micropatterned, 3D microfluidic vessels, fully enclosed in collagen. The microvessels are then seeded with cells by pipetting a small (10 µl) cell suspension into the inlet reservoir. (e) The microvascular network is perfused with gravity-driven or pump-driven culture medium or whole blood. Photographs of detailed device assembly steps that are not depicted are available in Supplementary Figure 3. A video showing the detailed preparation and assembly of the microfluidic culture device (Steps 21-53) is available as Supplementary Video 2.

6| Passivate the surface of the wafer to avoid adhesion to silicone (PDMS), as follows. Oxidize the master for 1 min at 100 W in a plasma cleaner. Place the wafer with the featured side facing up in a vacuum desiccator with a vial containing a few drops (~10 μl) of tridecafluoro-1,1,2,2-tetrahydrooctyl-1-trichlorosilane. Evacuate the wafer, close the valve and leave the wafer under vacuum for at least 2 h.

! CAUTION Avoid contact and inhalation of silane. Work and vent the vacuum pump in a fume hood.

 PAUSE POINT The master can be stored indefinitely (in a protective cover) until further use.

Fabrication of machined parts of the molding and culture jig ● TIMING 5 h

7| Create aluminum jigs for molding the PDMS stamp with features on the silicon wafer (ii–iii, vi–vii in Fig. 2a). This jig will generate a stamp of well-defined dimensions to facilitate alignment with the microfluidic culture device. Mechanical drawings of example parts are presented in Supplementary Figure 1.

! CRITICAL STEP We used aluminum in our device for durability to prevent the jig from undesired deformation (when plastic was used) through multiple uses and because of its ease of machining.

! CRITICAL STEP Molding biological hydrogels directly onto microfabricated structures in rigid materials such as silicon and SU-8 photoresist leads to difficulties in demolding (separating a structured gel from a micromold). For this reason, the structure should be transferred to a PDMS stamp (described in Steps 9–11).

8| Create a microfluidic device to contain culture (iv–v in Fig. 2a). Mechanical drawings of parts are presented in Supplementary Figure 2.

! CRITICAL STEP We used polycarbonate in our device for its transparency, biocompatibility and absence of autofluorescence.

Fabrication of the PDMS stamp ● TIMING 10 h

9| Assemble the aluminum casting jig for casting the PDMS stamp from the silicon master as shown in Figure 2b.

10| Mix the PDMS components in the weight ratio of 1/11 curing agent to 10/11 base. Remove the air bubbles by applying weak vacuum. Pour the liquid PDMS into the aluminum casting jig, carefully to prevent the formation of air bubbles. Partially cure it overnight at room temperature. Cure it for 1 h at 60 °C to finish hardening.

! CRITICAL STEP Curing directly at an elevated temperature will lead to distortions of the features in the stamp caused by the thermal expansion of the aluminum jig.

11| Disassemble the aluminum casting jig and remove the PDMS stamp slowly (viii in Fig. 2a); applying small volumes of ethanol facilitates easier demolding.

Sterilization of materials for device assembly ● TIMING 30 min

! CRITICAL All components must be sterilized with an autoclave or plasma cleaner, or by using another appropriate method such as gas sterilization with ethylene oxide.

12| Sterilize the following components by autoclaving them: four stainless steel machine screws for the microfluidic culture device (xi in Fig. 2a; 4–40 (thread size)); two stainless steel dowel pins

(16-gauge diameter; x in Fig. 2a); tweezers, scalpel handle(s), a spatula, and a screwdriver; PDMS flat squares (30 mm × 30 mm; 3–5 mm in thickness; ix in Fig. 2a); glass culture dishes; paper towels; and autoclavable tubing and pump connections (for operation with pump only).

13| Sterilize all polycarbonate components in 10% (vol/vol) bleach for 30 min. Rinse them with sterile water and dry them with compressed air.

14| Sterlize all polycarbonate components (top piece of the microfluidic culture device for housing the 1 mm deep, 20 × 5 mm inset for bottom layer of collagen and bottom 50 mm × 50 mm piece of the microfluidic culture device with no. 1.5, 25 mm × 25 mm glass coverslip on top of it) in plasma cleaner for 5 min at 100 W.

15| Transfer the components to a sterile biosafety cabinet using sterile techniques.

16| Sterilize 1% (wt/vol) PEI and 0.1% (wt/vol) GA using a 0.22-μm sterile filter.

! CRITICAL STEP All remaining steps must be performed in a sterile biosafety cabinet, while wearing sterile gloves, until fixation.

Coating of devices with sterile PEI and GA ● TIMING 45 min

17| Soak a glass coverslip (xii in Fig. 2a) in 1% (wt/vol) PEI for 10 min. Meanwhile, apply 1% (wt/vol) PEI via a 200-μl micropipette to the 1-mm-deep well (collagen reservoir) in the top piece of the microfluidic device (v in Fig. 2a) for 10 min (do not let it dry).

18| Aspirate the PEI from the coverslip and device surface. Rinse the coverslip in sterile-filtered deionized water. Wash the device surface thoroughly with 10 ml of sterile water. Aspirate water

from the coverslip and device, and then dry it with dry air (sterilized through a sterile filter). If sterile air is not available, air-dry the device for 30 min.

! CRITICAL STEP To avoid residue, do not allow PEI to dry on the device without aspirating it. Only apply PEI to the tissue culture region.

19| Soak the glass coverslip in 0.1% (wt/vol) GA for 30 min. Apply 0.1% (wt/vol) GA via a 200-µl micropipette into the 1-mm-deep well (collagen reservoir) in the top piece of the microfluidic culture device for 30 min (do not let it dry).

20| Aspirate the GA from the coverslip and device surface to avoid deposition of residue. Rinse it thoroughly with sterile water and dry it in sterile air. If sterile air is not available, air-dry it for 30 min. Place the top and bottom pieces of the device and the microscope coverslip in a refrigerator (4 °C) in a sterile, sealed container to chill, both while mixing the collagen (Step 21) and before injection-molding the collagen (Step 24).

! CRITICAL STEP The device must be thoroughly rinsed after coating because free GA will be toxic to the cells. To avoid residue, do not let GA dry on the device without aspirating it. Only apply GA to the tissue culture region.

! CRITICAL STEP The device should be chilled in a refrigerator (4 °C) before injection-molding the collagen (Step 24). This step will slow the rate of nucleation during collagen gelation and enable the proper formation of the collagen protein fibers.

 PAUSE POINT The devices can be stored in a refrigerator (4 °C) for several days before injecting the collagen (Step 24), provided that they are kept in a sterile, sealed container.

Preparation of 1% (wt/wt) collagen gel ● TIMING 10 min

21| Use a 1-ml syringe with tapered Luer lock tip to transfer stock collagen with a desired volume to a sterile 30-ml conical tube. See Supplementary Video 1 for further guidance. For an acellular scaffold, calculate the volume of stock collagen by using the following formula: $V_{s\_collagen} = V_f \times C_{f\_collagen}/C_{s\_collagen}$, where $V_{s\_collagen}$ is the volume of stock collagen, V_f is the final volume of neutralized collagen, $C_{f\_collagen}$ is the final concentration of neutralized collagen, and $C_{s\_collagen}$ is the concentration of stock collagen. Each device requires a final volume of ~1 ml of neutralized collagen gel, depending on jig geometry. To avoid forming air bubbles during transfer, take up an initial small amount of collagen (~100 ml) into the syringe tip and move the plunger up and down to remove air bubbles. Next, push the collagen to the end of the syringe until it protrudes slightly from the tip and take up the remaining volume. Transfer the stock collagen to a sterile 30-ml conical tube.

22| Prepare the neutralizing reagent, using micropipettes to collect it into a 15-ml conical tube. The neutralizing reagent consists of Lonza M199 EC medium (1× and 10×) and NaOH. For an acellular scaffold, calculate the volume of each reagent using these formulas:

$$V_{10\times} = 0.1\times V_f$$

$$V_{NaOH} = 0.022\times V_{s\_collagen}$$

$$V_{1\times} = V_f - V_{s\_collagen} - V_{10\times} - V_{NaOH}$$

where $V_{10\times}$ is the volume of 10× Lonza M199 medium, V_f is the final volume of neutralized collagen (from Step 21), V_{NaOH} is the volume of NaOH, $V_{s\_collagen}$ is the volume of stock collagen (from Step 21), and $V_{1\times}$ is the volume of 1× Lonza M199 medium.

23| Mix the solution of neutralizing reagent prepared in the previous step and pipette it carefully on top of the collagen in the 30-ml conical tube in order to avoid air bubbles. Use a sterilized spatula to gently mix the gel until it is homogeneous. Avoid introducing any bubbles into the collagen.

For cellular scaffolds, prepare the mixed, neutralized collagen gel at a concentration above that desired (see sample calculations in Steps 21 and 22), and then add cells suspended in an appropriate volume of medium (V_{s_cell}) to reduce the collagen to a 1% (vol/vol) solution, and then mix it again until it is homogeneous. Calculate the appropriate volume of medium for the cell suspension (V_{s_cell}) as follows:

$$V_{s\_cell} = V_{f\_cell} - V_f$$

$$V_{f\_cell} = V_f \times C_{f\_collagen} / C_{f\_cell}$$

where V_{s_cell} is the volume of cell suspension, V_{f_cell} is the final volume of neutralized collagen after adding the cell suspension, V_f is the volume of neutralized collagen before adding the cell suspension (from Step 21), $C_{f\_collagen}$ is the concentration of neutralized collagen before adding the cell suspension (from Step 21), and C_{f_cell} is the final concentration of collagen after adding the cell suspension (1% (vol/vol)).

! CRITICAL STEP To make a different concentration of collagen, vary the reagent volumes according to the above formulas.

! CRITICAL STEP Neutralized collagen gels rapidly at room temperature. Keep all reagents on ice. Confirm appropriate pH with litmus paper and add small volumes (1 µl dropwise) of NaOH until the pH reaches a physiological value of 7.4.

! CRITICAL STEP Dense collagen (>5 mg ml^{-1} or 0.5 % (wt/wt)) is highly viscous. Use a 1-ml taper-tip syringe to transfer collagen solutions, moving the plunger up and down to remove air bubbles. Mix the collagen gently with a sterile stainless steel spatula to avoid generating bubbles. To ensure homogeneity, stir the mixture for about 2 min after the color becomes uniform. If bubbles form, centrifuge the mixture at 1,950*g* at 4 °C for 5 min.

! CRITICAL STEP For cell-laden scaffolds, neutralize the stock collagen to pH 7.4 before introducing the cells. Ensure that the collagen is at pH 7.4 or the cells will die. Prepare this collagen at an initial concentration that is above that desired (see sample calculation in Step 23), and then add cells suspended in an appropriate volume of medium to reduce the collagen to a 1% (vol/vol) solution.

Injection-molding microstructured collagen ● TIMING 15 min

24| Immediately after preparing the collagen gel with or without suspended cells present (Steps 21–23), sterilize and oxidize the surface of the PDMS stamp with the microstructure pattern by exposure to oxygen plasma for 5 min at 30 W (or 1 min at 100 W). The collagen will wet onto the oxidized surface of the PDMS such that the entrapment of bubbles is minimized. See Supplementary Video 1 for further details.

25| Place the top piece of the microfluidic culture device (v in Fig. 2a) onto the PDMS stamp (viii in Fig. 2a) as shown in Figure 2c. Align the inlet and outlet ports of the micropatterned network on the PDMS stamp with the inlet and outlet ports on the top piece of the microfluidic culture device (Supplementary Fig. 3).

! CRITICAL STEP When you design the device, ensure that the inlet and outlet ports of the microfluidic network will align with reservoir ports in the top piece of the microfluidic culture device (Fig. 2c and Supplementary Fig. 3).

26| Gently insert the 16-gauge stainless steel dowel pins (x in Fig. 2a) into the reservoir holes on the top piece of the microfluidic culture device. They should be loose within the reservoir holes and rest stably on top of the PDMS stamp without pushing down on it (Fig. 2c and Supplementary Fig. 3). These dowels are required to create the inlet and outlet ports within the bulk collagen (the ports for GM) by preventing the entry of collagen during the injection molding.

27| Use a 1-ml taper-tip syringe to extract ~0.5–0.6 ml of collagen. Remove the bubbles in the syringe by gently moving the plunger up and down vertically. Slowly and steadily inject the collagen into the injection port on the top piece of the microfluidic culture device (Fig. 2c).

28| Transfer the entire assembly to a fully enclosed, sterile glass dish, and then place it in an incubator at 37 °C for 30 min to allow for gelation.

Molding collagen coating onto a glass coverslip ● TIMING 5 min

29| Place the precoated glass microscope coverslip onto the bottom piece of the microfluidic device, and use a micropipette to dispense ~170 µl of collagen onto the glass microscope coverslip (xii in Fig. 2a) homogeneously (Fig. 2c and Supplementary Fig. 3). See Supplementary Video 1.

30| Gently place the flat square of PDMS (ix in Fig. 2a) on top of the collagen and microscope coverslip to spread the collagen evenly across the coverslip (Fig. 2c and Supplementary Fig. 3).

31| By using two pairs of tweezers, one to push down at the edge of the PDMS square to hold it in place and the other to spread the collagen, gently move the tweezers across the top of the PDMS

square to spread the collagen evenly across the coverslip. Ensure that the collagen covers the gaps between the microscope coverslip and the microfluidic culture device on all four sides and that it does not accumulate in the center (Supplementary Fig. 3).

Collagen gelation ● TIMING 30 min

32| Transfer the entire assembly to a fully enclosed, sterile glass dish, and place it in an incubator at 37 °C for 30 min to allow for gelation.

33| Remove the top and bottom pieces of the microfluidic culture device from the incubator after gelation and return them to the sterile biosafety cabinet.

Assembling the device (top and bottom pieces) ● TIMING 15 min

34| Pick up the top piece of the microfluidic culture device and hold it so that the PDMS stamp is on the top. See also Supplementary Video 1.

35| Remove the PDMS stamp from the top piece of the microfluidic culture device by applying ~250 µl of PBS around the interface of the stamp with the device. Gently lift the PDMS stamp from the surface of the top Plexiglas piece (Supplementary Fig. 3). If the collagen scaffold contains cells, use cell culture medium instead of PBS.

! CRITICAL STEP The PDMS stamp is held against the top piece of the microfluidic culture device by surface tension. Be careful not to bump the stamp, because it may damage the collagen channels. The small volume of PBS (or cell culture medium for a cellularized collagen scaffold) applied around the interface serves as a lubricant for easier removal.

36| Remove stainless steel dowel pins from the top piece of the microfluidic culture device with sterile tweezers.

37| Place the top piece of the device on a Petri dish cover, collagen side up, and dispense ~0.5–1 ml of PBS on top of the micropattern in the collagen gel to prevent it from drying. If the collagen scaffold contains cells, use cell culture medium instead of PBS.

38| Use a 3-ml syringe to add PBS around the perimeter of the PDMS flat square on the bottom piece of the microfluidic culture device (Supplementary Fig. 3). Gently remove the PDMS flat square from the bottom piece. Remove any excess collagen from the edges with a spatula. If the collagen scaffold contains cells, use cell culture medium instead of PBS.

39| Pick up the bottom piece with a pair of tweezers or forceps and flip it upside down so that the collagen is facing the collagen on the top piece.

40| Balance the bottom piece between two Petri dishes, with the collagen facing down, and place screws into three of its four corner holes, such that the pointed ends of the screws face down and the screw heads rest in the corner holes.

41| Gently assemble the two pieces (joining the micropatterned collagen of the top piece with the flat collagen layer of the bottom piece) as follows. First, place the top piece into a large Petri dish with the collagen facing up. Then, dispense PBS onto the top piece so that it completely covers both the collagen and the surrounding polycarbonate of the device. If the collagen scaffold contains cells, use cell culture medium instead of PBS. Finally, carefully place the bottom piece (with collagen facing down) onto the top piece (that has the collagen facing up), by holding the bottom piece at an angle and inserting the tips of the two screws from one side of the bottom piece into the corresponding, matching holes of the top piece, and then gently roll (rotate the alignment) the bottom piece across the top piece to insert the third screw into position on the opposite side. This motion should displace the PBS liquid between the two pieces of the microfluidic culture device

and prevent the formation of air bubbles as the collagen from the top and bottom pieces join. See Supplementary Figure 3. If the collagen scaffold contains cells, use cell culture medium instead of PBS.

42| Insert the fourth screw on the jig and use a screwdriver to gently tighten all four screws.

! CRITICAL STEP To ensure that both collagen pieces are joined with a uniform, level seal, tighten the screws in the rotating manner of an automobile tire. Be careful not to tighten the screws too much or the channels will collapse (Supplementary Fig. 3).

43| Aspirate excess PBS (or cell culture medium, for a cellularized scaffold) from the device.

44| Use autoclaved paper towels or an aspirator to remove any remaining PBS (or cell culture medium, for a cellularized scaffold) surrounding the surfaces of the microfluidic culture device, and then put the device into an autoclaved glass dish.

45| Turn the device over and remove the PBS (or cell culture medium, for a cellularized scaffold) from the reservoirs on the top of the device (Supplementary Fig. 3).

46| Add cell culture medium to the inlet reservoir.

47| Place the device in a fully enclosed, sterile Petri dish and inspect it under a light microscope to confirm the channel fidelity and the absence of air bubbles (Supplementary Fig. 3).

! CRITICAL STEP Air bubbles must not be present in the channel. They will grow in the incubator and rupture the channel. If air bubbles are present in the channel, place the device (in a fully enclosed, sterile glass dish) in a refrigerator (4 °C) until the bubbles dissolve (~20 min).

Device incubation in preparation for seeding channels ● TIMING 1 h

48| Place the device in the incubator for at least 1 h to allow the collagen to equilibrate with the cell culture medium and to attain the proper physiological pH. See Figure 2 for a summarized schematic diagram of the assembly process.

 PAUSE POINT The device can be stored in the incubator overnight before the channels are seeded with cells.

Seeding channels with endothelial cells ● TIMING 40 min

49| Trypsinize HUVECs or other endothelial cell types and prepare a cell suspension, using appropriate cell culture medium (see Reagents), at a cell density of ~4–6 × 10^6 cells per ml.

50| In a sterile biohood, remove the GM from the reservoirs in the device by using 200-µl pipette tips. If necessary, remove any residual GM remaining in the reservoir by using gel-loading tips (while in the biohood), being careful not to press the tips into the collagen.

! CRITICAL STEP Do not attempt to remove medium from the channels, as this will introduce air bubbles. Air bubbles will grow upon incubation and rupture the channels.

51| Inspect the channels with a bright-field microscope to ensure that no air bubbles are present in the channels.

52| Add a 10-µl cell suspension into one reservoir at the entrance to the collagen channel (but without touching the bottom of the collagen channel) using a gel-loading pipette (Supplementary Fig. 3). The flow should start immediately, but it should be slow. It should balance between the inlet and outlet reservoirs within 10 min. (See Supplementary Fig. 4 and Supplementary Video 2

for examples of successful seeding. See Supplementary Videos 3 and 4 for examples of unsuccessful seeding.)

! CRITICAL STEP To prevent introduction of air bubbles into the channel, before inserting the pipette tip into the reservoir entrance to the channel, push a droplet of medium to the tip of the pipette so that it protrudes.

! CRITICAL STEP When you seed cells into the device, do not allow the tip of the gel-loading pipette to touch the collagen, as doing so will destroy the channel integrity.

! CRITICAL STEP If the flow is too fast, add 2 μl of culture medium to the outlet reservoir before incubation. Reservoirs should equilibrate and the flow will stop during the first 10 min of incubation.

53| Allow the cells to attach to the collagen for 30 min in the incubator (in a fully enclosed, sterile dish), and then transfer the device to the biohood and add cell culture medium to the inlet reservoir. Wash out any unattached cells from the channel or network by enabling flow, and then remove them from the outlet reservoir. Proceed with culturing the cells (Supplementary Fig. 3). A confluent monolayer of endothelial cells should form in the channel within 24 h.

Perfusion culture

54| If desired, set up perfusion via gravity (option A) or pump (option B). See also Figure 2e. Pump-driven perfusion provides more precise and stable flow rates than gravity-driven flow, and it can improve culture efficiency by recirculating the medium, thereby eliminating the need to replace it. In addition, a pump has the ability to impose different flow regimes (e.g., with respect to waveform, frequency and amplitude). Alternative experiments involving perfusion of the

endothelialized networks, such as measuring endothelial permeability (Box 1) or characterizing interactions with whole blood (Box 2), are presented herein.

(A) Gravity-driven perfusion culture ● TIMING 5 min

(i) Add cell culture medium, as appropriate, to the inlet reservoir and recycle or replace the medium as necessary during 14 d of culture.

(ii) Select the desired shear stress for the culture and calculate the required volumetric flow accordingly. In the case of gravity-driven flow, the reservoir height will define the volumetric flow rate, Q (m^3 s^{-1}), and shear stress at the channel wall, τ (kg m^{-1} s^{-2}). As an example, for a single channel of uniform dimensions, we have:

$$Q = \frac{\rho g}{R}\Delta h(t)$$

$$\tau = \frac{d}{4L}RQ$$

where ρ (kg m^{-3}) is the fluid density, g (m s^{-2}) is the gravitational acceleration, R is the hydraulic resistance of the channel, Δh(t) (m) is the difference in height of fluid between the reservoirs, d (m) is the diameter of the channel, and L (m) is the length of the channel. For this single-channel example,

$$R = \frac{128\,\mu L}{\pi d^4}$$

where μ (kg m^{-1} s^{-1}) is the viscosity of the medium. As the reservoirs equilibrate over time, the height difference decays according to the following equation:

$$\Delta h(t) = \Delta h_0 e^{\frac{-2\rho g}{AR}t}$$

where Δh_0 (m) is the initial difference in height, A (m^2) is horizontal cross-section of the reservoir, and t (s) is time.

! CRITICAL STEP To maintain approximately steady-state flow with the gravity-driven system, slow the rate of change of $\Delta h(t)$ by using large reservoirs (A), by using an overflow system (46), or by periodically restoring the inlet and outlet fluid levels.

(B) Pump-driven perfusion culture ● TIMING 15 min

(i) Select an appropriate pump for the experiment. Syringe pumps present challenges for driving flow within μVNs; recycling of medium is difficult, and they are prone to fluctuations in pressure that can destroy the endothelium. Conventional peristaltic pumps are compatible with medium recirculation, but they generate unsteady flows and are susceptible to air bubbles. An effective solution is to use a high-precision, continuous-flow pump with an in-line flow sensor with submicroliter-per-minute flow accuracy based on feedback control and a bubble trap. Such a pump is available from CorSolutions (http://www.mycorsolutions.com/products/fluidic_pumps.html).

(ii) For pump-driven flow, determine the desired shear stress for the endothelium and calculate the required flow rate as described in Step 54A(ii). Insert the appropriate pump connectors into the inlet and outlet reservoirs.

! CRITICAL STEP Be very careful not to introduce air bubbles into either the connectors or the device. To prevent bubble formation, fill the connection ports with medium before inserting them into the inlet and outlet reservoirs.

(iii) Attach sterile, nontoxic tubing (e.g., CorSolutions) to the pump and gently connect it to the device: first to the inlet reservoir and then to the outlet reservoir.

! CRITICAL STEP To prevent air bubbles from being introduced to the microchannels, allow a drop of medium to collect at the opening of the tube before attaching it to the inlet connector port.

Similarly, allow a droplet of medium to collect at the surface of the outlet reservoir connector before connecting the tubing (Fig. 2e).

Imaging of cells

55| Cultures can be imaged and evaluated via live fluorescence microscopy (option A), for example, to characterize the permeability of the matrix and epithelium (Box 1). Alternatively, confocal fluorescence microscopy can be performed on fixed samples (option B), or greater resolution can be obtained via TEM (option C). Live imaging (option A and Boxes 1 and 2) allows the dynamics of the endothelial cells within the endothelium (e.g., proliferation, alignment and migratory behavior) to be tracked in the presence of well-defined luminal flow (Fig. 3, Supplementary Video 1). Confocal fluorescence microscopy (option B), which can also be performed following live fluorescence microscopy, enables the visualization of the molecular-level features of the microvasculature, such as nuclei, individual proteins in the membrane or cytoplasm, and polysaccharide chains of the glycocalyx. TEM (option C) enables the identification of additional molecular level features, such as cell-cell junctions and the basal lamina, that are not readily distinguishable by other techniques.

(*A) Live imaging of fluorescent cells* ● TIMING variable, 1 h or 2–3 d

(i) To perform live imaging of fluorescent cells, use a microscope with an incubating stage (sterile with humidified and controlled temperature and carbon dioxide). Mount the device on the microscope stage and verify that it is level by checking the focus across the sample.

! CRITICAL STEP Maintenance of a stable environment (humidity and CO_2 level) is crucial to the health of the culture. The use of a secondary container of smaller volume with regulated

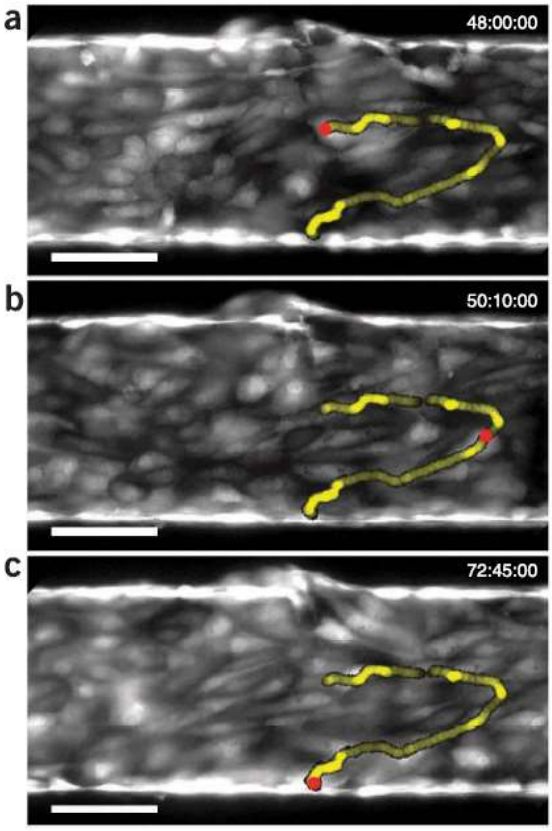

Fig. 3. Live fluorescence imaging of GFP-expressing HUVECs in µVNs, as described in Step 55A. (a-c) The culture was run under physiological shear flow (-11 µl min^{-1}, 17 dyne cm^{-2}) with a feedback-controlled peristaltic pump (Step 54B). The flow direction is from left to right. The snapshots reveal dynamic cell motility throughout the vessel wall. Cell tracking (red dots) traces an individual cell's path (yellow lines) as it migrates upstream and downstream within the endothelium. Yellow intensity corresponds to instantaneous velocity along the path length, with dark zones representing faster motion. Scale bars, 50 µm. Time stamps show hours:minutes:seconds after onset of flow. See Supplementary Video 1 for the full image sequence.

humidity and CO_2 may be required to maintain physiologic levels of CO_2 and adequate humidity around the culture.

(ii) To ensure that photographs captured during the culture are clear, focus the image with the microscope focus knob for coarse and fine adjustment while viewing it through the camera, not through the microscope ocular lens.

(iii) For perfusion cultures, establish the flow using the procedures above (Steps 54A and 54B).

(iv) Set the desired frequency of time-lapse images (e.g., once every 2.5–5 min). See Figure 3 and Supplementary Video 5 for examples of long-term, live images of GFP^+ HUVECs in a microvessel.

(B) Confocal fluorescence microscopy on fixed and stained samples ● TIMING 14 h

! CRITICAL STEP Note that fluorescence imaging can be performed without disassembling the microfluidic culture device. Perform this step by flowing reagents through the channels and imaging through the microscope coverslip in the base of the device.

(i) Fixing and staining. To fix the cells and the matrix at the end of the culture, replace the medium in the reservoir with 3.7% (wt/vol) formaldehyde in PBS and allow it to flow through the device at room temperature for 30 min.

! CAUTION Wear suitable protective clothing and gloves when you work with 3.7% (wt/vol) formaldehyde.

(ii) To remove the formaldehyde, perform three 5-min washes with PBS.

 PAUSE POINT The device can be stored with the reservoirs filled with PBS for up to 12 h if refrigerated and protected from light and evaporation (e.g., covered with aluminum foil).

(iii) To block against nonspecific binding and to permeabilize the cell membranes to enable staining, incubate the cells in 3% (wt/vol) BSA and 1% (vol/vol) Triton X-100 in PBS for 1 h.

(iv) Remove BSA/Triton X-100, but do not wash the cells with PBS. Incubate them with primary antibodies in PBS with supplemental 1% (wt/vol) BSA overnight at 4 °C in the following ratios: either Rb primary, polyclonal antibody (pAb) to CD31 (Abcam) at a ratio of 1:50 or Rb pAb to VE-cadherin (Abcam) at a ratio of 1:50; and mouse primary monoclonal antibody to α-SMA (Abcam) at a ratio of 1:100. They can be used for co-staining because they are from different species and are targeted by different secondary antibodies (Step 55B(vi)).

(v) Remove excess, unbound primary antibodies by performing three 5-min washes with PBS.

(vi) In a dark room, incubate the cells with secondary antibody in PBS with supplemental 1% (wt/vol) BSA for 1 h at room temperature in these ratios: Goat anti-rabbit Alexa Fluor 568 (CD31 or VE-cadherin), 1:50; Goat anti-mouse Alexa Fluor 647 (α-SMA), 1:100; Alexa Fluor phalloidin 488 (endothelial cell F-actin), 1:100; DAPI, dilactate (nucleus), 1:1,000.

(vii) To remove unbound, excess secondary antibodies, perform three 5-min washes with PBS.

! CRITICAL STEP Procedures with secondary antibodies, DAPI and phalloidin (i.e., any antibody conjugated to a light-sensitive, fluorescent dye) should be performed in the dark. Visible light will degrade the fluorophores that are conjugated to the antibodies and will prevent successful fluorescence imaging. Wrap the culture devices in aluminum foil during incubation and at all times afterward to prevent exposure to light.

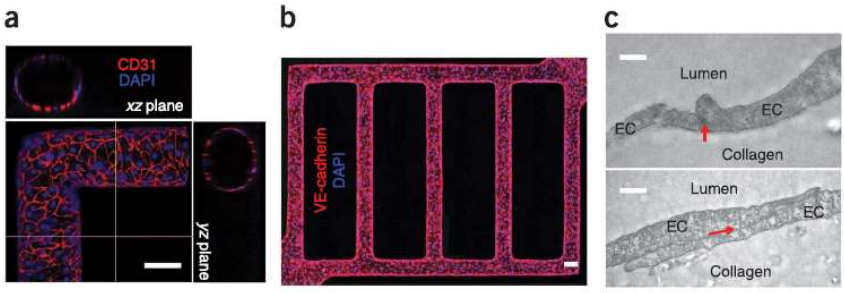

Fig. 4. Characterization of vessel structure by confocal fluorescence microscopy (Step 55B) and transmission electron microscopy (Step 55C). (a,b) Complex geometrical features such as corners, junctions, and bifurcations are readily visualized by confocal fluorescence imaging, and cross-sections of microchannels reveal rounded vessel morphology. Immunohistochemistry of CD31 (a, red) and VE-cadherin (b, red) are used to demonstrate confluent and healthy endothelium throughout the network. Blue, nuclei; scale bars, 100 μm. (c) Transmission electron micrographs enable imaging of cell-cell junctions, including focal contacts (arrow, top) and overlapping junctions (arrow, bottom); scale bars, 1 μm. EC, endothelial cell. Adapted with permission from Zheng *et al.* (2).

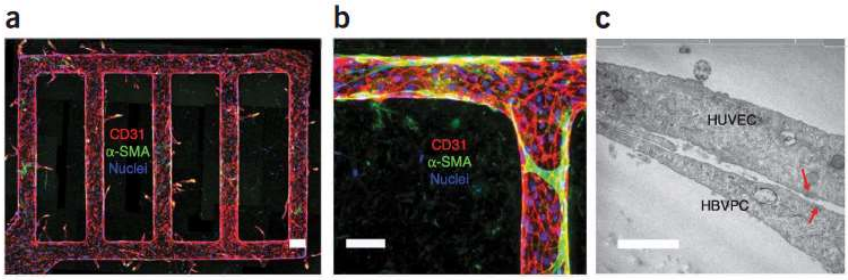

Fig. 5. Heterotypic cell culture. (a) Endothelial cells (HUVECs) respond to stimulation in the presence of cells (human brain vascular pericytes, H BVPCs) seeded in the matrix (Step 23) by sprouting new branches, as visualized by confocal microscopy (Step 55B). (b) Smooth muscle cells seeded in the matrix (Step 23) associate with the endothelium, as visualized by confocal microscopy (Step 55B). (c) Ultrastructure of the cellular interfaces formed between HUVECs and HBVPCs, including a deposited layer of basal lamina, can be visualized by transmission electron microscopy (Step 55C). In a,b: CD31, red; DAPI, blue; α-SMA, green; scale bars, 100 µm. In c, scale bar, 1 µm. Adapted with permission from Zheng *et al.* (2).

! CRITICAL STEP For best results, perform confocal imaging analysis (Step 55B(viii–xii)) as soon as possible after completing procedures with secondary antibodies (Step 55B(v–vii)) (Figs. 4 and 5).

(viii) Confocal imaging and analysis. Select an objective lens with appropriate working distance (>0.4 mm) to allow for imaging of cells around channels through the coverslip and the bottom layer of the matrix. For example, we used an ×25 objective lens with a numerical aperture of 0.8 with a Zeiss confocal microscope LSM 710 to acquire the images presented in Figures 4a,b and 5a,b (use an ×0.6 zoom to increase the field of view if necessary).

(ix) Acquire z-stacks of horizontal images through the scaffold. Use a spacing of 2–3 μm between images in order to provide sufficient vertical resolution for 3D analysis. Collect images with excitation and emission filters appropriate for the fluorescent dyes used in staining.

(x) Evaluate cellular positions and densities in culture using the color channel of the nuclei (for example, blue for DAPI). Threshold images and use cell counting routines available in software such as ImageJ.

(xi) Evaluate the health of the endothelium according to CD31 or VE-cadherin staining. A healthy endothelium will have contiguous staining surrounding each cell membrane.

(xii) Evaluate the degree of alignment of the cells according to the staining of the actin fibers via the phalloidin conjugate. Endothelial cells will align in the direction of flow when subjected to physiologic levels of shear stress. Staining the actin fibers of the cytoskeleton will identify the extent to which cells in perfusion culture have aligned.

(xiii) Perform 3D analysis of the stack of images. For example, to evaluate morphology, reorient the volume to view vertical cross-sections as shown in Figure 4a. The 3D Viewer plugin embedded in ImageJ provides this functionality.

(C) Transmission electron microscopy ● TIMING 3 d

! CRITICAL STEP Perform cell fixation steps (Steps 55C(i–viii)) on the intact culture within the jig by flowing reagents through the channels. Remove the scaffold from the jig (Step 55C(ix)) for embedding, sectioning and staining for TEM imaging.

(i) *Fixing, embedding, sectioning, and staining for TEM*. At the end of the culture, replace the medium in the reservoir with 0.1M cacodylate buffer, $Na(CH_3)_2AsO_2 \cdot 3H_2O$ containing 0.05% (wt/vol) ruthenium red to stain the glycocalyx for 5 min.

! CAUTION Perform procedures with ruthenium red in a chemical hood; wear gloves, goggles and suitable protective clothing.

! CRITICAL STEP To stain the glycocalyx, the cells must be incubated in ruthenium red before fixing the cells with GA in Step 55C(ii).

(ii) Fix the cells and the matrix for 2 h using 2% (wt/vol) GA in 0.1M cacodylate buffer containing 0.05% (wt/vol) ruthenium red.

(iii) Perform three 5-min rinses of the cells with 0.1M cacodylate buffer containing 0.05% (wt/vol) ruthenium red.

(iv) Incubate the cells for 1 h in 0.1 M cacodylate buffer containing 1% (wt/vol) osmium tetroxide (OsO_4) to cross-link lipids and embed a heavy metal in the cell membranes. The buffer should also be supplemented with 0.05% (wt/vol) ruthenium red to stain the glycocalyx.

! CAUTION Osmium tetroxide is extremely toxic, even at low concentrations, and it can cause severe damage to the respiratory tract and corneas. Perform all procedures with osmium tetroxide in a chemical hood; wear gloves, goggles and suitable protective clothing.

(v) Perform three 5-min rinses of the cells with pure 0.1 M cacodylate buffer.

(vi) Dehydrate the cells by incubation in increasing concentrations of ethanol: first 25% (vol/vol) ethanol for 10 min and then 50% (vol/vol) ethanol for 10 min.

(vii) Incubate the cells in 75% (vol/vol) ethanol, with 2% (wt/vol) uranyl acetate ($UO_2(CH_3COO)_2 \cdot 2H_2O$), to stain proteins, for 24 h.

! CAUTION Uranyl acetate is both radioactive and toxic. Perform all procedures with uranyl acetate in a chemical hood; wear gloves, goggles and suitable protective clothing.

(viii) Perform three 5-min rinses of the cells with 75% (vol/vol) ethanol. At this point, the cells are stable and can be stored.

 PAUSE POINT The cells can be stored, refrigerated (4 °C), in 75% (vol/vol) ethanol for several months.

(ix) Carefully remove the collagen scaffold (containing the vessels) from the microfluidic device. Cut the sample into 1-mm^2 squares. Place each square in a glass vial containing 95% (vol/vol) ethanol (~2 ml).

! CRITICAL STEP In disassembling the device, carefully separate collagen from the glass coverslip by using a scalpel.

(x) Replace the 95% (vol/vol) ethanol with 100% ethanol (a stock of 100% ethanol should be stored over a molecular sieve to ensure dryness) and allow the sample to be submerged for 5 min.

(xi) Replace the 100% ethanol with 100% acetone and allow the sample to be submerged for 5 min.

(xii) Repeat the 5-min incubation with fresh 100% acetone and allow the sample to be submerged for 5 min.

(xiii) The samples must be gradually embedded in epoxy. This process can be performed in a simple-but-slow single procedure or done more quickly. For the slow procedure, add epoxy to the acetone/cell sample in a 1:1 ratio and mix it by gently pipetting up and down. Place the samples on a rotisserie and let them sit for 3 d (e.g., over a weekend). Alternately, to proceed more rapidly, incubate the samples in progressively higher ratios of epoxy:acetone as follows: 3 parts acetone:1 part epoxy for 8 h; 1 part acetone:1 part epoxy for 8 h; and finally 1 part acetone:3 parts epoxy for 8 h.

(xiv) Embed the samples in coffin molds and fill them with 100% epoxy and incubate for 24 h.

(xv) Trim the epoxy with a razor blade and then use a high-precision microtome to cut the samples into 60-nm slices.

(xvi) Transfer the 60-nm slices to copper TEM disks with copper grids and store them in a grid box for imaging.

! CRITICAL STEP When you prepare the samples, ensure that all instruments are cleaned with a solvent such as methanol, that the grids have been cleaned with a solvent and the grid box is clean.

(xvii) *TEM imaging procedure.* Follow your institution's procedures for operating the TEM (see Figs. 4c and 5c for sample images).

Troubleshooting

Troubleshooting advice can be found in the following table:

Step	Problem	Possible reason	Solution
21–23	Air bubbles form in the collagen during mixing	Lifting the spatula above the surface level of the collagen	Centrifuge at 1,950*g*, 4 °C for 5 min
26	Inlet and outlet reservoir ports are blocked with collagen, preventing flow through the device	The dowel pins temporarily inserted into the inlet and outlet reservoir ports for collagen injection were not in contact with the PDMS stamp, or they became dislodged during injection	The inlet and outlet reservoir port holes should be machined widely enough to allow the dowel pins to be loose within the reservoir holes and rest stably on top of the PDMS stamp. The pins should not be 'press fit' to the holes because it will potentially create a gap between the device and the stamp. If necessary, gently hold the pins in place during collagen injection
41, 42	The channel is deformed after device assembly	The top and bottom pieces of device are screwed together too tightly	During assembly, stop tightening the screws when resistance is first encountered
47	Air bubbles form in channels during assembly	Mishandling of the joints between the top and bottom pieces	To prevent the formation of air bubbles, ensure that the collagen is completely covered with buffer before assembling the top and bottom pieces together If bubbles are present after assembly, place the device in the refrigerator (4 °C) for ~20 min until bubbles dissolve
53	Nonconfluent monolayer of cells after 24 h	Insufficient seeding density	Allow cells to grow for more 24 h. If the cells are still not confluent, increase seeding density
	Unhealthy endothelium	Evaporation of the medium, pH drift of the medium, or buildup of waste in the medium	Keep the device in a covered, humidified chamber. Ensure the stability of humidity and CO2 in the incubator. Replace the medium regularly

● TIMING

Steps 1–6, fabrication of a master mold of microfluidic channels by photolithography: 3 h

Steps 7 and 8, fabrication of machined parts of the molding and culture jig: 5 h

Steps 9–11, fabrication of the PDMS stamp: 10 h

Steps 12–16, sterilization of materials for device assembly: 30 min

Steps 17–20, coating of devices with sterile PEI and GA to enable adhesion to collagen: 45 min

Steps 21–23, preparation of collagen gel: 10 min

Steps 24–28, injection-molding microstructured collagen: 15 min

Steps 29–31, molding collagen coating onto a glass coverslip: 5 min

Steps 32 and 33, collagen gelation: 30 min

Steps 34–47, device assembly: 15 min

Step 48, device incubation in preparation for seeding channels: 1 h

Steps 49–53, seeding channels with endothelial cells: 40 min

Step 54A, gravity-driven perfusion culture: 5 min

Step 54B, pump-driven perfusion culture: 15 min

Step 55A, live fluorescence microscopy: variable, 1 h or 2–3 d

Step 55B, confocal fluorescence microscopy on fixed and stained samples: 14 h

Steps 55C, transmission electron microscopy: 3 d

Box 1, characterization of permeability of matrix and endothelium: 30 min

Box 2, characterization of blood-endothelial interactions: 1 h

Anticipated results

The fundamental platform comprises an endothelialized network of microchannels embedded within a bioremodelable hydrogel scaffold (Fig. 1a). This protocol allows for diverse

experimental design and analysis for the study of microvascular phenomena with precise control of geometry, coculture seeding, distributions of soluble signals, and mechanical stresses. The assay is amenable to *in situ* fluorescence confocal microscopy, histological analysis, or TEM for high-resolution imaging. Furthermore, media or cell extracts can be used for proteomic or genomic biochemical analysis such as ELISA.

Without stimulation, the culture yields a confluent monolayer of endothelial cells on the walls of the microchannels with appropriate morphology and cell-cell junctions. Via live imaging (Step 55A), the dynamics of the endothelial cells within the endothelium can be tracked in the presence of well-defined luminal flow (Fig. 3). Immunohistochemically stained cultures (Step 55B) show that the endothelium remodels the walls to yield rounded vessels (Fig. 4a), expresses CD31 (Fig. 4a) and VE-cadherin (Fig. 4b) with appropriate localization, and presents low nonspecific permeability (Fig. 6). One advantage of this platform is the opportunity to increase biological complexity incrementally, including the incorporation of additional cell types, the control of hemodynamic fluid forces, or the generation of biochemical gradients (Fig. 1d). In cocultures with perivascular cells seeded in the bulk of the matrix (Step 23), one sees endothelial cell–perivascular cell interactions with the induction of sprouting (Fig. 5a), recruitment of perivascular cells to the abluminal side (Fig. 5b), and deposition of basement membrane (Fig. 5c). Upon exposure to tumor-like proangiogenic signals, robust sprouting angiogenesis occurs and the barrier properties of the endothelium are compromised (2). Notably, perfusion of an unstimulated microvessel with citrate-stabilized whole blood leads to minimal adhesion of platelets and leukocytes to the vessel wall (Fig. 7a). Upon proinflammatory stimulation, the endothelium shows a strong response in the form of secreted von Willebrand factor (vWF), self-assembling of fibers

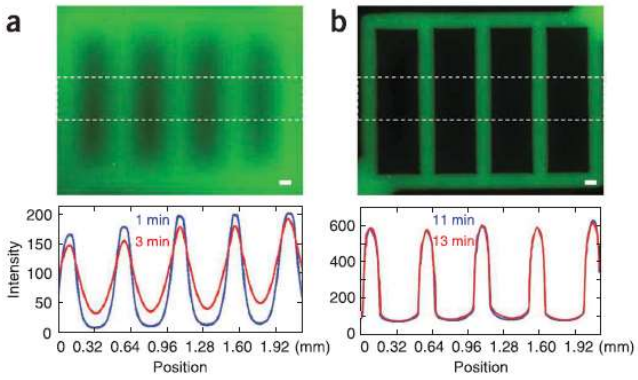

Fig. 6. Characterization of the permeability of matrix and live endothelium (Box 1). (a,b) Fluorescence micrographs show the distribution of 70-kDa FITC-dextran after injection into a network of channels in collagen with no endothelium (a) and with a live endothelium (b). Time evolution of the fluorescence intensity profiles (bottom) can be used to calculate the diffusivity of molecules in the matrix (acellular, a) and the permeability of the vessel membrane (cellular, b). For the complete method, see Zheng *et al.* (2). Figure adapted with permission from Zheng *et al.* (2). Scale bars, 100 μm.

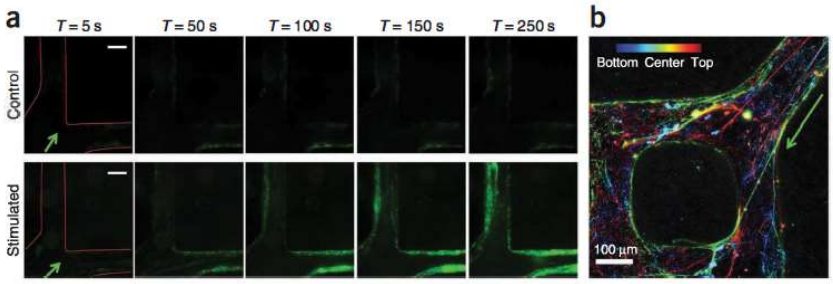

Fig. 7. Interaction with whole blood. (a) Time sequences of whole-blood perfusion through a µVN, either quiescent (control vessels, top images) or stimulated (bottom images), at a flow rate of 10 µl min^{-1} at time points of 5, 50, 100, 150 and 250 s after initiation of perfusion. The platelets are in green, labeled with CD41a to platelet-specific glycoprotein IIb (integrin αIIb); flow direction is indicated with arrows (scale bars, 100 µm). (b) vWF fibers were either coated on the walls of the activated vessel or traveled through the lumens. The locations of vWF fibers in the vessel are color coded: bottom in blue, center in light green and top in red. Adapted with permission from Zheng *et al.* (2). See Box 2.

of vWF, and formation of platelet-vWF–derived thrombi in a manner that depends on the vessel architecture (Fig. 7b).

One advantage of this platform is the assimilation of increasing biological complexity, including incorporation of additional cell types, control of hemodynamic fluid forces, or generation of biochemical gradients. Perivascular cells embedded within the collagen bulk migrated to and associated with the vascular network, and they stabilized vessel permeability under inflammatory assault. The device has been coupled to a sensitive pump apparatus for precise control of fluid dynamic forces, including various flow regimes, resulting in endothelial cell alignment. Finally, the inclusion of source and sink channels within the scaffold enables the steady-state generation of defined gradients to explore heterogeneous signals in the tissue microenvironment (3). Taken together, these efforts establish a novel assay for the study of physiological phenomena in a fully 3D context *in vitro*, which not only has considerable implications for the study of vasculature and vascular tissues in health, disease and therapy, but also has appealing potential for other emerging research areas such as brain (neuroglial) science and engineering.

Supplementary information

Supplementary information is available in the online version of the paper.

References

1. Choi NW, *et al.* (2007) Microfluidic scaffolds for tissue engineering. *Nature Materials* 6(11):908-915.

2. Zheng Y, *et al.* (2012) In vitro microvessels for the study of angiogenesis and thrombosis. *Proceedings of the National Academy of Sciences of the United States of America* 109(24):9342-9347.

3. Verbridge S, *et al.* (2013) Physicochemical regulation of endothelial sprouting in a 3D microfluidic angiogenesis model. *Journal of Biomedical Materials Research Part a* 101(10):2948-2956.

4. Stroock AD & Fischbach C (2010) Microfluidic Culture Models of Tumor Angiogenesis. *Tissue Engineering Part A* 16(7):2143-2146.

5. Verbridge S, *et al.* (2010) Oxygen-Controlled Three-Dimensional Cultures to Analyze Tumor Angiogenesis. *Tissue Engineering Part a* 16(7):2133-2141.

6. Song JW & Munn LL (2011) Fluid forces control endothelial sprouting. *Proceedings of the National Academy of Sciences of the United States of America* 108(37):15342-15347.

7. Song J, Bazou D, & Munn L (2012) Anastomosis of endothelial sprouts forms new vessels in a tissue analogue of angiogenesis. *Integrative Biology* 4(8):857-862.

8. Shin Y, *et al.* (2011) In vitro 3D collective sprouting angiogenesis under orchestrated ANG-1 and VEGF gradients. *Lab on a Chip* 11(13):2175-2181.

9. Shin Y, *et al.* (2012) Microfluidic assay for simultaneous culture of multiple cell types on surfaces or within hydrogels. *Nature Protocols* 7(7):1247-1259.

10. Davis G, Bayless K, & Mavila A (2002) Molecular basis of endothelial cell morphogenesis in three-dimensional extracellular matrices. *Anatomical Record* 268(3):252-275.

11. Yannas IV & Burke JF (1980) DESIGN OF AN ARTIFICIAL SKIN .1. BASIC DESIGN PRINCIPLES. *Journal of Biomedical Materials Research* 14(1):65-81.

12. Langer R & Vacanti JP (1993) TISSUE ENGINEERING. *Science* 260(5110):920-926.

13. Jain RK, Au P, Tam J, Duda DG, & Fukumura D (2005) Engineering vascularized tissue. *Nature Biotechnology* 23(7):821-823.

14. Stroock AD & Cabodi M (2006) Microfluidic biomaterials. *Mrs Bulletin* 31(2):114-119.

15. Mikos AG, *et al.* (1993) PREVASCULARIZATION OF POROUS BIODEGRADABLE POLYMERS. *Biotechnology and Bioengineering* 42(6):716-723.

16. Levenberg S, *et al.* (2005) Engineering vascularized skeletal muscle tissue. *Nature Biotechnology* 23(7):879-884.

17. Du Y, *et al.* (2011) Sequential Assembly of Cell-Laden Hydrogel Constructs to Engineer Vascular-Like Microchannels. *Biotechnology and Bioengineering* 108(7):1693-1703.

18. Neumann T, Nicholson BS, & Sanders JE (2003) Tissue engineering of perfused microvessels. *Microvascular Research* 66(1):59-67.

19. Cabodi M, *et al.* (2005) A microfluidic biomaterial. *Journal of the American Chemical Society* 127(40):13788-13789.

20. Chrobak KM, Potter DR, & Tien J (2006) Formation of perfused, functional microvascular tubes in vitro. *Microvascular Research* 71(3):185-196.

21. Miller JS, *et al.* (2012) Rapid casting of patterned vascular networks for perfusable engineered three-dimensional tissues. *Nature Materials* 11(9):768-774.

22. Whitesides GM, Ostuni E, Takayama S, Jiang XY, & Ingber DE (2001) Soft lithography in biology and biochemistry. *Annual Review of Biomedical Engineering* 3:335-373.

23. Qin D, Xia Y, & Whitesides GM (2010) Soft lithography for micro- and nanoscale patterning. *Nature Protocols* 5(3):491-502.

24. Tang MD, Golden AP, & Tien J (2003) Molding of three-dimensional microstructures of gels. *Journal of the American Chemical Society* 125(43):12988-12989.

25. Nelson CM, VanDuijn MM, Inman JL, Fletcher DA, & Bissell MJ (2006) Tissue geometry determines sites of mammary branching morphogenesis in organotypic cultures. *Science* 314(5797):298-300.

26. Bellan LM, *et al.* (2009) Fabrication of an artificial 3-dimensional vascular network using sacrificial sugar structures. *Soft Matter* 5(7):1354-1357.

27. McGuigan AP & Sefton MV (2006) Vascularized organoid engineered by modular assembly enables blood perfusion. *Proceedings of the National Academy of Sciences of the United States of America* 103(31):11461-11466.

28. Gauvin R, Guillemette M, Dokmeci M, & Khademhosseini A (2011) Application of microtechnologies for the vascularization of engineered tissues. *Vascular Cell* 3.

29. Borenstein JT, *et al.* (2002) Microfabrication technology for vascularized tissue engineering. *Biomedical Microdevices* 4(3):167-175.

30. Fidkowski C, *et al.* (2005) Endothelialized microvasculature based on a biodegradable elastomer. *Tissue Engineering* 11(1-2):302-309.

31. Bettinger CJ, *et al.* (2007) Silk fibroin microfluidic devices. *Advanced Materials* 19(19):2847-+.

32. Ling Y, *et al.* (2007) A cell-laden microfluidic hydrogel. *Lab on a Chip* 7(6):756-762.

33. Nelson CM & Tien J (2006) Microstructured extracellular matrices in tissue engineering and development. *Current Opinion in Biotechnology* 17(5):518-523.

34. Golden AP & Tien J (2007) Fabrication of microfluidic hydrogels using molded gelatin as a sacrificial element. *Lab on a Chip* 7(6):720-725.

35. Iruela-Arispe ML & Davis GE (2009) Cellular and Molecular Mechanisms of Vascular Lumen Formation. *Developmental Cell* 16(2):222-231.

36. Asahara T, Kawamoto A, & Masuda H (2011) Concise Review: Circulating Endothelial Progenitor Cells for Vascular Medicine. *Stem Cells* 29(11):1650-1655.

37. Feener EP & King GL (1997) Vascular dysfunction in diabetes mellitus. *Lancet* 350:SI9-SI13.

38. Muschler GE, Nakamoto C, & Griffith LG (2004) Engineering principles of clinical cell-based tissue engineering. *Journal of Bone and Joint Surgery-American Volume* 86A(7):1541-1558.

39. Sung JH, Kam C, & Shuler ML (2010) A microfluidic device for a pharmacokinetic-pharmacodynamic (PK-PD) model on a chip. *Lab on a Chip* 10(4):446-455.

40. Wong KHK, Chan JM, Kamm RD, & Tien J (2012) Microfluidic Models of Vascular Functions. *Annual Review of Biomedical Engineering, Vol 14,* Annual Review of Biomedical Engineering, ed Yarmush ML), Vol 14, pp 205-230.

41. Cross VL, *et al.* (2010) Dense type I collagen matrices that support cellular remodeling and microfabrication for studies of tumor angiogenesis and vasculogenesis in vitro. *Biomaterials* 31(33):8596-8607.

42. King KR, Wang CCJ, Kaazempur-Mofrad MR, Vacanti JP, & Borenstein JT (2004) Biodegradable microfluidics. *Advanced Materials* 16(22):2007-+.

43. Vickerman V, Blundo J, Chung S, & Kamm R (2008) Design, fabrication and implementation of a novel multi-parameter control microfluidic platform for three-dimensional cell culture and real-time imaging. *Lab on a Chip* 8(9):1468-1477.

44. Bornstein MB (1958) RECONSTITUTED RAT-TAIL COLLAGEN USED AS SUBSTRATE FOR TISSUE CULTURES ON COVERSLIPS IN MAXIMOW SLIDES AND ROLLER TUBES. *Laboratory Investigation* 7(2):134-137.

45. Rajan N, Habermehl J, Cote M-F, Doillon CJ, & Mantovani D (2006) Preparation of ready-to-use, storable and reconstituted type I collagen from rat tail tendon for tissue engineering applications. *Nature Protocols* 1(6):2753-2758.

46. Haessler U, Pisano M, Wu M, & Swartz MA (2011) Dendritic cell chemotaxis in 3D under defined chemokine gradients reveals differential response to ligands CCL21 and CCL19. *Proceedings of the National Academy of Sciences of the United States of America* 108(14):5614-5619.

47. Franco C & Gerhardt H (2012) TISSUE ENGINEERING: Blood vessels on a chip. *Nature* 488(7412):465-466.

CHAPTER 5

A PHYSICAL SCIENCES – ONCOLOGY PERSPECTIVE ON CANCER METABOLISM

Peter DelNero, Benjamin Hopkins, Lewis Cantley, and Claudia Fischbach (*In review).* A physical sciences-oncology perspective on cancer metabolism. *Sci Transl Med.*

Abstract

Advances in the culturing of patient-derived cells has enabled analyzing drug sensitivity of individual patient samples. However, our ability to translate these findings to the clinic is constrained by the failure of culture models to accurately recapitulate the diversity of metabolic states within tumors. Here we outline the myriad environmental factors that regulate cell metabolism in native tumors and describe how advances in engineered culture models could enhance the predictive power of precision medicine pipelines.

Introduction

Aberrant cell metabolism is a hallmark of cancer that influences cancer risk and prognosis and that is increasingly being pursued as a target for therapy (1–3). The biochemical repertoire present in cells, tissues, and body fluids arises from complex interactions between genetic alterations, tissue perturbations, energy balance, treatment history, and environmental exposures (Figure 1) (4). However, the interdependent mechanisms linking cell metabolism and cancer pathogenesis are not completely understood, and therapeutic agents that interfere with metabolic processes have yielded inconsistent and underwhelming clinical results.

Interdisciplinary collaborations are critical for turning cancer metabolism into an actionable target for intervention. The mutual exchange of knowledge and expertise across disciplines affords a more complete and sophisticated understanding of cell metabolism for cancer prevention, detection, and management. In this spirit, the National Cancer Institute initiated the Physical Sciences Oncology Network

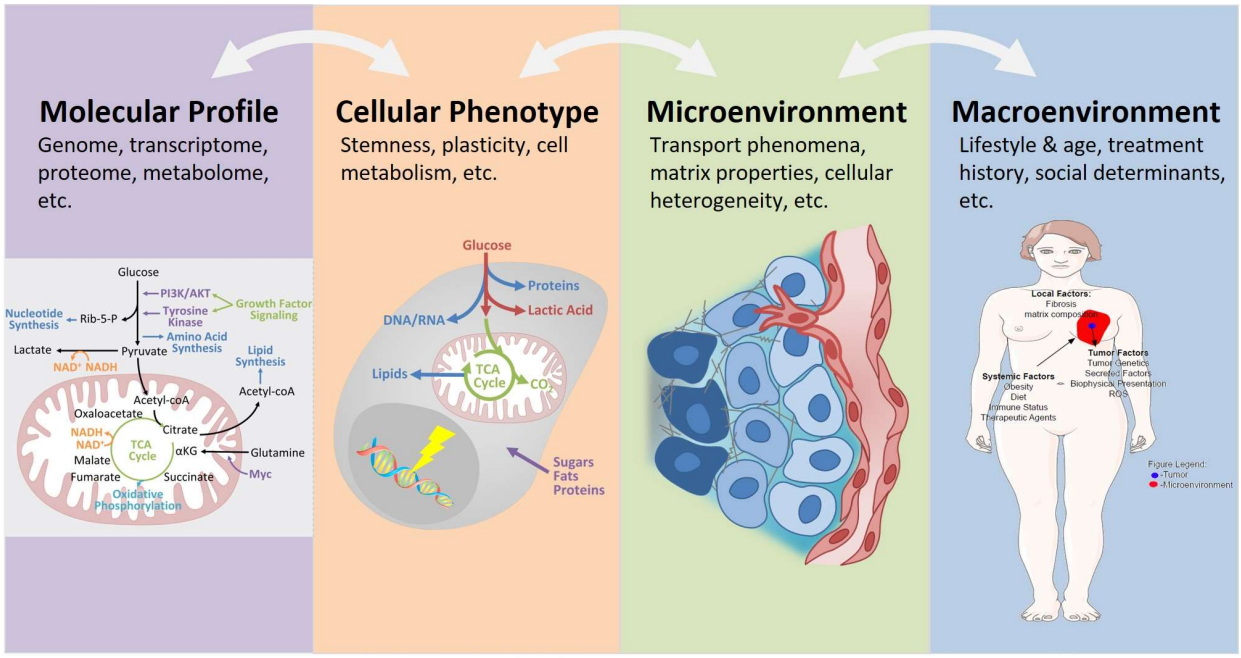

Fig. 1. Determinants of cancer metabolism. Metabolism is a multiscale process, comprising the full range of biological factors. In order to understand the interdependent regulatory mechanisms, it is essential that model systems simulate salient features that govern metabolic networks across multiple scales.

(PS-ON) to promote dialogue between oncologists, engineers, and cancer biologists. As a new component of the PS-ON, the Cornell Center for the Physics of Cancer Metabolism aims to foster unconventional partnerships across disciplines to generate clinically-translatable insights on tumor metabolism and advance the understanding and treatment of cancer. This article presents a physical sciences-oncology perspective on the theme of cancer metabolism, with special emphasis on the physical tumor microenvironment and precision medicine.

Metabolic Transport: Convection-Diffusion-Reaction Kinetics

Metabolic processes govern the conversion of biomass, molecular energy, and redox equivalents required for virtually all biological functions (5, 6). Although one of the earliest recognized molecular signatures of cancer, tumor metabolism is not a unique, monolithic alteration. Instead, it is an adaptive biochemical network, which is responsive to both internal signaling and extracellular conditions and synchronizes the flux of metabolites through numerous interdependent pathways. Sustained efforts have yielded considerable progress in mapping the sequence of these biochemical events, but major gaps remain in our understanding of how these pathways are regulated.

The Warburg effect (aerobic glycolysis) is the dominant metabolic phenotype for proliferating cells. Compared to normal counterparts, Warburg-like cells exhibit elevated nutrient uptake and glycolysis. Many intermediate products are diverted from the tricarboxylic acid (TCA) cycle toward biosynthetic pathways, presumably to generate building blocks for cell division (7). This reprogramming supports tumor growth, allows cells to survive adverse conditions (stresses), and promotes invasive behaviors. Warburg-like changes are associated with driver mutations that activate oncogenic signaling pathways such as Ras/MAPK (mitogen-activated protein kinase) and PI3K (phosphoinositide 3-kinase)/Akt. However, these metabolic processes are also the cause and consequence of a perturbed microenvironment, which plays a significant role in producing the diversity of metabolic phenotypes that can be found in different regions of a tumor (8–10).

Metabolic processes are controlled in part by soluble factors in the tumor microenvironment, including transport-limited availability of oxygen, accumulation of lactic acid, and irregular concentrations of metabolic substrates. The distribution of these factors is primarily defined by the microcirculatory system (11). Dysfunctional tumor vasculature causes deregulated transport phenomena, in part by altering hydrostatic forces and therefore the spatial and temporal presentation of respiratory gases, metabolites, and soluble factors. Abnormal tissue perfusion and reaction kinetics result in heterogeneous biochemical gradients throughout the tumor. Hypoxia and lactic acidosis are principle consequences of aberrant microvascular transport (12).

A small number of highly conserved regulatory systems control metabolic wiring to support tumor cell survival, growth, and proliferation in response to adverse microenvironmental conditions, including those mediated by hypoxia inducible factor (HIF) (13), mammalian target of rapamycin complex (mTORC) (14, 15), and AMP-activated protein kinase (AMPK) (16, 17). These metabolic sensors are interconnected with oncogene signaling (e.g. MYC, PI3K, MAPK, PTEN, p53, OCT1) and hormone balance (e.g. insulin) to monitor cellular energy and nutrient status (6).

The combination of microenvironmental and signaling changes favors cancer cells that exhibit metabolic plasticity. Metabolic flexibility allows tumor cells to regulate glycolytic and oxidative flux in order to overcome adverse tissue conditions, including hypoxia, acidosis, and limited nutrient availability at the interior of a tumor. For example, during lactic acidosis, cancer cells exhibit non-glycolytic metabolism, characterized by reduced glucose uptake and negligible lactate production (18). This non-glycolytic phenotype provides a protective effect when cells are subsequently exposed to hypoglycemic conditions (18). Importantly, metabolic plasticity appears to be independent of genetic profile, as environmental changes can induce isogenic populations of cancer cells to switch from glycolytic to oxidative phenotypes (19).

Complementary modes of metabolism, which enable cells to adapt to fluctuating tissue conditions, also lead to the emergence of distinct subpopulations. Adjacent tumor niches interact through asymmetric "supply and demand" for intermediate metabolites, bioactive byproducts, and oxygen (20). For example, some oxygenated cancer cells express monocarboxylate transporter 1 (MCT1), which allows them to consume the energy-rich metabolites produced by Warburg-like cells (21, 22). This mechanism of nutrient exchange, known as "metabolic symbiosis," uses lactate from hypoxic cells to fuel oxidative metabolism in aerobic tumor compartments (23). Cancer cells can even manipulate the metabolic properties of stromal fibroblasts to shift toward aerobic glycolysis, thus promoting metabolic efficiency and proliferative capacity.

Spatial and temporal variations are a key feature of the metabolic landscape; tumor cells mutually shape and respond to their soluble environment. The full continuum of biochemical niches distributed throughout the tumor produces a mosaic of metabolic phenotypes that ultimately affect a patient's response to treatment.

Biophysical Forces: The Mechanics of Tumor Metabolism

In addition to the soluble microenvironment, metabolic pathways are also sensitive to variations in tumor mechanical properties (24). Increased tumor stiffness can be attributed to a variety of parameters (25, 26). In particular, increased cell density and deposition and contraction of fibrillar extracellular matrix (ECM) proteins due to the formation of an activated tumor stroma play important roles. Furthermore, increased levels of glycosylated matrix components control tissue hydration and interstitial osmotic pressure (27). Water absorption, in turn, causes swelling, which further contributes to the palpable stiffness of solid tumors (28).

The resulting changes in tissue architecture, as well as matrix structure and mechanics, can significantly impact cell behavior and regulate tumor metabolism (29). Through mechanotransduction, cells convert extracellular mechanical cues into biochemical outputs. Indeed, ECM structural elements that were

once considered to be static architectural features are now known to regulate an intricate network of force-sensitive signaling functions, which have a critical role in the development of disease (30).

Mechanotransduction from the ECM is primarily mediated by integrin receptors, which are transmembrane heterodimers that physically link the ECM and the actin cytoskeleton (31). Integrin-mediated mechanosignaling can be induced by external forces applied by the ECM or via cell-mediated contraction caused by phosphorylation of myosin light chain (MLC) by Rho kinase (ROCK) (32). Under mechanical tension, actin filaments bundle into stress fibers and integrins cluster to form focal adhesions, which both play active roles in regulating multiple aspects of cell metabolism (30).

Integrin-mediated focal adhesions are important elements of mechanical signal transduction, and multiple signaling pathways converge at this interface that regulate metabolic processes. Focal adhesions are canonically associated with activation of focal adhesion kinase (FAK) and c-Src tyrosine kinase (CTK), which activate Ras and the MAPK pathway (33). In addition, the PI3K-AKT-mTOR pathway is a core element of focal adhesion signaling by operating as a transducer for growth factor receptors and Ras. Through receptor clustering, focal adhesions directly enhance growth factor-dependent PI3K signaling and a host of downstream functions (34–36). By exerting mechanical control over tyrosine kinase effector networks, focal adhesions directly contribute to malignant invasion, as demonstrated by the loss of tissue organization and concomitant changes in metabolic activity on stiffer substrates (37). Inhibiting the focal adhesion apparatus, or restoring appropriate matrix mechanics, results in cell quiescence and tissue homeostasis (38–40). Physical properties of the tumor microenvironment use focal adhesions to regulate diverse signaling networks responsible for malignant behavior and subsequent changes in metabolic status.

While it is well-established that cytoskeletal remodeling is a key component of mechanosignaling, it was recently found that it also regulates a key step in glycolysis. Actin polymerization involves the rapid assembly and disassembly of fiber bundles that provide the structural framework of the cell. When actin fibers disassemble, they release the metabolic enzyme aldolase, which catalyzes the conversion of 6-carbon

fructose molecules to the 3-carbon molecules glyceraldehyde and dihydroxyacetone (41). The release of aldolase from the cytoskeleton accelerates glycolysis, as demonstrated by a sustained decrease in NADH:NAD+ ratio (41). This mechanism sensitizes glucose catabolism to external mechanical forces, thus establishing a direct link between matrix mechanical properties and cell metabolism.

Vice versa, metabolic changes also affect the way cells interpret their mechanical environment. For example, glutamine metabolism appears to play a key role in mechanosignaling (42). A recent study reported that glutamine regulation partly controls the activity of RhoA, an oncogenic GTPase involved in focal adhesions and actin stress fiber assembly (43, 44). Hyperactive RhoA signaling typically causes oncogenic transformation, but this effect could be reversed using a small molecule inhibitor of glutaminase (GLS1), the amidohydrolase enzyme that converts glutamine to glutamate for entry into the TCA cycle (43). A new study corroborated this observation by showing that stiffness-induced changes in glutamine flux were mediated in part by transcriptional regulation of GLS1 (45), suggesting reciprocal feedback between mechanosignaling and glutamine metabolism.

Although metabolic activity is most often attributed to differences in cell and molecular biology, matrix mechanics also regulates metabolic functions. It is increasingly clear that denser, thicker, and mechanically rigid ECM promotes cancer growth and metastasis (46). Therefore, strategies to target cancer cell metabolism must carefully consider the physical context. By exploring the role of biophysical factors in tumor metabolism and incorporating these factors into our models of patient disease, we expect to improve the predictiveness of our assays and thereby enhance our ability to identify effective therapeutic strategies.

Experimental Platforms: Engineering Model Systems

Culture-based model systems are central to the investigation of spatial, temporal, and physical elements of cancer metabolism. Although *in vitro* models can never capture a complete representation of the tumor microenvironment, they can be useful for examining the effect of its most salient features on

cellular metabolism, including physical properties of the matrix and the impact of fluid transport. One of the greatest challenges in studying metabolism is navigating between levels of space, time, and complexity, from molecular details to whole-body physiology. This is one area in which new tissue-engineered model systems are proving especially useful.

Conventional *in vitro* assays are largely based on monotypic populations of cells cultured on plastic or glass substrates. Monolayer cultures of homogeneous cells, or mouse xenografts derived from commercial cell lines, diverge from the original tumor, most notably through the dramatic loss of heterogeneity and tissue structure (47). Even transient exposure to planar culture conditions causes irreversible changes in cell behavior (48, 49). A microarray analysis of cancer cells in 2D versus 3D culture revealed broad changes in hypoxia response and pro-inflammatory pathways (50). These observations reflect a growing consensus that the culture environment is a critical determinant of cell behavior, and that 2D monolayer culture drives abnormal function whereas exposure to a 3D environment mimics a more physiologic state (51, 52).

In the past twenty years, many labs have adopted 3D culture techniques to mimic microenvironmental aspects of native tissues. Merely embedding cells within 3D substrates can restore a mélange of important functions, including 3D morphogenesis, secretory functions, and tissue homeostasis (40, 53–55). However, "3D culture" has become an umbrella term that obscures a more nuanced reality. There are many differences between 2D, 3D, and physiological settings; dimensionality is complicated by the numerous parameters that define each model system. For example, "matrix mechanics" encompasses fiber architecture and conformation, matrix composition and porosity, covalent and ionic crosslinking, and cell density, polarity, and contractility (56–60). Similarly, "mass transport" is not merely a question of vascular proximity, but also involves osmotic and hydrostatic pressure gradients, fluid viscosity and shear stress, cell density and metabolic activity, concentrations of ions and dissolved gases, and matrix binding kinetics. Functional consequences emerge from the integrative effects of these manifold variables, rather than from a perfunctory switch from 2D to 3D (61, 62). 3D assays provide demonstrable evidence that

context is important, but we must carefully consider how various features of the experimental system provide instructive cues that alter cell behavior, especially with regard to metabolic programming.

Emerging tissue-engineering technologies now provide attractive tools to control the physical microenvironment for studies of cancer cell metabolism. Hydrogel-based biomaterials are frequently the basis for 3D culture, and a catalog of natural and synthetic materials are available that support cell adhesion, viability, and remodeling; nutrient and waste exchange; and appropriate mechanical properties. Natural ECM components include type I collagen, fibrin, reconstituted basement membrane (EHS or Matrigel), and decellularized matrices deposited by fibroblasts (63, 64). Natural materials possess inherent biological functions, such as adhesive ligands and cleavage sites, but it can be difficult to precisely define and manipulate the composition and/or structural properties. On the other hand, synthetic gels afford greater control over materials properties, and can be readily manipulated with biological moieties such as matrix metalloproteinase (MMP)-cleavable domains, integrin binding sites, or specified fiber properties and crosslinking, but lack the biological complexity of native tumor-associated ECM (65–73). As modifications to the physical culture environment have a profound impact on tumor cell metabolism, accurate modeling of the ECM and spatiotemporal variations thereof is critical for proper characterization of metabolic behavior.

Both natural and synthetic materials are readily integrated with microfluidic technologies to recapitulate matrix mechanics and fluid transport processes that affect tumor metabolism. For example, microfluidic biomaterials can be generated using a confined gel, whereby microchannels are patterned within a transparent silicone mold (74, 75). Alternatively, dense hydrogels allow imprinting of microfluidic conduits directly within the scaffold to control the spatial and temporal gradients of exogeneous factors or drugs, reminiscent of microvascular function (76–79). Both strategies have been used to construct biomimetic vascularized tissue constructs to recapitulate the individual and combinatorial effects of matrix structure, solute transport, and cellular composition that define the metabolic environment.

Microfluidic biomaterials can also be integrated with live cell imaging techniques to acquire spatial and temporal information about the complex interdependencies between the microenvironment and cell metabolism. These tools can be used to readily manipulate and measure real-time, single-cell dynamics by using endogenous or genetically-encoded fluorescent sensors. For example, a vascularized microtumor (VMT) model was used to map metabolic activity within different regions of hybrid microfluidic-organoid via fluorescence lifetime imaging of NAD^+ and NADH (80). The VMT platform mimicked stromal composition, matrix structure, and vascular function, and it simulated metabolic response to pharmacologic agents (80).

Advances in biomaterials and microfabrication technologies (like the VMT model described above) afford new methods to integrate vascular, stromal, and epithelial compartments with precise arrangements of parenchymal and interstitial elements (81–83). In addition, emerging tissue culture techniques have produced a new generation of microphysiological devices ("tissue chips") that capture increasingly accurate representations of whole organs, including liver, kidney, heart, lungs, brain, GI system, blood vessels, skin, adipose, cervix, uterus, and ovaries (81, 84, 85). These culture analogs mimic the structure and function of human physiology, with particular attention toward the cellular microenvironment and tissue heterogeneity (86). Originally designed for pre-clinical drug screening, organ-on-a-chip models have been used to simulate first-pass metabolism, activation of anti-cancer prodrugs, synergistic actions of drug combinations, modulation of tissue bioavailability, membrane barrier function, off-target toxicity, and mechanisms of drug adsorptions, distribution, metabolism, excretion (ADME) (87). Tumor metabolism is a multiscale phenomenon, and these platforms make it possible to simulate higher-order metabolic regulation *in vitro.*

The next milestone for microphysiological platforms involves the serial integration of multiple organs within a single device (87). A complete "body-on-a-chip" would simulate interactions between organs, such as drug adsorption through GI-tract, metabolism in the liver, clearance in the kidneys, and cytotoxic effects in the heart or other tissues (87). Already, pioneering systems have been strategically validated as physical analogs for pharmacokinetic/pharmacodynamic modeling (88). By carefully

controlling tissue volume and fluid residence time, integrated microphysiological systems can mimic drug distribution, uptake, and activity in surrogate organs (89). One such platform predicted nontarget drug retention in adipose tissue and nephrotoxicity. Similarly, a commercial model, called Hurel, was instrumental for identifying drug metabolites that were not present in traditional, monotypic cell culture (90).

Collectively, microphysiological devices present a promising opportunity to navigate across cell, tissue, and organ systems when investigating cancer metabolism and drug response. Importantly, micro-tissue devices are not delicate, "artisan" products, but increasingly robust platforms for broad application in the laboratory and the clinic. Several platforms are commercially available with high simplicity, reliability, and throughput. Multiwell plate and microscope slide formats make these technologies immediately suitable for implementation in non-engineering labs.

Clinical Translation: Metabolism in Precision Oncology

The manifold variables that influence metabolism and drug response make it challenging to infer susceptibility to targeted pharmaceutical agents. Factors related to metabolism and energetics (diet, physical activity, weight control, and vascular health) interact with genetic, physiological, and environmental variables to influence cancer risk, prognosis, and treatment outcomes in ways that are often impossible to predict. Every patient manifests a unique and ever-changing gene expression, metabolic profile, and tissue microenvironment.

The precision medicine paradigm has been championed as a strategy to account for the dynamic, patient-specific variations in tumor behavior. Originally, precision oncology used molecular information to prioritize therapies for patients that expressed specific biomarkers. Now, comprehensive approaches integrate pathology, -omics analyses, and functional diagnostics (e.g. rapid drug screening and animal modeling) to pre-determine the safety and efficacy of personalized treatments for individual patients (Figure 2) (91–93). Information about the genetic aberrations, the gene expression profiles, and the patient-specific

drug responses helps guide new off-label use of FDA-approved therapies, which could not have been predicted from sequencing alone. By integrating data from multiple independent methodologies, these approaches can cross validate personalized therapies for cancer patients. These approaches have special significance for patients with advanced disease or multi-drug resistant cancers, where standard therapies have failed.

In order to formulate and test patient-specific combination therapies, clinicians require model systems that accurately recapitulate the salient characteristics of the native tumor. Microenvironmental and systemic metabolic feedback mechanism (such as increases in insulin secretion upon treatment with PI3K inhibitors) have the capacity to significantly alter tumor responses to therapy but are frequently not accounted for in culture platforms being utilized in the precision medicine setting (94). Such shortcomings may account for divergence between *in vitro* and *in vivo* responses observed in the precision medicine context (95). Therefore, model systems must be attentive toward the constellation of interdependent variables that influence drug sensitivity, including the genetic composition, proximal microenvironment, and systemic factors. This is especially true for drugs that target metabolic processes, in which the microenvironmental context plays an essential role in regulating aberrant behavior. As the tumor microenvironment is a major factor in determining drug efficacy, the use of models that recapitulate patient-specific tissue properties may be critical for the success of precision medicine approaches.

Patient-derived xenograft (PDX) models seem to be the most suitable platform to preserve the clonal architecture of the original patient sample, as well as its gene expression, histology, and epigenetic profile (96, 97). Indeed, PDXs, for which pieces of a patient's primary tumor are propagated in immunodeficient mice, enable highly representative, co-clinical testing of drug combinations (98). However, this approach is extremely time consuming and expensive, and lacks the capacity for high-throughput screening or precise experimental manipulation. Furthermore, PDXs select for specific cell types over time, lack a functional immune system, and significant differences between humans and animals can lead to discrepancies with regard to drug metabolism and signaling mechanisms (99). These challenges

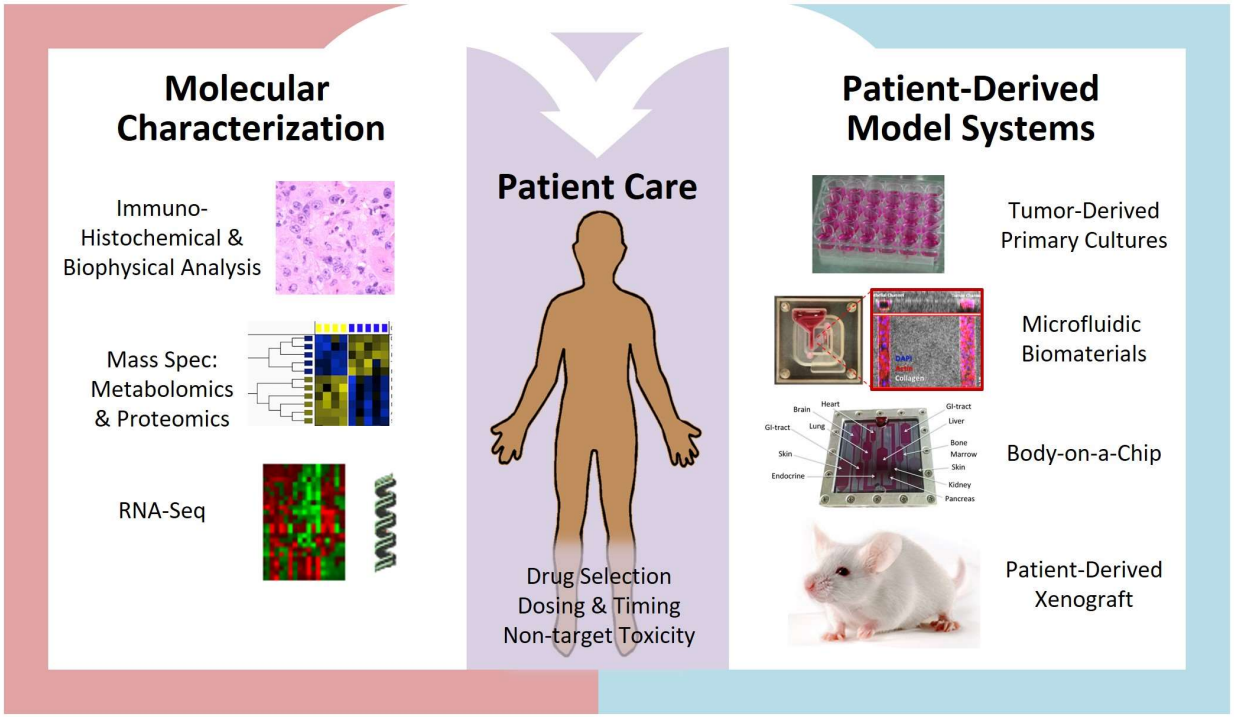

Fig. 2. A comprehensive precision medicine toolkit. A comprehensive approach to precision oncology integrates pathology and sequencing analyses (left) with functional diagnostic platforms (right). More complete information about individual patient susceptibility will help guide personalized treatment strategies (center).

might be overcome by complementing PDX models with physiologically relevant *in vitro* assays that can be utilized to quickly and accurately perform high-throughput screening with potential therapeutic agents and provide mechanistic information to guide treatment (100, 101).

Biomaterial-based, microfluidic tumor models that contain patient-derived cells should become an important component in a comprehensive approach to precision medicine. Patient-derived microphysiological systems combine the biological complexity of primary tissue samples with the simplicity of *in vitro* analysis (102). The fast timing, low cost, and small tissue volume permits testing large numbers of drug permutations and dose regimens, thereby ranking optimal combinations to be tested *in vivo* (98). These platforms avoid some of the limitations of traditional tissue culture systems, and they complement more intensive methods like PDXs.

Engineered, clinically-derived culture models might help improve the use of anti-metabolic agents in precision oncology (92). Efforts to study cancer metabolism *in vitro* rarely consider the ubiquitous effects of vascular transport phenomena and matrix mechanical properties. This poses a challenge for determining the impact of pharmacological agents that target metabolic processes, as vascular transport not only affects local concentrations of biochemical factors, but also the bioavailability of drugs. Additionally, matrix mechanical properties not only affect metabolic signaling pathways as outlined above, but also directly contribute to therapy resistance by acting as a physical barrier to the delivery of therapeutic agents. Indeed, the tumor microenvironment and limited bioavailability of drugs is viewed as a major determinant of resistance to therapy, but is often overlooked in molecular analyses of clinical specimens and in chemo-sensitivity testing. Functional screening platforms that incorporate a full range of biophysical cues might help predict whether a specific patient is likely to benefit from treatments with drugs that target the unique vulnerabilities afforded by tumor metabolism.

Incorporating patient samples into sophisticated microphysiological systems may provide insight into underlying determinants of disease progression and drug response. For example, spatial information

about the activity of cells in different regions of a controlled microenvironment might simulate heterogeneous response to targeted therapies. When combined with quasi-physiological culture models, patient-derived samples can be used to determine how tissue-scale heterogeneity impacts tumor progression and response to pharmacological agents. As microphysiological culture platforms move toward clinical settings, they offer a promising strategy for guiding patient-specific drug selection and treatment modalities.

Conclusions

Physical scientists and engineers can contribute new tools and insights on the mechanisms by which cells, tissues, and organ systems regulate metabolic processes. Such outcomes require the expertise of biologists and clinical oncologists, who are most directly familiar with the physiology of patient tissues. The cross-disciplinary exchange of knowledge ensures the advancement of technologies and treatments to preserve or restore human health. This dialogue is especially critical for developing patient-derived model systems that faithfully recapitulate matrix mechanics and transport properties to evaluate anti-metabolic therapies in precision medicine settings.

References

1. Vander Heiden MG (2011) Targeting cancer metabolism: a therapeutic window opens. *Nat Rev Drug Discov* 10(9):671–684.

2. Tennant D a, Durán R V, Gottlieb E (2010) Targeting metabolic transformation for cancer therapy. *Nat Rev Cancer* 10(4):267–277.

3. Kroemer G, Pouyssegur J (2008) Tumor Cell Metabolism: Cancer's Achilles' Heel. *Cancer Cell* 13(6):472–482.

4. Beger RD, et al. (2016) Metabolomics enables precision medicine: "A White Paper, Community Perspective." *Metabolomics* 12(10). doi:10.1007/s11306-016-1094-6.

5. Pavlova NN, Thompson CB (2016) The Emerging Hallmarks of Cancer Metabolism. *Cell Metab* 23(1):27–47.

6. Cairns RA, Harris IS, Mak TW (2011) Regulation of cancer cell metabolism. *Nat Rev Cancer* 11(2):85–95.

7. Vander Heiden MG, Cantley LC, Thompson CB (2009) Understanding the Warburg Effect: The Metabolic Requirements of Cell Proliferation. *Science (80-)* 324(5930):1029–1033.

8. Anastasiou D (2016) Tumour microenvironment factors shaping the cancer metabolism landscape. *Br J Cancer* 116:277–286.

9. Vaupel P, Kallinowski F, Okunieff P (1989) Blood flow, oxygen and nutrient supply, and metabolic microenvironment of human tumors: a review. *Cancer Res* 49:6449–6465.

10. Hsu PP, Sabatini DM (2008) Cancer cell metabolism: Warburg and beyond. *Cell* 134(5):703–707.

11. Munn LL (2003) Aberrant vascular architecture in tumors and its importance in drug-based therapies. *Drug Discov Today* 8(9):396–403.

12. Hirschhaeuser F, Sattler UGA, Mueller-Klieser W Lactate: A Metabolic Key Player in Cancer. doi:10.1158/0008-5472.CAN-11-1457.

13. Nakazawa MS, Keith B, Simon MC (2016) Oxygen availability and metabolic adaptations. *Nat Rev Cancer* 16(10):663–73.

14. Saxton RA, Sabatini DM (2017) mTOR Signaling in Growth, Metabolism, and Disease. *Cell* 168(6):960–976.

15. Laplante M, Sabatini DM (2012) MTOR signaling in growth control and disease. *Cell* 149(2):274–293.

16. Hardie DG (2014) AMPK—Sensing Energy while Talking to Other Signaling Pathways. *Cell Metab* 20(6):939–952.

17. Hardie DG, Ross FA, Hawley SA (2012) AMPK: a nutrient and energy sensor that maintains energy homeostasis. *Nat Rev Mol Cell Biol* 13(4):251–262.

18. Xie J, et al. (2014) Beyond Warburg effect--dual metabolic nature of cancer cells. *Sci Rep* 4:4927.

19. Saga I, et al. (2014) Integrated analysis identifies different metabolic signatures for tumor-initiating cells in a murine glioblastoma model. *Neuro Oncol* 16(8):1048–1056.

20. Nakajima EC, Van Houten B (2013) Metabolic symbiosis in cancer: Refocusing the Warburg lens. *Mol Carcinog* 52(5):329–337.

21. Feron O (2009) Pyruvate into lactate and back: From the Warburg effect to symbiotic energy fuel exchange in cancer cells. *Radiother Oncol* 92(3):329–333.

22. Sonveaux P, et al. (2008) Targeting lactate-fueled respiration selectively kills hypoxic tumor cells in mice. *J Clin Invest* 118(12):3930–3942.

23. Pisarsky L, et al. (2016) Targeting Metabolic Symbiosis to Overcome Resistance to Anti-angiogenic Therapy. *Cell Rep* 15(6):1161–1174.

24. Tung JC, et al. (2015) Tumor mechanics and metabolic dysfunction. *Free Radic Biol Med* 79:269–280.

25. Pickup MW, Mouw JK, Weaver VM (2014) The extracellular matrix modulates the hallmarks of cancer. *EMBO Rep* 15(12):1243–1253.

26. Nia HT, et al. (2016) Solid stress and elastic energy as measures of tumour mechanopathology. *Nat Biomed Eng* 1(November):1–11.

27. Wiig H, Tenstad O, Iversen P, Kalluri R, Bjerkvig R (2010) Interstitial fluid: the overlooked component of the tumor microenvironment? *Fibrogenesis Tissue Repair* 3(1):12.

28. Stylianopoulos T, et al. (2013) Coevolution of solid stress and interstitial fluid pressure in tumors during progression: Implications for vascular collapse. *Cancer Res* 73(13):3833–3841.

29. Munn LL, Jain RK (2016) The Forces of Cancer. *Sci*.

30. Alonso JL, Goldmann WH (2016) Cellular mechanotransduction. *AIMS Biophys* 3(1):50–62.

31. Desgrosellier JS, Cheresh DA (2010) Integrins in cancer: biological implications and therapeutic opportunities. *Nat Rev Cancer* 10(1):9–22.

32. Chen CS (2008) Mechanotransduction - a field pulling together? *J Cell Sci* 121(20):3285–3292.

33. Mitra SK, Schlaepfer DD (2006) Integrin-regulated FAK-Src signaling in normal and cancer cells. *Curr Opin Cell Biol* 18(5):516–523.

34. Levental KR, et al. (2009) Matrix Crosslinking Forces Tumor Progression by Enhancing Integrin Signaling. *Cell* 139(5):891–906.

35. Rubashkin MG, et al. (2014) Force Engages Vinculin and Promotes Tumor Progression by Enhancing PI3K Activation of Phosphatidylinositol (3,4,5)-Triphosphate. *Cancer Res* 74(17):4597–4611.

36. Mouw JK, et al. (2014) Tissue mechanics modulate microRNA-dependent PTEN expression to regulate malignant progression. *Nat Med* 20(4):360–367.

37. Paszek MJ, et al. (2005) Tensional homeostasis and the malignant phenotype. *Cancer Cell* 8(3):241–254.

38. Weaver VM, et al. (1997) Reversion of the malignant phenotype of human breast cells in three-dimensional culture and in vivo by integrin blocking antibodies. *J Cell Biol* 137(1):231–45.

39. Petersen OW, R0nnov-Jessen L, Howlettt AR, Bissellt MJ (1992) Interaction with basement membrane serves to rapidly distinguish growth and differentiation pattern of normal and malignant human breast epithelial cells (extracelular matrix/rapid transformation assay/breast cancer/tissue structure and function). *Cell Biol* 89:9064–9068.

40. Kenny P a, Bissell MJ (2003) Tumor reversion: correction of malignant behavior by microenvironmental cues. *Int J Cancer* 107(5):688–95.

41. Hu H, et al. (2016) Phosphoinositide 3-Kinase Regulates Glycolysis through Mobilization of Aldolase from the Actin Cytoskeleton. *Cell* 164(3):433–446.

42. Haikala HM, Marques E, Turunen M, Klefström J (2016) Myc requires RhoA/SRF to reprogram glutamine metabolism. *Small GTPases*:1–9.

43. Wang J Bin, et al. (2010) Targeting mitochondrial glutaminase activity inhibits oncogenic transformation. *Cancer Cell* 18(3):207–219.

44. Walsh CT, Stupack D, Brown JH (2008) G protein-coupled receptors go extracellular: RhoA integrates the integrins. *Mol Interv* 8(4):165–173.

45. Bertero T, et al. (2016) Vascular stiffness mechanoactivates YAP/TAZ-dependent glutaminolysis to drive pulmonary hypertension. *J Clin Invest* 126(9):3313–3335.

46. Butcher DT, Alliston T, Weaver VM (2009) A tense situation: forcing tumour progression. *Nat Rev Cancer* 9(2):108–22.

47. Johnson JI, et al. (2001) Relationships between drug activity in NCI preclinical in vitro and in vivo models and early clinical trials. *Br J Cancer* 84(10). doi:10.1054/bjoc.2001.1796.

48. Daniel VC, et al. (2009) A primary xenograft model of small-cell lung cancer reveals irreversible changes in gene expression imposed by culture in vitro. *Cancer Res* 69(8):3364–73.

49. Guo S, et al. (2016) Molecular Pathology of Patient Tumors, Patient-Derived Xenografts, and Cancer Cell Lines. *Cancer Res* 76(16):4619–4626.

50. DelNero P, et al. (2015) 3D culture broadly regulates tumor cell hypoxia response and angiogenesis via pro-inflammatory pathways. *Biomaterials* 55(1):110–118.

51. Baker BM, Chen CS (2012) Deconstructing the third dimension: how 3D culture microenvironments alter cellular cues. *J Cell Sci* 125(Pt 13):3015–24.

52. Cukierman E, Pankov R, Stevens DR, Yamada KM (2001) Taking cell-matrix adhesions to the third dimension. *Science* 294(5547):1708–1712.

53. Fischbach C, et al. (2007) Engineering tumors with 3D scaffolds. *Nat Methods* 4(10):6–11.

54. Bissell MJ, Radisky D (2001) Putting tumours in context. *Nat Rev Cancer* 1(1):46–54.

55. Debnath J, Muthuswamy SK, Brugge JS (2003) Morphogenesis and oncogenesis of MCF-10A mammary epithelial acini grown in three-dimensional basement membrane cultures. *Methods* 30(3):256–268.

56. Buxboim A, Ivanovska IL, Discher DE (2010) Matrix elasticity, cytoskeletal forces and physics of the nucleus: how deeply do cells "feel" outside and in? *J Cell Sci* 123(Pt 3):297–308.

57. Baker BM, et al. (2015) Cell-mediated fibre recruitment drives extracellular matrix mechanosensing in engineered fibrillar microenvironments. *Nat Mater* 14(12):1262–8.

58. Chandler EM, Saunders MP, Yoon CJ, Gourdon D, Fischbach C (2011) Adipose progenitor cells increase fibronectin matrix strain and unfolding in breast tumors. *Phys Biol* 8(1):15008.

59. Smith ML, et al. (2007) Force-induced unfolding of fibronectin in the extracellular matrix of living cells. *PLoS Biol* 5:e268.

60. Chaudhuri O, et al. (2014) Extracellular matrix stiffness and composition jointly regulate the induction of malignant phenotypes in mammary epithelium. *Nat Mater* 13(10):970–978.

61. Wang K, et al. (2015) Stiffening and unfolding of early deposited-fibronectin increase proangiogenic factor secretion by breast cancer-associated stromal cells. *Biomaterials* 54:63–71.

62. McCoy MG, Seo BR, Choi S, Fischbach C (2016) Collagen I hydrogel microstructure and composition conjointly regulate vascular network formation. *Acta Biomater* 44:200–208.

63. Seo B, et al. (2015) Obesity-dependent changes in interstitital ECM mechanics promote breast tumorigenesis. *Sci Transl Med* 7(301).

64. Serebriiskii I, Castelló-Cros R, Lamb A, Golemis EA, Cukierman E (2008) Fibroblast-derived 3D matrix differentially regulates the growth and drug-responsiveness of human cancer cells. *Matrix Biol* 27(6):573–585.

65. Patterson J, Martino MM, Hubbell J a. (2010) Biomimetic materials in tissue engineering. *Mater Today* 13(1–2):14–22.

66. Lutolf MP, Hubbell J a (2005) Synthetic biomaterials as instructive extracellular microenvironments for morphogenesis in tissue engineering. *Nat Biotechnol* 23(1):47–55.

67. Bray LJ, et al. (2015) Multi-parametric hydrogels support 3D in vitro bioengineered microenvironment models of tumour angiogenesis. *Biomaterials* 53:609–620.

68. Chwalek K, Tsurkan M V, Freudenberg U, Werner C (2014) Glycosaminoglycan-based hydrogels to modulate heterocellular communication in in vitro angiogenesis models. *Sci Rep* 4:4414.

69. Kloxin AM, Tibbitt MW, Anseth KS (2010) Synthesis of photodegradable hydrogels as dynamically tunable cell culture platforms. *Nat Protoc* 5(12):1867–87.

70. Kloxin AM, Kasko AM, Salinas CN, Anseth KS (2009) Photodegradable hydrogels for dynamic tuning of physical and chemical properties. *Science* 324(5923):59–63.

71. Fischbach C, et al. (2009) Cancer cell angiogenic capability is regulated by 3D culture and integrin engagement. *Proc Natl Acad Sci U S A* 106(2):399–404.

72. Gill BJ, et al. (2012) A synthetic matrix with independently tunable biochemistry and mechanical properties to study epithelial morphogenesis and EMT in a lung adenocarcinoma model. *Cancer Res* 72:6013–6023.

73. Hahn MS, Miller JS, West JL (2006) Three-dimensional biochemical and biomechanical patterning of hydrogels for guiding cell behavior. *Adv Mater* 18(20):2679–2684.

74. Vickerman V, Chung S, Kamm RD (2008) Design, Fabrication and Implementation of a Novel Multi Parameter Control Microfluidic Platform for Three-Dimensional Cell Culture and Real-Time Imaging. *Lab Chip* 8(9):1468–1477.

75. Song JW, Bazou D, Munn LL (2012) Anastomosis of endothelial sprouts forms new vessels in a tissue analogue of angiogenesis. *Integr Biol (Camb)* 4(8):857–62.

76. Miller JS, et al. (2012) Rapid casting of patterned vascular networks for perfusable engineered three-dimensional tissues. *Nat Mater* 11(9):768–74.

77. Zheng Y, et al. (2012) In vitro microvessels for the study of angiogenesis and thrombosis. *Proc Natl Acad Sci U S A* 109(24):9342–7.

78. Morgan JP, et al. (2013) Formation of microvascular networks in vitro. *Nat Protoc* 8(9):1820–36.

79. Chrobak KM, Potter DR, Tien J (2006) Formation of perfused, functional microvascular tubes in vitro. *Microvasc Res* 71:185–196.

80. Sobrino A, et al. (2016) 3D microtumors in vitro supported by perfused vascular networks. *Sci Rep* 6(August):31589.

81. Ingber DE (2016) Reverse Engineering Human Pathophysiology with Organs-on-Chips. *Cell* 164(6):1105–1109.

82. Young EWK (2013) Cells, tissues, and organs on chips: challenges and opportunities for the cancer tumor microenvironment. *Integr Biol* 5:1096–1109.

83. Moraes C, Mehta G, Lesher-Perez SC, Takayama S (2011) Organs-on-a-Chip: A Focus on Compartmentalized Microdevices. *Ann Biomed Eng*. doi:10.1007/s10439-011-0455-6.

84. Tanner K, Gottesman MM (2015) Beyond 3D culture models of cancer. *Sci Transl Med* 7(283):7–10.

85. Yum K, Hong SG, Healy KE, Lee LP (2014) Physiologically relevant organs on chips. *Biotechnol J* 9(1):16–27.

86. Wikswo JP (2014) The relevance and potential roles of microphysiological systems in biology and medicine. *Exp Biol Med (Maywood)* 239(9):1061–72.

87. Esch MB, King TL, Shuler ML (2011) The Role of Body-on-a-Chip Devices in Drug and Toxicity Studies. *Annu Rev Biomed Eng Vol 13* 13:55–72.

88. Oleaga C, et al. (2016) Multi-Organ toxicity demonstration in a functional human in vitro system composed of four organs. *Sci Rep* 6(1):20030.

89. Sung JH, Kam C, Shuler ML (2010) A microfluidic device for a pharmacokinetic-pharmacodynamic (PK-PD) model on a chip. *Lab Chip* 10:446–455.

90. Novik E, Maguire TJ, Chao P, Cheng KC, Yarmush ML A microfluidic hepatic coculture platform for cell-based drug metabolism studies. *Biochem Pharmacol*. doi:10.1016/j.bcp.2009.11.010.

91. Friedman A a., Letai A, Fisher DE, Flaherty KT (2015) Precision medicine for cancer with next-generation functional diagnostics. *Nat Rev Cancer* 15(12):747–756.

92. Pauli C, et al. (2017) Personalized *In Vitro* and *In Vivo* Cancer Models to Guide Precision Medicine. *Cancer Discov* (May). doi:10.1158/2159-8290.CD-16-1154.

93. Morelli MP, et al. (2012) Prioritizing phase I treatment options through preclinical testing on personalized tumorgraft. *J Clin Oncol* 30(4):e45-8.

94. Fruman DA, et al. (2017) The PI3K Pathway in Human Disease. *Cell* 170(4):605–635.

95. Pauli C, et al. (2017) Personalized In Vitro and In Vivo Cancer Models to Guide Precision Medicine. *Cancer Discov*.

96. Hidalgo M, et al. (2014) Patient-derived Xenograft models: An emerging platform for translational cancer research. *Cancer Discov* 4(9):998–1013.

97. Kopetz S, Lemos R, Powis G (2012) The promise of patient-derived xenografts: the best laid plans of mice and men. *Clin Cancer Res* 18(19):5160–2.

98. Capulli AK, et al. (2014) Approaching the in vitro clinical trial: engineering organs on chips. *Lab Chip* 14(17):3181.

99. Byrne AT, et al. (2017) Interrogating open issues in cancer precision medicine with patient-derived xenografts. *Nat Rev Cancer* 17(4):254–268.

100. Berridge BR, Pettit SD, Sarazan RD (2014) Opportunities to meet clinical cardio-oncology needs with new approaches to non-clinical safety assessment. *Prog Pediatr Cardiol* 36(1–2):31–32.

101. Heylman C, Sobrino A, Shirure VS, Hughes CC, George SC (2014) A strategy for integrating essential three-dimensional microphysiological systems of human organs for realistic anticancer drug screening. *Exp Biol Med* 239(9):1240–1254.

102. Ruppen J, et al. (2015) Towards personalized medicine: chemosensitivity assays of patient lung cancer cell spheroids in a perfused microfluidic platform. *Lab Chip* 15(14):3076–3085.

CHAPTER 6

FROM PATIENTS TO PARTNERS

Peter DelNero and Alexandra McGregor. (2017) From patients to partners. *Science* 358(6361):414.

Manuscript

When we started graduate school 5 years ago, we were determined to learn everything we could about cancer. We spent all our time in the lab developing an arsenal of experimental techniques. However, in our daily work with petri dishes and microscopes, we felt that something was missing. We learned all about tumor biology, but we knew very little about the human dimensions of cancer. Even though our research is far from the clinic, we believed that interacting with patients and survivors would improve our understanding of cancer and the quality of our science.

With permission from our advisers, we contacted the director of a local cancer center to find out whether he might be interested in working with us. He was enthusiastic about connecting scientists-in-training with the cancer community; in fact, he was already discussing this idea with another group at our university. Together, we started hosting monthly seminars where researchers and patients interact and learn from each other. Some months, a graduate student gives a lay-language presentation about an important aspect of cancer research. Other months, community members describe their experiences of living with cancer. We also organize informal activities that promote patient-researcher dialogue, such as lab tours, book clubs, and participation in cancer support groups. One lung cancer survivor even spent a summer conducting experiments with us. Our relationship with the cancer center created a continuous stream of new opportunities.

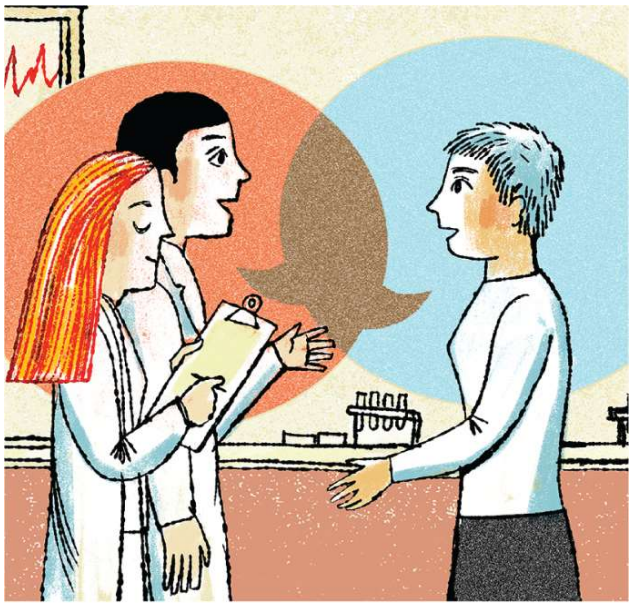

Fig. 1. Cancer patients contribute to all stages of the research process, beginning with the training of new scientists. Illustration by Robert Neubecker.

The partnership with the patient community has deeply influenced our formation as scientists. Our conversations have revealed gaps in our knowledge, exposed biases and assumptions, and even opened new paths for inquiry. We have learned about the hidden costs of cancer and the day-to-day obstacles patients face with their work, health insurance, family life, and plans for the future. By speaking with cancer patients, we have also learned to exercise openness, empathy, and reflective listening. Over time, we have fostered special relationships with patients and family members, and many have become our closest friends. Occasionally, we come face-to-face with the devastating reality that current treatments are not good enough.

The patient-researcher partnership transformed our research from an intellectual exercise into a deeply personal endeavor. It reminds us that people with cancer are not merely cells or molecular pathways. They are neighbors, colleagues, friends, and relatives. They are valued partners in the fight against cancer. As one of our colleagues explained, "I used to care about accomplishments and great publications, but now I simply want to generate data that will be most reliable and important for improving cancer therapy."

Early in the process, we felt nervous about taking time and energy away from our lab work to develop this program. We felt we were "breaking the rules" for graduate student conduct. But we decided to ignore this nagging anxiety, and we gave ourselves permission to continue. With help from a team of faculty members, the partnership evolved into a formal curriculum for public engagement in cancer research. This aspect of our work became a highlight of our graduate experience.

Through our partnership, we discovered that research is not the only way that scientists can make a positive difference in the fight against cancer. Outside the lab, we can nurture personal

relationships with individual patients, survivors, and families. Researchers are well placed to disseminate information, dispel common misconceptions, and share the scientific process with the cancer community. Most importantly, we can be good, supportive listeners. As we pursue the next phase in our research careers, we know that our patient involvement will continue. For us, it has become an integral part of what it means to be a cancer scientist.

CHAPTER 7

NAVIGATING A WAYWARD PATH TOWARD PUBLIC ENGAGMENT

Peter DelNero. (*In press*) Navigating a wayward path toward public engagement. *Michigan Journal of Community Service Learning*.

Abstract

Graduate school is an intense period of identity formation, where scholars-in-training form the attitudes and values that shape their research. While pursuing their degree, graduate students navigate an evolving sense of personal and professional self-concept. This process is modulated by the presence or absence of public engagement paradigms. The extent to which students assimilate public engagement into their academic formation may depend on the system of beliefs that underpin their particular field of study. In some fields, public engagement disrupts the conventional forms of scholarship and elicits a peculiar tension. How can graduate students overcome a misalignment between their personal goals, values, and interests and those of their discipline? If graduate students are trained to think and act in certain ways, then what happens to people who choose to think and act differently in order to cultivate a community-engaged mindset? In this essay, I examine these questions through my experiences as a community-engaged doctoral student in biomedical engineering.

Manuscript

Graduate school represents a critical stage in the academic pipeline, where professional attitudes and priorities are internalized by future faculty and administrators. During graduate education, students construct the aspirations, commitments, and identities that ultimately define their careers. As such, there is growing appreciation for preparing graduate students for

professional roles that advance the practice of community-engaged scholarship (1, 2). But what if graduate students are trained in departments that do not value or reward these activities? Will emerging scholars perpetuate traditional attitudes toward teaching, research, and service?

In this narrative, I reflect on my experience of disrupting a cycle of social reproduction in order to accommodate a community-engaged mindset. The article is autoethnographic in that I connect my personal experiences with an analysis of my academic culture (3, 4)*. I present this essay as a scholarly personal narrative* (5)*; the italicized sections represent my personal experiences and interpretations.*

Graduate education is an intense period of cognitive and affective development. Through a process of socialization, students acquire specialized knowledge and skills, while coming to recognize the cultural norms, ideologies, and world views that characterize their profession (6, 7). At the same time, graduate students have entered a stage of self-authorship, where they exercise the capacity to define their own beliefs, identities, and social relations (8). Students play an active role in shaping their academic formation while learning to navigate professional norms and boundaries.

I am a doctoral candidate in biomedical engineering, specializing in cancer biology. As a graduate student, I fall into an uncomfortable gap between advanced student and novice scholar. In addition to taking classes, I also teach, conduct research, and assume service roles at my institution. When I entered graduate school, I expected to receive instrumental training in biomedical research and become a credentialed professional in the field. During my first year, I quickly assimilated into the norms of my discipline.

Disciplinary norms are the values, behaviors, and responsibilities that characterize "business-as-usual" in an academic community. Academia is a diverse profession, but there is an implicit code-of-conduct that governs the epistemic culture within each field (9). This culture is often invisible to new students, concealed within the latent assumptions and biases of the discipline. As discussed by the Carnegie Initiative on the Doctorate, graduate education is largely a process of becoming acculturated to these norms (10).

Jackson (1968) introduced the concept of a "hidden curriculum" to describe the cultural transmission that occurs within and beyond the classroom. The hidden curriculum is the way in which institutional systems "persist and reproduce themselves without being consciously recognized by the people involved" (12). In graduate education, disciplinary norms play a substantial role in the socialization of emerging scholars, but they "remain an embedded and largely ignored element of academic life" (13).

As an engineering student, I inhabit a discipline where I perceive the culture to be relatively strict. Patterns of thought and behavior are enforced via institutional structures such as apprenticeship, peer-review, the curriculum, and the collective expectations of the community. The engineering identity, with its explicit maxim to "think like an engineer," is an unequivocal way of being.

Although socialization provides a stable mechanism for stewardship and knowledge transmission, the hidden curriculum can sometimes be problematic (14, 15). For example, the apprenticeship model of doctoral training has been criticized for perpetuating institutional discrimination (16). When experts evaluate prospective candidates, they "tend to look for someone like themselves, missing the valuable talents of people who are different" (17, 18).

Downey and Lucena connect the negative impact of socialization to the concept of "weeding out." During interviews, "students regularly asserted that the goal of certain courses was to 'weed out' students {…} For students who stayed, these and other courses also appeared to *weed out part of themselves as persons"* (19). Similarly, Weidman and colleagues reported that the principal conflict for many graduate students was the feeling that they must sacrifice their own interests and goals to fit the expectations and interests of their advisors (20). Students who embody nonconforming social or intellectual identities confront systematic resistance, which subverts efforts toward equity, innovation, and risk-taking.

Cech reported a "culture of disengagement" in engineering education, comprising a collection of ideologies that discourage civic awareness and activism (21). This culture is characterized by an exclusion of non-technical stakeholders in academic dialogue, the dismissal of public welfare concerns, and an inattention toward social justice, equity, and social responsibility (21, 22). As a result of socializing to these norms, engineering students lose the ability to reflect on the broader context of their work, to define and prioritize social concerns, and to assess problems, methods, or outcomes from multiple perspectives. In essence, students learn to dissociate public impacts as tangential to their field of study (21).

My acculturation into the biomedical engineering community was disrupted by an emerging partnership with a local cancer support center, which I helped initiate during my second year of graduate school. Our collaboration is logistically simple, comprising a monthly colloquium for patients, survivors, and students. Seminars are complemented by a variety of informal activities that facilitate dialogue between patients and scientists.

As my relationship with the cancer community grew stronger, it gradually infringed on my identity as an engineer. My priorities and attitudes toward research seemed misaligned with the expectations of my colleagues. For example, a faculty member once complained to me that the "broader impacts" criteria should be eliminated from the funding mechanisms of the National Science Foundation. The professor stated, "I don't write grants so that [my student] can do outreach. I'm training her to be a scientist, not a babysitter." According to this professor, broader impacts, such as public engagement activities, are a waste of time. Because of my involvement in the cancer community, I found myself becoming an outsider in my discipline.

In an analysis of participatory research, Nyden observed that "sometimes [academic] culture can be indifferent to community involvement; other times it is actually hostile" (23). For graduate students, "being in opposition does not simply mean confronting abstract ideas; frequently and most uncomfortably it means confronting one's professors" (18). Given these circumstances, "successful" students are often those who readily assimilate to disciplinary paradigms, while students who re-define these paradigms have a more difficult experience (13, 24). In some cases, this environment might tacitly discourage civic engagement activities, social justice concerns, and the retention of graduate students who espouse them.

Cognitive dissonance is a painful but important element of disciplinary learning. But in my case, the cognitive dissonance between the discipline of engineering and community engagement evoked feelings of guilt, shame, and self-doubt. Through my academic training, I had internalized the belief that public engagement was outside the purview of engineering. My relationships with community members challenged my assumptions about the purpose, process, and products of biomedical engineering research. At the time, I was unable to articulate this dissonance, but I felt an overwhelming anxiety surrounding what I was coming to perceive as my deviant patterns of

thought and behavior. My commitment to the community partnership violated my beliefs about what it meant to be an engineer.

Reflection, as a cornerstone of service-learning and with roots often attributed to the education theories of John Dewey (25) and David Kolb (26), is the vital link between experience and knowledge. In *Where's the Learning in Service-Learning,* reflective practices predicted learning outcomes associated with personal development, citizenship, problem-solving, and perspective transformation (27). In service-learning pedagogy, cognitive and emotional processes are inseparable dimensions of reflection (28), both of which are essential for making meaning from experience.

Self-reflection was facilitated through my role in developing curriculum, writing grant proposals, and drafting manuscripts. Through this process, I learned how to tell my story, and I gained a deeper understanding of my experiences. By pursuing community-engaged activities, I felt I was "breaking the rules" of what an engineering student is "supposed to do." But ultimately, who decides how an engineer should think or behave? Why did I maintain the inexorable conviction that community engagement was verboten?

As I reflected on this, I arrived at Walt Kelly's startling conclusion: "We have met the enemy and he is us." I discovered that I was trapped by tunnel-vision: I had internalized a system of values and beliefs from my discipline. But I also realized that I had the capacity to change those values and beliefs. This realization enabled me to construct a new, integrated concept of my professional identity: "I thought I knew what it meant to be an engineer, but that was partly a myth. It's okay to be different."

According to Mezirow, transformative learning "makes it possible for us to […] become emancipated from our constraining habits of expectation and move to a perspective that permits interpretations which are more inclusive, differentiating, permeable, and integrative of experience" (29). Transformative learning empowered me to step beyond my existing patterns of thought and behavior and to extend the definition of my profession.

My involvement in public engagement transformed my perspective of graduate education. I am no longer the passive recipient of professional socialization. As a graduate student, I am responsible for my own academic development, including attentiveness toward the intellectual and social norms that permeate my discipline. I have agency to define the values, goals, and methods of my scholarship. I have an obligation to reflect on the usefulness of knowledge, the social consequences of my work, and its relation to the world beyond campus (30). *In short, I am a co-creator of the intellectual communities that I inhabit and an advocate for my ongoing formation as an engaged scholar.*

In graduate education, students internalize the profession's concept of ethical behavior and social norms. If community dialogue is marginalized, emerging scholars will continue to define public engagement as irrelevant to the practice of their discipline. Conversely, graduate students are uniquely positioned to disrupt the cycle of assimilation, and to cultivate an academic identity that accommodates public engagement. We can foster an intellectual community that "provides explicit emphasis on how to value and engage in such work" (1).

References

1. Austin A, Barnes B (2005) Preparing doctoral students for faculty careers that contribute to the public good. *Higher Education for the Public Good*, eds Kezar AJ, Chambers TC, Burkhardt JC (San Francisco, CA).

2. Stanton TK (2012) New times demand new scholarship II: research universities and civic engagement: opportunities and challenges. *J High Educ Outreach Engagem* 16(4):271–304.

3. Ellis C (2004) *The Ethnographic I: A Methodological Novel about Autoethnography* (AltaMira Press).

4. Ellis C, Adams TE, Bochner AP (2011) Autoethnography: An Overview. *Qual Soc Res* 12(1).

5. Nash RJ, Bradley DL (2011) *Me-Search and Re-Search: A Guide for Writing Scholarly Personal Narrative Manuscripts* (Information Age Publishing Inc).

6. Gardner SK (2008) Fitting the mold of graduate school: a qualitative study of socialization in doctoral education. *Innov High Educ* 33(2):125–138.

7. O'Meara K (2008) Graduate education and community engagement. *New Dir Teach Learn* (113):27–42.

8. Baxter Magolda MB (2006) Intellectual development in the college years. *Chang Mag High Learn* 38(3):50–54.

9. Margolis E, Romero M (1998) The Department Is Very Male, Very, White, Very Old, and Very Conservative": The Functioning of the Hidden Curriculum in Graduate Sociology Departments. *Harv Educ Rev* 68(Spring):33.

10. Walker GE, Golde CM, Jones L, Bueschel AC, Hutchings P (2008) *The formation of scholars* (Jossey-Bass, San Francisco, CA).

11. Jackson PW (1968) *Life in classrooms* (Holt, Rinehart and Winston, New York, NY).

12. Apple MW (1982) *Cultural and economic reproduction in education: essays on class, ideology, and the state* (Routledge & Kegan Paul, London).

13. Gair M, Mullins G (2001) Hiding in plain sight. *The Hidden Curriculum in Higher Education*, ed Margolis E (Routledge, New York, NY), pp 21–41.

14. Egan JM (1989) Graduate school and the self: a theoretical view of some negative effects of professional socialization. *Teach Sociol* 17(2):200–207.

15. Nyquist JD, et al. (2010) On the road to becoming a professor: the graduate student experience. *Chang Mag High Educ* 31(3):18–27.

16. Damrosch D (2006) Vectors of change. *Envisioning the Future of Doctoral Education: Preparing Stewards of the Discipline*, eds Golde CM, Walker GE (Jossey-Bass, San Francisco, CA), pp 34–45.

17. Lawrence CR, Matsuda MJ (1997) *We won't go back: making the case for affirmative action* (Houghton Mifflin, Boston, MA).

18. Margolis E, Romero M (2001) "In the image and likeness...": how mentoring functions in the hidden curriculum. *The Hidden Curriculum in Higher Education*, ed Margolis E (Routledge, New York, NY), pp 79–96.

19. Downey GL, Lucena JC (1997) Engineering selves: hiring into a contested field of education. *Cyborgs and Citadels: Anthropological Interventions in Emerging Sciences and Technologies*, eds Downey GL, Dumit J (The SAR Press, Santa Fe, NM), pp 117–142.

20. Weidman JC, Twale DJ, Stein EL (2001) *Socialization of Graduate and Professional Students in Higher Education: A Perilous Passage?*

21. Cech EA (2014) Culture of disengagement in engineering education? *Sci Technol Hum Values* 39(1):42–72.

22. Cech EA, Sherick HM (2015) Depoliticization and the Structure of Engineering Education. *International Perspectives on Engineering Education: Engineering Education and Practice in Context, Volume 1*, eds Christensen HS, et al. (Springer International Publishing, Cham, Switzerland), pp 203–216.

23. Nyden P (2003) Academic incentives for faculty participation in community-based participatory research. *J Gen Intern Med* 18(7):576–585.

24. Strouse AW (2014) Getting medieval on graduate education: queering academic professionalism. *Pedagog Crit approaches to Teach Lit Lang Compos Cult* 15(1):119–138.

25. Dewey J (1910) *How We Think* (D.C. Heath & Co.).

26. Kolb DA (1984) *Experiential Learning: Experience as The Source of Learning and Development*. (Prentice Hall, Inc).

27. Eyler J, Giles DEJ (1999) *Where's the Learning in Service-Learning?* (Jossey-Bass).

28. Felten P, Gilchrist LZ, Darby A (2006) Emotion and Learning: Feeling our Way Toward a New Theory of Reflection in Service-Learning. *Michigan J Community Serv Learn* 12(Spring):38–46.

29. Mezirow J (2001) Learning as Transformation: Critical Perspectives on a Theory in Progress. *J Acad Librariansh* 27(5):417.

30. Boyer EL (1990) *Scholarship reconsidered: priorities of the professoriate* (The Carnegie Foundation for the Advancement of Teaching, Princeton, NJ).

CHAPTER 8

CONCLUSION

There are countless elements that contribute to cancer pathogenesis, and it is important to determine which factors ultimately lead to better patient outcomes. This may include the physical properties of the tissue microenvironment, as well as the communities of people who are grappling with cancer in its full human complexity. Both basic science labs and community support organizations provide irreplaceable services to improve human health and reduce the burdens of cancer.

In Part I, I document the scientific approaches that are traditionally associated with biomedical research. My laboratory research demonstrates how the tumor microenvironment influences cancer cell behavior. The results show that the three-dimensional tissue context has substantial effects on hypoxia response and angiogenesis. These laboratory-based investigations led to sophisticated tools to study how the tumor microenvironment regulates cancer cell behavior and microvascular function.

Looking forward, it is exciting to consider the future implications that might emerge from these projects. With regard to the microvascular networks, there is potential application in multiple settings. In the clinic, these products may provide an important platform for precision medicine; microphysiological models containing patient-derived tissues might be used to test novel drug combinations, potentially improving personalized treatments for cancer patients. More elaborate body-on-a-chip platforms offer systemic models of metastasis or treatment. Appropriate vascular transport is essential for mimicking the physiology of health and disease in vitro.

A spectrum of biological questions are made tractable by well-controlled microvascular models. This technology might be used to assess the effects of matrix fiber architecture on vascular function or the influence of angiocrine signals in the tumor niche. The system is well suited for testing vessel response to new therapeutic agents or cell-derived cues like microvesicles. When combined with genetically-encoded fluorescent sensors, the device can be used to monitor cell status in response to exogenous factors. For example, we used a FRET-based lactate sensor to measure real-time, single-cell metabolic changes while manipulating nutrient availability, glycolysis, or oxidative phosphorylation. Finally, our platform may provide a suitable surrogate for validating computational models of disease. Mathematical models are useful for simulating metabolic processes or tumor evolution, and in vitro systems might allow researchers to test predictions from such experiments.

Two features will make the microphysiological platform even more useful. First, the platform should closely recapitulate the specific properties of host tissue. For example, in vitro models of breast cancer ought to include matrix and cellular components that reflect the adipose tissue microenvironment. This is also true in modeling metastatic processes like intra- and extravasation, where local tissue properties play a role in tumor colonization. Second, the devices must become more robust and reproducible for use in non-engineering labs. So far, sensitive device assembly prevents wide-spread application of these tissue engineering models. Improving the device fabrication procedure will significantly enhance the impact of these technologies. Appendix I presents one example of a facile tool for reconstructing elements of the tumor microenvironment, including spatially-resolved molecular characterization and autologous transport gradients.

In Part II, I report on an unconventional aspect of biomedical research: the patient-researcher partnership. This project is directly relevant to a convergence toward public engagement

in health research, higher education, and science communication. The approach is not focused on molecular mechanisms of disease; instead, the best possible outcome is a sustained and equitable partnership. Patient involvement reveals a different dimension of cancer: how cancer affects people's lives. The personal aspects of cancer are critical determinants of research training. By interacting with cancer patients and survivors, we gain concrete knowledge that cannot be replicated in a laboratory. Through my involvement in the patient-researcher partnership, I have discovered an entirely different way of understanding the purpose, process, and products of science. These relationships provide a more complete understanding of this disease.

The patient-researcher partnership transforms the relationship between scientists and community members. Scientists begin to see themselves as members of the patient support network, with a personal concern toward improving the wellbeing of individual patients and survivors. The parternship welcomes new forms of knowledge and expertise that arises from the lived-experiences of cancer patients and their families. The partnership allows new voices to influence our choices and perspectives when approaching scientific phenomena, and it offers the possiblity of seeing things that we miss in the laboratory. When we expose ourselves to diverse perspectives, we are more aware of the limitations and biases of our own worldviews. When science is inclusive to public participation, it engages a range of perspectives that would otherwise be excluded; the scientists who listen are rewarded with valuable insights and irreplaceable relationships.

The patient-researcher partnership leads to a more complete understanding of cancer and a stronger commitment toward reducing the burdens of this disease. Looking ahead, it is exciting to think that our simple collaboration might become a normative aspect of biomedical training. We hope that the concept of patient-researcher dialogue will be replicated at other research insitutions

and community support organizations. If successful, this paradigm could change the way that scientists perceive their role in the cancer landscape, just as it has for me.

There are many ways of producing knowledge. In biomedical sciences, discovery often progresses through an incremental process of generating and testing hypotheses. In addition to discoveries, scholarship can also involve the integration or application of knowledge in new ways, or the transmission of knowledge across new boundaries. Since the 1990's, there has been sustained interest in accommodating a wider variety of epistemologies within scholarly discourse, for example by elevating the practice of applied research, teaching, and outreach to equal status with traditional forms of inquiry. This shift reflects an appreciation for multiple responsibilities and forms of expertise that co-exist within universities.

Ultimately, my PhD was six years learning how to improve human health and reduce the burdens of cancer. I found three ways to do this: First, by developing laboratory models that better reflect the conditions in the body so that our experiments are most likely to lead to reliable and useful data. Second, by forming personal relationships with members of the Ithaca cancer community and taking actions to support people who are affected by cancer. And third, by training new cancer scientists to be diligent researchers who are also attentive and committed to listening to patient perspectives and maybe learning something unexpected. For me, all three outcomes are integral parts what it means to be a cancer scientist.

APPENDIX I

ENGINEERED TUMOURS: ROLL-ON SCAFFOLDS

Peter DelNero and Claudia Fischbach. (2016) Engineered tumours: roll-on scaffolds. *Nature Materials* 15(2):138-39.

Manuscript

Aberrant biological and physical properties of the microenvironment - such as vascular dysfunction and the ensuing perturbations of diffusive and convective transport - are both cause and consequence of malignant transformation (Fig. la). To study the underlying cellular and molecular mechanisms, biomaterials and tissue-engineering strategies that mimic specific physicochemical properties of tumours in vivo are increasingly applied (1). In contrast to conventional two-dimensional monolayers, cells embedded within a three- dimensional artificial extracellular matrix (ECM) recreate tissue structures and soluble gradients that resemble those of actual tumours (Fig. la) (2). Although biomaterials-based models achieve relative success in predicting cell signalling and drug response, they often conceal the exact mechanisms by which the microenvironment regulates disease, in part because of the difficulty of decoupling the feedback mechanisms by which extracellular conditions and intracellular pathways synergistically promote tumour aggressiveness. Reporting in Nature Materials, Alison McGuigan and colleagues introduce a ribbon-on-a-spool biocomposite (Fig. lb) that can help untangle these interactions by permitting the analysis of distinct, localized regions in quasi-physiological tumours (3).

In the scaffold-tumour construct, which McGuigan and colleagues termed tumour roll for analysis of cellular environment and response (TRACER), cancer cells are embedded on a biocomposite film, wrapped around an aluminium mandrel, and cultured in a standard well-plate.

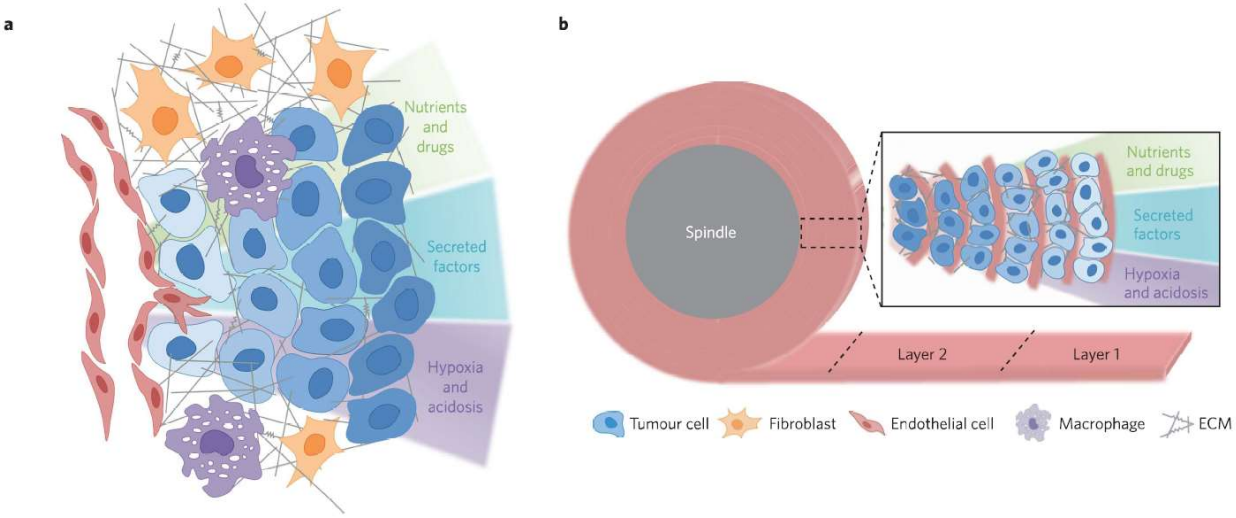

Fig. 1. a) Cancer initiation, progression, and therapy are controlled by aberrant features of the surrounding tissue environment, such as inflammation, angiogenesis and desmoplasia. The resulting heterogeneous distributions of nutrients and drugs (green), cell-secreted factors (blue), and oxygen and pH (purple), collectively contribute to tumour malignancy. To study the underlying biological and physical mechanisms, biomaterials-based tumour models attempt to recapitulate the corresponding tumour–host-cell interactions, soluble-factor gradients, and extracellular-matrix (ECM) properties. b) A cell-laden biocomposite roll allows for the correlation of phenotypic changes with specific microenvironmental niches. Within the spool, passive diffusion and cell-mediated processes generate gradients of soluble factors that mimic the spatial distributions imposed as a function of progressive distance from the nearest functional blood vessel. By unrolling the spindle and isolating cells from spatially distinct locations, specific extracellular conditions (such as hypoxia or acidosis) can be correlated with changes in intracellular signalling.

Consumption and secretion activities by encapsulated cells create radial molecular gradients (Fig. lb; inset). Subsequently, the film is unravelled, cut into sections, and analysed with conventional biological assays. Hence, this cell-culture platform offers an exquisite tool for the generation of well-defined autonomous gradients and for the characterization of cellular behaviours at precise regions along these gradients. Because the design of TRACER does not require sophisticated instrumentation or technical expertise, the platform is simple enough to be widely implemented as a pathologically relevant model of cancer.

Cancer-cell metabolism is a poignant example of the reciprocity between cells and their local microenvironment. It is commonly accepted that tumour cells dynamically adjust their metabolic signalling to meet the increased needs for macromolecule biosynthesis and for redox balance associated with excess cell prolife ration (4). These changes have been primarily associated with aberrant intracellular signalling pathways. However, asymmetric biochemical gradients caused by the combined effects of vascular transport and cellular consumption and secretion play a similarly important role, and may terminate in severe local hypoxia, lactic acidosis, and nutrient depletion (5). Cancer cells respond to these adverse conditions through a variety of adaptive responses, including a switch toward glycolytic metabolism. Therefore, the metabolic phenotype of an individual cancer cell is affected by both oncogenic alterations and spatial differences in microenvironmental stress.

McGuigan and co-authors first used TRACER to investigate the effect of spatial variations in oxygen concentration on the activity of hypoxia-inducible factor-I (HIF-1; a canonical regulator of the hypoxia response (6)) and resultant changes in tumour-cell metabolic reprogramming. Gene-expression and metabolomic analyses of TRACER layers confirmed that cellular phenotypes

varied as a function of their spatially distinct microenvironments. Interestingly, inhibition of HIF-1 with short-hairpin RNA (shHIF) broadly altered the metabolic profile in TRACER. Although some of these changes are expected, a number of surprising connections that may represent new, context-dependent metabolic pathways also emerged. Moreover, metabolic changes were corroborated by indirect measures of oxygen concentration in the TRACER system. TRACERs containing shHIF manifested a fixed oxygen gradient after 12 hours, whereas control experiments showed increasing oxygen levels. The authors attribute these observations to the inability of shHIF-treated cells to modulate their oxygen consumption under hypoxic conditions, possibly as a consequence of the altered metabolic profiles. Altogether, the authors directly correlated HIF-1-dependent changes in intracellular metabolic processes and extracellular oxygen gradients to unique regions in the tumour. Their analysis provides an excellent protocol for using TRACER to study the intersection of gene-regulatory pathways and the tumour microenvironment.

Although McGuigan and co-authors discuss their findings in the context of hypoxia, oxygen gradients are only one of the multiplexed environmental factors regulating tumour metabolism and thus malignancy. Distributions of lactic acid, paracrine signals, therapeutic drugs, and other soluble factors concomitantly affect cellular phenotype and could be studied with TRACER. Likewise, insoluble ECM components play a critical role, as their chemical, structural, and mechanical properties can affect cellular/metabolic behaviours directly by altering mechanotransduction and indirectly by modulating transport phenomena (7). In fact, hypoxia and ECM physical changes are dynamically linked, as hypoxia can promote tumorigenic physical changes of the ECM that may further perturb oxygen transport (for example, by increasing expression of the collagen crosslinking enzyme lysyl oxidase (8)). Moreover, tumours not only consist of tumour cells, but interactions with host cells are equally important. For example,

integrating endothelial cells or activated fibroblasts would improve the physiological relevance of the model system and enable studies focused on metabolic coupling between both cell types, such as through the reverse Warburg effect (9). TRACER provides an opportunity to carefully reconstruct (and subsequently analyze) the intersecting soluble gradients, matrix properties, and cellular components of the tumour microenvironment.

The cancer microenvironment is a diverse biological ecosystem. Biomaterials and tissue-engineering strategies provide well-defined and reproducible models that may afford a unique window into the evolutionary dynamics of cancer progression. By recreating physiologically appropriate conditions and gradients, engineered tumours could help elucidate adverse microenvironmental parameters that may select for the resilient or aggressive phenotypes that promote malignancy and drug resistance (10). Using TRACER, McGuigan and colleagues have developed an easily accessible and adaptable approach to correlate cellular phenotypes with local microenvironmental conditions. Ultimately, it is the design of such simple and versatile platforms that may lead to meaningful collaborations between biomaterials scientists, tissue engineers, and cancer biologists to accelerate the discovery of new therapeutic targets and advance the effective treatment of cancer.

References

1. Bissell MJ & Radisky D (2001) Putting tumours in context. *Nature Reviews Cancer* 1(1):46-54.

2. Fischbach C, *et al.* (2007) Engineering tumors with 3D scaffolds. *Nature Methods* 4(10):855-860.

3. Rodenhizer D, *et al.* (2016) A three-dimensional engineered tumour for spatial snapshot analysis of cell metabolism and phenotype in hypoxic gradients. *Nature Materials* 15(2):227-+.

4. Heiden MGV, Cantley LC, & Thompson CB (2009) Understanding the Warburg Effect: The Metabolic Requirements of Cell Proliferation. *Science* 324(5930):1029-1033.

5. Carmeliet P & Jain RK (2011) Principles and mechanisms of vessel normalization for cancer and other angiogenic diseases. *Nature Reviews Drug Discovery* 10(6):417-427.

6. Semenza GL (2009) Regulation of cancer cell metabolism by hypoxia-inducible factor 1. *Seminars in Cancer Biology* 19(1):12-16.

7. Tung JC, *et al.* (2015) Tumor mechanics and metabolic dysfunction. *Free Radical Biology and Medicine* 79:269-280.

8. Levental KR, *et al.* (2009) Matrix Crosslinking Forces Tumor Progression by Enhancing Integrin Signaling. *Cell* 139(5):891-906.

9. Pavlides S, *et al.* (2009) The reverse Warburg effect Aerobic glycolysis in cancer associated fibroblasts and the tumor stroma. *Cell Cycle* 8(23):3984-4001.

10. Nowell PC (1976) Clonal evolution of tumor-cell populations. *Science* 194(4260):23-28.

APPENDIX II

MICROENGINEERED TUMOR MODELS: INSIGHTS & OPPORTUNITIES FROM A PHYSICAL SCIENCES – ONCOLOGY PERSPECTIVE

Peter DelNero*, Young Hye Song*, and Claudia Fischbach. (2013) Microengineered tumor models: insights & opportunities from a physical sciences-oncology perspective. *Biomed Microdevices* 15(4):583–593.

**Authors contributed equally*

Abstract

Prevailing evidence has established the fundamental role of microenvironmental conditions in tumorigenesis. However, the ability to identify, interrupt, and translate the underlying cellular and molecular mechanisms into meaningful therapies remains limited, due in part to a lack of organotypic culture systems that accurately recapitulate tumor physiology. Integration of tissue engineering with microfabrication technologies has the potential to address this challenge and mimic tumor heterogeneity with pathological fidelity. Specifically, this approach allows recapitulating global changes of tissue-level phenomena, while also controlling microscale variability of various conditions including spatiotemporal presentation of soluble signals, biochemical and physical characteristics of the extracellular matrix, and cellular composition. Such platforms have continued to elucidate the role of the microenvironment in cancer pathogenesis and significantly improve drug discovery and screening, particularly for therapies that target tumor-enabling stromal components. This review discusses some of the landmark efforts in the field of micro-tumor engineering with a particular emphasis on deregulated tissue organization and mass transport phenomena in the tumor microenvironment.

Introduction

Despite sustained progress in our knowledge of biological signaling events regulating tumor malignancy, the clinical prognosis for many cancer types has scarcely changed since 1950 {Howlader 2012}. Increasing experimental evidence suggests that this discrepancy may be due in part to an under-appreciation of physical phenomena contributing to disease progression. As a result, cancer biologists are increasingly collaborating with physical scientists and engineers to study physicochemical characteristics of solid tumors and their role in modulating intracellular signaling (1). Particular emphasis is placed on analyzing microenvironmental changes that fundamentally influence tumor progression and therapy, including aberrant mechanical properties (e.g. cell forces, matrix stiffness), transport phenomena (e.g. mass and energy transfer, fluid dynamics), and growth/reaction kinetics (e.g. metabolism, signaling, proliferation). For example, quantifying therapy-associated mass transport, reaction rates, and the resulting cellular growth kinetics may help to better understand the evolution of drug resistance and inform more efficacious dosing regiments (2, 3). To determine such variables, new experimental platforms are needed that accurately recapitulate salient characteristics of the tumor microenvironment.

By integrating strategies from tissue engineering, microfabrication, and cancer biology, biologically-inspired culture models (a.k.a. tumor surrogates) enable studies of physicochemical disease dynamics across multiple scales (4, 5). Tissue engineering technologies, including biomaterials, scaffold fabrication techniques, and bioreactor design, allow facile manipulation of tissue-level phenomena such as culture dimensionality, cell-cell and cell-extracellular matrix (ECM) interactions, and soluble factor transport and signaling. Complementing these tools, microfabrication principles can exert exquisite control over the chemical and physical environment on the cellular scale, for example via incorporation of microfluidic channels or precise variation

of mechanical and topographical properties, respectively (6, 7). Hence, the combination of tissue engineering and microfabrication affords the development of novel *in vitro* approaches to quantitatively assess constitutive microenvironmental features that are frequently neglected by conventional tissue culture methods or obscured by the complexity of *in vivo* models (8-10). Moreover, these platforms may interface in real-time with sensitive analytical instrumentation, such as confocal microscopy or mass spectrometry, for unprecedented access to cellular and biomolecular dynamics (11, 12).

Here, we briefly introduce prominent characteristics of the tumor microenvironment, describe current state-of-the-art *in vitro* technologies to quantify these phenomena, and provide a perspective on future opportunities for micro-engineered tumor platforms in cancer research and clinical application with the ultimate goal of illuminating the multiscale regulation of cancer pathogenesis and therapy response.

Biological and physical hallmarks of the tumor microenvironment

Carcinomas comprise the majority of all solid tumors, and their malignancy is driven not only by the genetic transformation of epithelial cells, but also by the remodeling of contiguous stromal tissue to foster growth, metastasis, and therapy resistance (13-15). This tumor stroma derives from reciprocal tumor-host cell crosstalk, whereby tumor cell-secreted growth factors and cytokines stimulate the otherwise quiescent host cells to initiate a variety of processes, including desmoplasia and angiogenesis (16-19). The ensuing physiological changes resemble wound healing processes; however, tumor-associated stromal cells undermine tissue homeostasis rather than normalizing it, eliciting the analogy that tumors function as ‘wounds that do not heal’ (20, 21). As a result, an asymmetric distribution of physical and chemical cues emerges, comprising spatiotemporally altered matrix mechanical properties and mass transport (18, 19, 22). Below, we

describe these pathological consequences of tumor-stroma interactions from both biological and physical science perspectives and summarize microscale tissue engineering strategies to explore the underlying mechanisms.

Deranged tissue organization: Dimensionality and ECM characteristics

Structural ramifications of malignant transformation begin with the transition from 2D to 3D tissue architecture caused by the hyper-proliferation of epithelial cells. Healthy epithelia are generally organized in polarized sheet structures, with a basolateral surface supported by a basement membrane, an apical lumen with secretory function, and tight junctions between neighboring cells in a confluent pseudo-monolayer (Fig. 1). Disruption of this arrangement by aberrant proliferation, loss of E-cadherin-mediated cell-cell contact, or secretion of matrix-degrading enzymes such as matrix metalloproteinases (MMPs) subverts epithelial homeostasis and promotes carcinogenesis (23-26). Independent of other environmental conditions, this dimensional shift affects tumor cell growth (27, 28), migration (29, 30), signaling (31), and drug response (32, 33). Conversely, restoration of appropriate geometrical context, or inhibition of integrin receptors that mediate 3D cellular engagement to the ECM, can normalize the malignant phenotype of transformed epithelial populations, in part by interrupting bidirectional cross-talk between growth factor and cell adhesion receptors {Wang 1998; Kenny 2003; Weigelt 2010}. For these reasons, appropriate choice of culture dimensionality is critical for the development of and interpretation of results collected with biomimetic tissue constructs in cancer research (9, 34, 35).

Moreover, ECM properties, such as elasticity, nano- and microstructure, as well as composition affect tumorigenesis and need to be considered when designing matrices for *in vitro* culture models (36-38). Namely, desmoplastic matrix remodeling by tumor-associated myofibroblasts entails the assembly of a highly dense ECM (Fig. 1), whose physicochemical

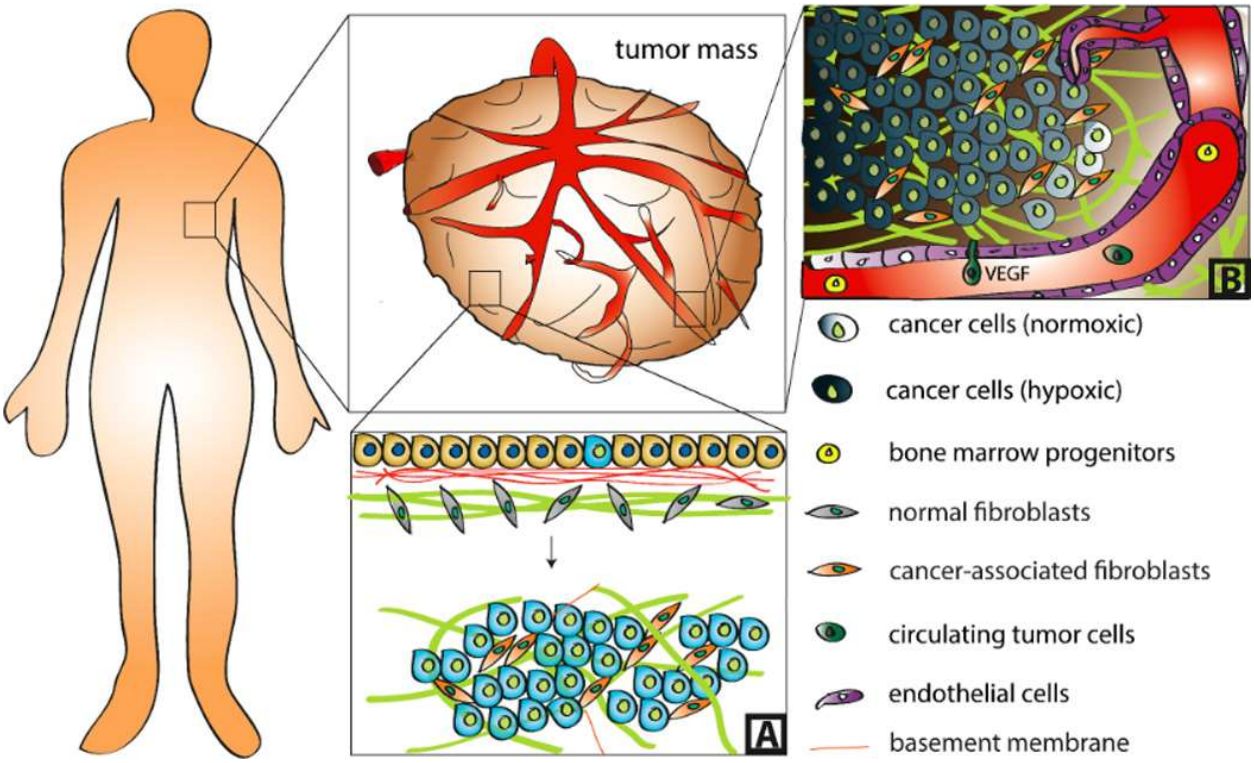

Fig. 1. Biological and physical changes inherent to the tumor microenvironment. Tumors are characterized by aberrant tissue organization (A) and mass transport (B). While normal epithelia form sheets that adhere to a layer of basement membrane, which is anchored to the underlying stroma, malignant transformation perturbs this architecture and leads to the development of a 3D tumor mass. During this process, basement membrane integrity is compromised and ECM composition, conformation, and mechanical properties are altered due in part to transformation of normal fibroblasts into cancer-associated fibroblasts (A). Excessive tumor cell proliferation results in diffusion-limited oxygen and waste transport and consequential development of hypoxia and acidosis. This induces secretion of pro-angiogenic factors including VEGF that activate neovascularization via angiogenesis and recruitment of bone marrow progenitors. These newly formed vessels, in turn, enable tumor growth and metastasis by providing vascular conduits for nutrients and extravasated circulating tumor cells, respectively (B).

attributes enhance malignancy through morphogenic deregulation, tumor cell proliferation, vascular recruitment, and myofibroblastic differentiation (19, 39, 40). Mediated by increased deposition, unfolding, and crosslinking of fibrillar adhesion proteins (e.g. fibronectin, collagen type I), desmoplastic stiffening contributes to epithelial transformation in part through integrin-mediated increases in cell contractility (41, 42). This change in cell contractility, in turn, can directly and indirectly alter gene expression via altering transcription factor activity and the release of matrix-bound, pro-tumorigenic growth factors (e.g., transforming growth factor beta; TGFbeta), respectively (43, 44). Similarly, changes in the distribution of pore sizes, chemical composition, and fiber arrangement due to myofibroblastic remodeling can control aspects of tumor cell phenotype such as adhesion, mechanics, and motility (30, 45). Recapitulating these diverse physical aspects of biological matrices comprises a critical design criterion for tissue-engineered tumor models.

Engineered models to evaluate the effect of tissue dimensionality and ECM interactions

Microfabrication techniques in conjunction with natural or artificial ECM molecules afford investigations into the role of 3D cell-cell and cell-ECM interactions (38, 46-48). Originally pioneered on planar surfaces, micropatterning of natural ECM molecules (e.g. fibronectin) onto cell culture substrates by polydimethylsiloxane (PDMS)-based microcontact printing or soft lithography has been extensively utilized to interrogate topographical and biochemical effects on individual cells and small cell populations (10, 49). For example, such studies were used to decouple the effects of cell shape, spreading, and receptor ligation on cell fate (50). However, the sagging and swelling of PDMS in solution limits homogeneous patterning of large surface areas as necessary for proteomic or transcriptional analysis of protein expression. Parylene patterning can address this challenge and has enabled seeding of individual cells or small cell clusters on

fibronectin-functionalized surfaces of varying area to examine the role of direct cell-cell contact on tumor cell behavior (51). Although both techniques have provided numerous insights regarding cell-matrix and cell-cell interactions, by maintaining monolayer cell culture, they neglect authentic tissue architecture. In contrast, fully-enclosed 3D tissue culture has proved its utility for mimicking the structural environment of tumor-associated stroma and subsequent effects on disease progression. For example, organotypic culture arrays comprising lithographically-defined epithelial tissue structures sandwiched between layers of collagen were used to study geometrical influences on neoplastic progression (52). Likewise, hydrogel-based 3D microwell arrays have emerged as a robust platform to examine cell culture space and intercellular interactions, including their effects on drug response {Charnley 2009, Håkanson 2012}. One particular advantage of microscale 3D matrices is the reduction of diffusion barriers to allow homogeneous, temporally-controlled stimulation of cell populations (53). Furthermore, such systems can be incorporated with lithographically defined microchannels to mimic cellular confinement within 3D tissue, an approach which has revealed that lower ECM porosity due to increased stiffness may promote cell migration (54).

In order to explore the role of matrix composition, structure, and mechanical properties in cancer pathogenesis, biomaterials from regenerative medicine and drug delivery can be adapted to microfabricated culture systems discussed above (55), including complex mixtures of biological ECM (e.g., Matrigel®, a basement membrane preparation isolated from Engelbreth-Holm-Swarm murine sarcoma) and isolated ECM components from animal tissue (e.g., collagen I, fibronectin) (56). These natural biomaterials offer unique advantages due to their inherent provision of cell binding sites and the fact that porosity, fiber structure, and stiffness can be readily tailored via adjusting gelling conditions such as temperature, concentration, gel thickness, and media

composition (38, 47, 57). Nevertheless, natural polymers suffer from batch to batch variations and provide limited parameter space for the above-described physical variables. In fact, their modulation often simultaneously alters other materials properties that independently affect cell behavior (e.g. concentration changes affect stiffness but also density of adhesion ligands and porosity) (58, 59). Artificially combining functional protein building blocks via protein engineering strategies provides an attractive route to overcome these shortcomings and generate biological materials systems with unprecedented control over cell adhesion, proteolytic degradation, or stiffness (60). However, the fabrication of such molecules is highly specialized and therefore frequently not amenable for routine applications.

Biologically-inspired partially or fully synthetic hydrogels may help to overcome some of the inherent limitations of natural biomaterials. They can be produced in large quantities, a highly reproducible manner, and are increasingly used by both the cancer biology and engineering community to selectively tune the physicochemical composition and structure of cell culture matrices. For example, synthetically modified fibrin or hyaluronic acid have been developed previously to guide endothelial cell behavior for regenerative approaches (61, 62), but are also relevant in the context of cancer as the deposition of these ECM components is increased during tumorigenesis (63, 64). Modifying natural ECM components takes advantage of the inherent cell affinity to the polymer backbone, while introducing selective variations of matrix mechanical properties and degradation via synthetic side chains {Hanjaya-Putra 2012; Anathanarayanan 2011}. Polyacrylamide gels covalently coated with ECM components provide another system to independently control elastic moduli and ECM ligand presentation and revealed mechanoregulatory mechanisms of perturbed epithelial tissue homeostasis (36). These substrates are widely utilized by many labs for 2D studies, but as they cannot be remodeled by cells,

translation to 3D culture formats or animal studies (i.e., for verification of *in vitro* data) is limited. Furthermore, recent findings indicate that stiffness-related changes in porosity of polyacrylamide gels may affect the conformation of covalently attached cell adhesion proteins, which, in turn, could also regulate cell behavior (65). Poly(ethylene glycol) (PEG)-based scaffolds provide an attractive alternative as not only the stiffness of these materials can be readily adjusted, but also the density of conformation-independent cell adhesion sites and/or proteolytically degradable crosslinkers ultimately enabling studies of cellular invasion in 3D culture formats (66). Modifications of PEG-based materials in which molecular moieties have been introduced to enable *in situ* photo-degradation or crosslinking are particularly exciting because this approach affords an opportunity to determine cellular response to dynamic changes of matrix stiffness that may result from tumor development or drug treatments (67, 68).

Cancer, A mass transport problem

Within the tumor stroma, convective and diffusive forces are intrinsic mediators of the biochemical landscape that sustains neoplastic development (35, 69, 70). The predominant conduits of mass transport, microvascular networks define the spatial distribution of oxygen, nutrients, endocrine signals, and therapeutic drugs. Moreover, as a consequence of diffusion-limited nutrient and waste transport, the absence of a functional vasculature regulates the development of hypoxia and acidosis during tumor initiation and at interior regions of advanced cancers (Fig. 1). These microenvironmental conditions promote malignancy by driving the selection of cells that mitigate oxidative stress via autonomous energy production, typically through glycolysis (71-73). Metabolic rewiring, known as the ‘Warburg effect’, can further enhance the proliferative, metastatic, and therapy-resistant behavior of the adapted cell population. Furthermore, hypoxia is known to dramatically alter the secretion profile of tumor cells,

particularly by inducing pro-angiogenic factors (e.g. vascular endothelial growth factor [VEGF], interleukin-8 [IL-8], basic fibroblast growth factor [bFGF]) that promote angiogenesis and vasculogenesis via the recruitment of adjacent blood vessels and bone marrow-derived progenitor cells, respectively (74). This process of sustained neovascularization constitutes a hallmark capability of cancer and, by surmounting nutrient limitations and providing vascular conduits, enables tumor growth and metastasis (75). However, compared to healthy vasculature, tumor-associated blood vessels exhibit increased leakiness, tortuosity, instability via absence of mural cells, and subsequent aberrant fluid mechanical forces {Hashizume 2000; Nagy 2008, 2012}. As a result, they fail to normalize the hypoxia/acidosis of the tumor core, but instead cause spatial and temporal variations of these conditions (76). Notably, by contributing to elevated fluid pressure in the tumor, dysfunctional vasculature compromises drug delivery and modulates interstitial flow at the tumor margins (77). Pressure gradients and subsequent drainage from the tumor perimeter directly and indirectly guide the behavior of tumor and stromal cells by redistributing morphogen and chemokine gradients and by mechanically-inducing stromal differentiation (78-80). From a physical science perspective, these integrated fluid mechanical forces establish the prevailing biochemical profile of the tumor microenvironment and direct disease progression (81). Likewise, tools to deconvolute convection-diffusion-reaction kinetics, paracrine signaling, vascular supply, and interstitial fluid mechanics are required for the comprehensive study of pathophysiological transport processes, including metabolic maintenance, drug delivery, and evolution of therapy resistance (82).

Biomimetic approaches to study tumor-associated transport phenomena

Whereas conventional *in vitro* technologies lack spatiotemporal variations of soluble chemicals, and animal studies prohibit quantitative control over mass transport, microfabricated

tissues can effectively access these critical pathological parameters (83). Therefore, researchers have employed microfabrication technologies to mimic physiological transport processes, including perfusion for metabolic maintenance, diffusion-controlled soluble factor gradients, convective transport through microfluidic conduits, and more recently, tissue-engineered biomimetic vasculature (7, 84, 85). For example, microfabrication technologies have surmounted diffusion-limited metabolic maintenance in 3D culture by the development of microscale perfusion bioreactors and by providing access to scaffold geometries within the Krogh length (i.e., to control hypoxia-associated effects in culture studies) (86, 87). From the profusion of tissue-engineered, microfabricated assays with well-controlled tissue structure and transport conditions, surprising data has emerged. For example, studies comparing 2D-cultured tumor cells with tumor cells incorporated within microfabricated hydrogel disks have revealed that changes in tissue dimensionality may be similarly if not even more important to the proangiogenic capability of tumor cells as oxidative stress (88). Moreover, by the tuning of physical and chemical stimuli as well as cellular complexity, microfabricated platforms afford a unique opportunity to examine both the isolated and integrated effects of multiplexed parameters.

Another aspect to consider is that cell responses to gradients of soluble factors, for example, may be different in 2D vs. 3D culture systems, and not only depend on the specific morphogen applied, but also its combination with other molecules as well as the specific spatial and temporal dynamics of exposure. Two-dimensional microfluidic models have proved their utility in the generation of stable, linear concentration gradients to independently evaluate directional responses to biomolecular assymetries, such as chemotaxis and morphogenesis {Jeon 2002; Selimović 2011; Saadi 2007; Dertinger 2001; Georgescu 2008; Mak 2011}. Three-dimensional microfluidic gradient generators with single- or multi-layered factor gradients will

additionally be able to distinguish biochemical synergies in a physiologically relevant tissue context, which is essential for the study of tumor cell migration and perturbed morphogenesis {Choi 2007; Chung 2009, 2010; Shamloo 2008, 2010; Shin 2011}.

While most of the current approaches are still relatively low-throughput, automated 3D microfluidic co-culture arrays may revolutionize this limitation. Such systems will be critical for economically more effective low-volume, high-throughput drug screening, and have already proved efficacious for interrogating tumor-stromal signaling within 3D culture formats without typical drug-diffusion limitations (89-92). By coupling biomaterials with microfabrication, further 3D platforms have emerged to study cellular responses to spatial distribution of physical and chemical stimuli. For example, collagen-based microfluidic channels enable studies of endothelial sprouting in response to VEGF gradients (93, 94) and the presence of pericytes (95), and aqueous two-phase systems allow patterning of cells as well as delivery of biochemical factors (96). Together, these systems can recapitulate the heterogeneity of tumor and stromal cell-secreted factors, drug distribution and reaction kinetics, or the gradients of hypoxia and acidosis described above.

In the particular case of tumor angiogenesis, tissue-engineered microvascular constructs will undoubtedly advance the development of artificial tumor surrogates and can be fabricated by a variety of techniques (Fig. 2). Whereas some models employ surface-cultured endothelial monolayers to study tumor-endothelial signaling and angiogenic invasion independent of transport effects, other assays generate fully-enclosed endothelial networks in remodelable matrices (53, 95, 97-102). For the fabrication of the latter, microfluidic conduits may be incorporated into biomimetic hydrogels through a variety of approaches including pull-through technique, sacrificial fiber molds, modular assembly and soft lithography (87, 103-106). Incorporating such

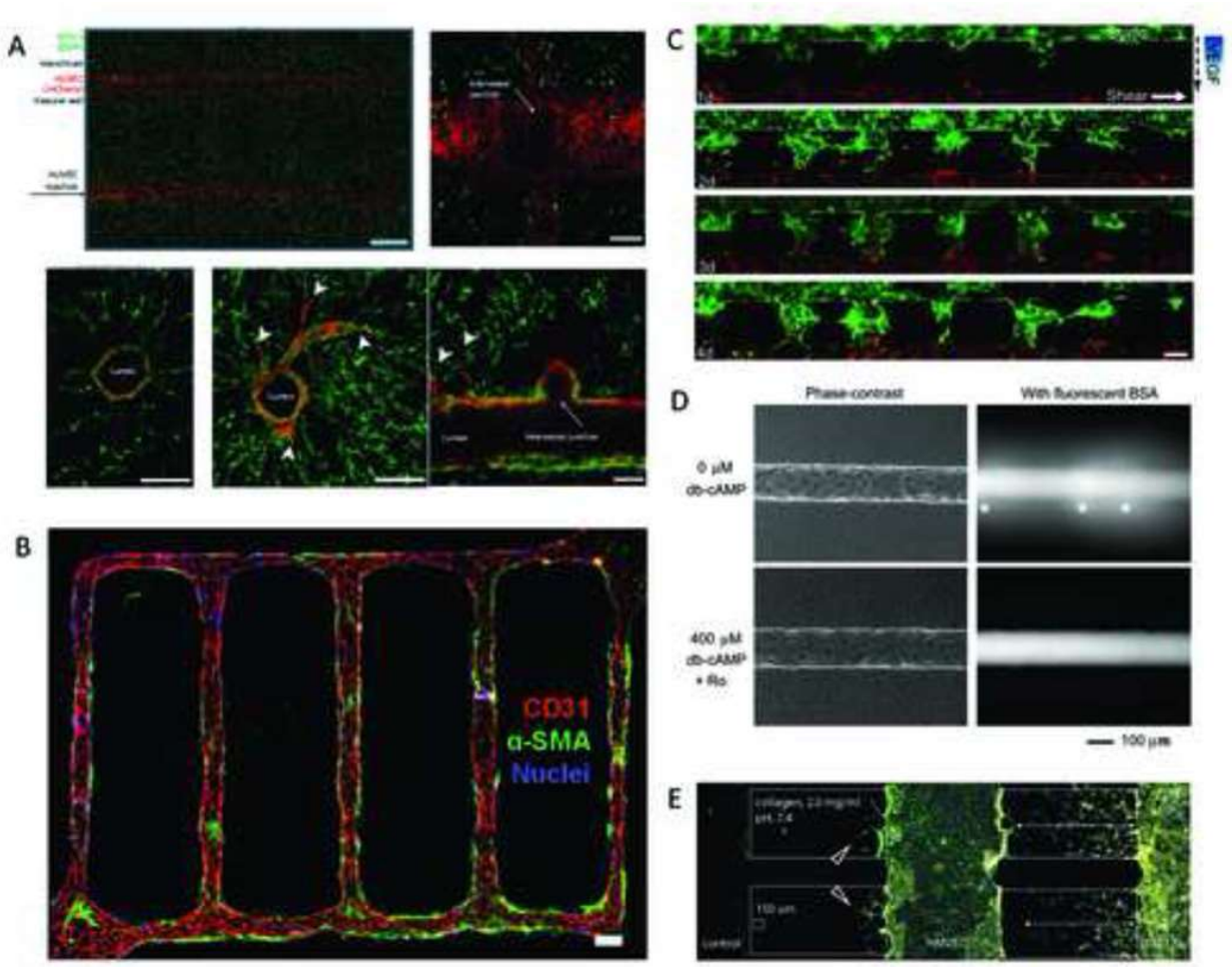

Fig. 2. Microfabrication techniques to recapitulate vascular networks *in vitro.* Cylindrical 3D networks can be incorporated into hydrogels using carbohydrate glass as sacrificial templates. Labeled human umbilical vein endothelial cells (HUVECs) seeded into these channels form perfusable vascular networks that can be induced to sprout (arrowheads), while incorporation of a second labeled cell type (e.g.10T1/2 cells) into the hydrogel bulk permits recapitulation of stromal tissue. Scale bars represent 1 mm and 200 μm (Miller 2012) (A). Similarly, lithographically patterned microfluidic devices may be used to generate functional vascular networks within remodelable hydrogels. In particular, incorporation of pericytes (indicated by α-SMA staining) into the bulk leads to the recruitment of these cells to HUVEC-lined vessels (indicated by CD31 staining) and their corresponding stabilization. Scale bar, 100 μm (Zheng 2012) (B). Microdevices composed of two parallel endothelial cell-coated channels (GFP-labeled HUVECs in top and dsRed-labeled HUVECs in bottom channel) separated by an invadable collagen matrix allow studies of vascular anastomosis in response to VEGF gradients as well as interstitial flow (dashed arrow) and axial shear flow (solid arrow). Scale bar, 100 μm (Song 2012) (C). Microvascular structures generated in microfluidic type I collagen gels using a pull-through technique can be stabilized by cyclic AMP (cAMP)-elevating agents as shown via perfusion of endothelial cell-coated vessels with fluorescently labeled BSA; *indicates focal leaks. Scale bar, 100 μm (Wong 2010) (D). Culture of stromal cells (10T1/2) and endothelial cells (HMVEC) in adjacent channels separated by a 3D collagen scaffold allows studying the effect of bi-directional paracrine signaling on invasion and sprouting behavior of these cells, respectively. 10T1/2 invaded at an enhanced rate in the presence of HMVECs. Additionally, HMVECs formed sprouts towards the blank collagen scaffold located in the left channel (red arrowheads), whereas vessels were stabilized in regions directed towards 10T1/2s (Chung 2009) (E). Images are modified and reproduced with permissions from the publishers.

microfabricated, endothelial-coated vessels into engineered tumor models will undeniably improve *in vitro* studies of sprouting angiogenesis, endothelial barrier function, and drug delivery {Zheng 2012, Chung 2009, Zervantonakis 2011}. In fact, pulsed injections of fluorophores or fluorescently-labeled proteins as mimics of small and large therapeutic molecules allows the measurement of their diffusivity and permeability from microengineered vasculature and permits the analysis of changes in leakiness due to exposure to excess concentrations of proangiogenic molecules (95). Likewise, these devices can be utilized in the quantification of diffusion-reaction metabolic processes in 3D and determination of cell growth rate constants, which are significantly different from suspension and monolayer culture (86).

In addition to solute delivery, microvascular models can be used to introduce a permissive mechanical regulator of the microenvironment, namely convective transport via interstitial flow (9, 107). In fact, interstitial flow can affect tumor progression via multiple mechanisms; for example, through biasing the distribution of cell-secreted factors, forcing mechanical aberrations of the tumor microenvironment by promoting stroma remodeling, and regulating endothelial sprouting (78-80, 108, 109). Integrated in tumor-engineered platforms selective perfusion of microvascular network recreates inherent pathological properties such as hypoxia/acidosis, compromised drug delivery, edema, and in some cases the direct visualization of migration and intravasation. By quantifying hitherto unexplored responses to transport processes, this unprecedented control of multiple-parameter *in vitro* models is indispensable for the improved understanding of tumor growth and clinical treatment.

Future opportunities

Over the past decade or so, reductionist approaches have helped to decipher the biological and physicochemical complexity of tumors, but as the discipline of tumor engineering matures and

technologies improve, we encounter the question of what can be gained by adding complexity. We propose applications for microengineered tumor-mimetic assays in drug development and delivery strategies, simulation of whole-body physiologically-based pharmacokinetic models, and screening of rationally-designed therapeutic regimens. Furthermore, experimental integration of convective-diffusion-reaction processes will provide unprecedented access to quantitative parameters that are instrumental to the validation of comprehensive computational models describing the intra- and extracellular signaling networks underlying tumorigenesis.

Engineering of functional, fully-human and/or patient-specific micro-tissues

The immediate advantage of complex microengineered tumor models derives from the opportunity to observe interactions between various constituents of the tumor microenvironment in real time with implications for both basic research and drug development. Whereas certain physicochemical parameters may be independently important, it is likely that combinatorial effects accentuate or attenuate their functional significance. Thus, robust platforms that can controllably add or subtract layers of physiological complexity will be indispensable for interrogating variates and co-variates in cancer therapy. For example, the emergence of drug resistant subpopulations may rely on microenvironmental signatures dictated by the cellular and acellular heterogeneity of the tumor mass; identification of the underlying molecular mechanisms has the potential to identify novel therapeutic targets that may improve current therapeutic interventions (110-112). Likewise, tumor-engineered assays will provide unprecedented ability to disambiguate the indirect effects of targeted cancer drugs. As one poignant example, the underwhelming clinical benefit of VEGF-inhibiting, anti-angiogenic therapies has received considerable attention (113, 114). Low therapeutic efficacy is due in part to a poor understanding of the mechanisms underlying vessel growth and drug response as well as the forced upregulation of alternative proangiogenic factors

(e.g., bFGF and IL-8) that render vessels VEGF-independent (74, 115-118). To explore these questions, our lab is developing microengineered tumor models to determine cooperative parameters that may control endothelial cell sprouting, including cell density, vessel geometry, and endothelial cell autocrine signaling mechanisms (119). As biomimetic vascular assays continue improving, the pros and cons of anti-angiogenic therapy and drug delivery (e.g. mechanisms of actions, delivery mode, dosing intervals) will become more apparent and therapies can be adjusted (118, 120-122).

Validation of whole-body PBPK-PD models

Knowledge and treatment of the primary tumor site only locally palliates a more pernicious systemic disorder. Through metastasis and colonization, circulating tumor cells can infiltrate distant tissues, often with morbid consequences; similarly, organ distribution and side effects are critical considerations during drug development. Therefore, pre-clinical tools that contribute to holistic understanding of both disease progression and treatment will benefit the development of better pharmaceuticals and dosing strategies. To this end, microengineered tumor cultures may integrate with current "body-on-a-chip" technologies for comprehensive culture models of disease progression across multiple tissues {Esch 2011; Sin 2004; Sung 2010; Vivaraidya 2004}. Such systems have already been used to validate whole-body physiologically-based pharmacokinetic (PB-PK) models and improve estimation of critical parameter such as Theile modulus or Peclet number, dimensionless coefficients that describe relative rates of transport and reaction kinetics, and measurement of variability and co-variation with disease or treatment among different organs (123). These systems will potentially contribute to the prediction of metastatic homing, dosing regimens, and side-effects, or selection of patients for specific clinical trials (124). For example, priming an *in vitro* tumor with downstream osteogenic or pulmonary compartments to resemble

the pre-metastatic niche may help determine mechanisms of organ homing, including characteristics or organ-specific tropisms such as stages of lung inflammation due to smoking (Fig. 3A-B). In addition, microfluidic PB-PK models can inform pharmacodynamic computational models and assist in the extrapolation of such models to animal and human predictions (Fig. 3C). While such devices have been used in toxicity and dosing studies (125, 126), testing of new cancer therapies may also benefit from this technology. Particularly, it could help to better understand the current disconnect between promising preclinical data and lack of clinical efficacy of new compounds, as well as inform dosing strategies and combination therapies to optimize biological response.

In vitro platforms for integrative mathematical oncology

A final application for tissue-engineered tumor surrogates lies in the realization of comprehensive mathematical cancer models (127). By selective incorporation of individual or multiplexed physiological components of the tumor microenvironment, *in vitro* tumor models can be used to determine critical *in silico* parameters, including correlation or interaction coefficients between various elements (82, 128-131). For example, it is known that integrin engagement, matrix stiffness, and growth factor receptor signaling are intimately linked, but quantitative parameters and modeling of co-variation are yet undetermined. Tissue-engineered models could test predictive behaviors and confirm computational hypotheses regarding disease dynamics. One example where such systems may prove beneficial is the modeling of tumor evolution, by which malignant or resistant populations propagate by somatic selection in resource-constrained tissues (132-135). Computational models of this process show that microenvironmental conditions are key determinants of population phenotype. This observation is consistent with emerging appreciation for the local heterogeneity within primary tumor site and in distant metastases, and it

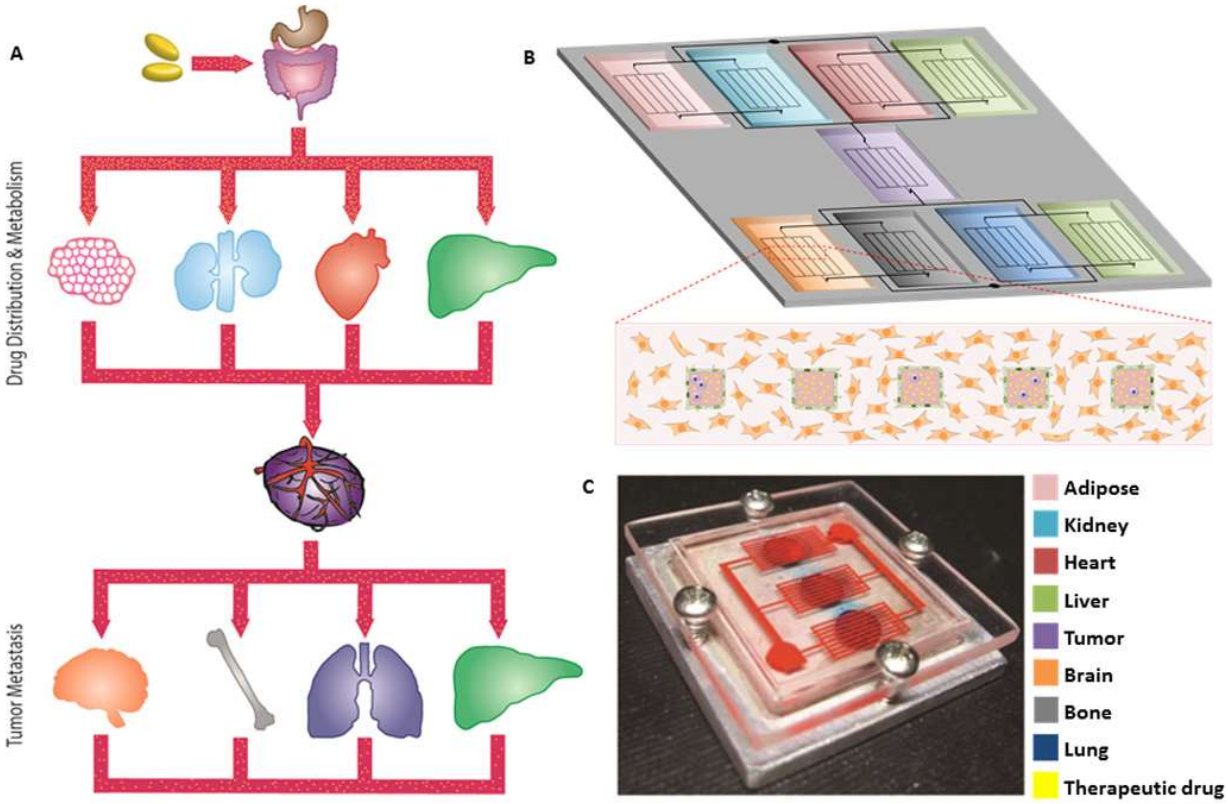

Fig. 3. Integration of microengineered tumor cultures with "body-on-a-chip" models. Cancer progression and therapy are controlled by systemic interactions. For example, endocrine signaling between tumors and distant tissues such as brain, bone, lungs, and liver regulate the tropism of certain cancers to particular sites (e.g. breast cancer to bone). Additionally, the efficacy of anti-cancer therapies is regulated by systemic distribution and metabolism in various tissues and organs such as adipose tissue, kidney, heart and liver. Therefore, connecting multiple organ components via vascular conduits in 'cancer on a chip' models has the potential to improve our understanding of metastatic homing mechanisms of tumor cells as well as drug therapy (A–B). Already, microscale cell culture analogs have been used to improve the predictability of pharmacokinetic-pharmacodynamic models in vitro (Sung 2010) (C). This platform, comprising bone, liver, and tumor compartments, was used to assess the toxicity of 5-fluorouracil in a 3D tissue context with multi-organ interactions. The combination of in vitro experimental data and mathematical PB-PK modeling may improve screening for drug development, as well as inform our understanding of cancer pathogenesis during therapy. Images are reproduced with permission from the publisher.

has spawned new hypotheses for therapeutic dosing regiments based on ecological principles {Basanta 2012, 2012; Maruskyk 2012; Navin 2011; Snuderl 2011}. However, such simulations are difficult to examine biologically. *In vitro* systems that include diverse cell populations and heterogeneous physicochemical environment would help validate the mathematical models and perhaps elucidate novel parameters to improve such systems.

Conclusions

Microfabrication techniques have the potential to yield important new insights into the pathogenesis of cancer. While great progress has been made in developing model systems for deciphering mechanisms of tumorigenesis, improved throughput and applicability by non-engineers (e.g. cancer biologists and clinicians) will further enhance the significance of these platforms. Moreover, exploring currently unrealized opportunities of recapitulating cancer complexity will help in elucidating molecular, cellular, tissue, and systems level phenomena that could be explored in the future for more efficacious clinical therapies.

References

1. Michor F, Liphardt J, Ferrari M, & Widom J (2011) What does physics have to do with cancer? *Nature Reviews Cancer* 11(9):657-670.

2. Foo J, Chmielecki J, Pao W, & Michor F (2012) Effects of Pharmacokinetic Processes and Varied Dosing Schedules on the Dynamics of Acquired Resistance to Erlotinib in EGFR-Mutant Lung Cancer. *Journal of Thoracic Oncology* 7(10):1583-1593.

3. Podlaha O, Riester M, De S, & Michor F (2012) Evolution of the cancer genome. *Trends in Genetics* 28(4):155-163.

4. Ghajar CM & Bissell MJ (2010) Tumor Engineering: The Other Face of Tissue Engineering. *Tissue Engineering Part A* 16(7):2153-2156.

5. Wlodkowic D & Cooper JM (2010) Tumors on chips: oncology meets microfluidics. *Current Opinion in Chemical Biology* 14(5):556-567.

6. Huh D, Hamilton GA, & Ingber DE (2011) From 3D cell culture to organs-on-chips. *Trends in Cell Biology* 21(12):745-754.

7. Walker GM, Zeringue HC, & Beebe DJ (2004) Microenvironment design considerations for cellular scale studies. *Lab on a Chip* 4(2):91-97.

8. Burdett E, Kasper FK, Mikos AG, & Ludwig JA (2010) Engineering Tumors: A Tissue Engineering Perspective in Cancer Biology. *Tissue Engineering Part B-Reviews* 16(3):351-359.

9. Griffith LG & Swartz MA (2006) Capturing complex 3D tissue physiology in vitro. *Nature Reviews Molecular Cell Biology* 7(3):211-224.

10. Khademhosseini A, Langer R, Borenstein J, & Vacanti JP (2006) Microscale technologies for tissue engineering and biology. *Proceedings of the National Academy of Sciences of the United States of America* 103(8):2480-2487.

11. Enders JR, *et al.* (2010) Towards monitoring real-time cellular response using an integrated microfluidics-matrix assisted laser desorption ionisation/nanoelectrospray ionisation-ion mobility-mass spectrometry platform. *Iet Systems Biology* 4(6):416-427.

12. Paguirigan AL, Puccinelli JP, Su X, & Beebe DJ (2010) Expanding the Available Assays: Adapting and Validating In-Cell Westerns in Microfluidic Devices for Cell-Based Assays. *Assay and Drug Development Technologies* 8(5):591-601.

13. Bissell MJ & Radisky D (2001) Putting tumours in context. *Nature Reviews Cancer* 1(1):46-54.

14. Mueller MM & Fusenig NE (2004) Friends or foes - Bipolar effects of the tumour stroma in cancer. *Nature Reviews Cancer* 4(11):839-849.

15. Joyce JA & Pollard JW (2009) Microenvironmental regulation of metastasis. *Nature Reviews Cancer* 9(4):239-252.

16. Kim JB, Stein R, & O'Hare MJ (2005) Tumour-stromal interactions in breast cancer: The role of stroma in tumourigenesis. *Tumor Biology* 26(4):173-185.

17. Ronnov-Jessen L & Bissell MJ (2009) Breast cancer by proxy: can the microenvironment be both the cause and consequence? *Trends in Molecular Medicine* 15(1):5-13.

18. Hanahan D & Coussens LM (2012) Accessories to the Crime: Functions of Cells Recruited to the Tumor Microenvironment. *Cancer Cell* 21(3):309-322.

19. Otranto M, *et al.* (2012) The role of the myofibroblast in tumor stroma remodeling. *Cell Adhesion & Migration* 6(3):203-219.

20. Dvorak HF, Flier J, & Frank H (1986) TUMORS - WOUNDS THAT DO NOT HEAL - SIMILARITIES BETWEEN TUMOR STROMA GENERATION AND WOUND-HEALING. *New England Journal of Medicine* 315(26):1650-1659.

21. Coussens LM & Werb Z (2002) Inflammation and cancer. *Nature* 420(6917):860-867.

22. Fukumura D & Jain RK (2007) Tumor microenvironment abnormalities: Causes, consequences, and strategies to normalize. *Journal of Cellular Biochemistry* 101(4):937-949.

23. Beliveau A, *et al.* (2010) Raf-induced MMP9 disrupts tissue architecture of human breast cells in three-dimensional culture and is necessary for tumor growth in vivo. *Genes & Development* 24(24):2800-2811.

24. Nelson CM & Bissell MJ (2005) Modeling dynamic reciprocity: Engineering three-dimensional culture models of breast architecture, function, and neoplastic transformation. *Seminars in Cancer Biology* 15(5):342-352.

25. Bissell MJ & Hines WC (2011) Why don't we get more cancer? A proposed role of the microenvironment in restraining cancer progression. *Nature Medicine* 17(3):320-329.

26. Chen A, *et al.* (2009) Endothelial Cell Migration and Vascular Endothelial Growth Factor Expression Are the Result of Loss of Breast Tissue Polarity. *Cancer Research* 69(16):6721-6729.

27. Weaver VM, *et al.* (1997) Reversion of the malignant phenotype of human breast cells in three-dimensional culture and in vivo by integrin blocking antibodies. *Journal of Cell Biology* 137(1):231-245.

28. Wang F, *et al.* (1998) Reciprocal interactions between beta 1-integrin and epidermal growth factor receptor in three-dimensional basement membrane breast cultures: A different perspective in epithelial biology. *Proceedings of the National Academy of Sciences of the United States of America* 95(25):14821-14826.

29. Fraley SI, *et al.* (2010) A distinctive role for focal adhesion proteins in three-dimensional cell motility. *Nature Cell Biology* 12(6):598-U169.

30. Zaman MH, *et al.* (2006) Migration of tumor cells in 3D matrices is governed by matrix stiffness along with cell-matrix adhesion and proteolysis. *Proceedings of the National Academy of Sciences of the United States of America* 103(29):10889-10894.

31. Fischbach C, *et al.* (2009) Cancer cell angiogenic capability is regulated by 3D culture and integrin engagement. *Proceedings of the National Academy of Sciences of the United States of America* 106(2):399-404.

32. Dhiman HK, Ray AR, & Panda AK (2005) Three-dimensional chitosan scaffold-based MCF-7 cell culture for the determination of the cytotoxicity of tamoxifen. *Biomaterials* 26(9):979-986.

33. Fischbach C, *et al.* (2007) Engineering tumors with 3D scaffolds. *Nature Methods* 4(10):855-860.

34. Pampaloni F, Reynaud EG, & Stelzer EHK (2007) The third dimension bridges the gap between cell culture and live tissue. *Nature Reviews Molecular Cell Biology* 8(10):839-845.

35. Kenny PA, Nelson CM, & Bissell MJ (2006) The ecology of tumors. *Scientist* 20(4):30-35.

36. Paszek MJ, *et al.* (2005) Tensional homeostasis and the malignant phenotype. *Cancer Cell* 8(3):241-254.

37. Discher DE, Janmey P, & Wang YL (2005) Tissue cells feel and respond to the stiffness of their substrate. *Science* 310(5751):1139-1143.

38. Carey SP, Kraning-Rush CM, Williams RM, & Reinhart-King CA (2012) Biophysical control of invasive tumor cell behavior by extracellular matrix microarchitecture. *Biomaterials* 33(16):4157-4165.

39. Kalluri R & Zeisberg M (2006) Fibroblasts in cancer. *Nature Reviews Cancer* 6(5):392-401.

40. Chandler EM, *et al.* (2012) Implanted adipose progenitor cells as physicochemical regulators of breast cancer. *Proceedings of the National Academy of Sciences of the United States of America* 109(25):9786-9791.

41. Chandler EM, Saunders MP, Yoon CJ, Gourdon D, & Fischbach C (2011) Adipose progenitor cells increase fibronectin matrix strain and unfolding in breast tumors. *Physical Biology* 8(1).

42. Levental KR, *et al.* (2009) Matrix Crosslinking Forces Tumor Progression by Enhancing Integrin Signaling. *Cell* 139(5):891-906.

43. Hinz B (2009) Tissue stiffness, latent TGF-beta1 activation, and mechanical signal transduction: implications for the pathogenesis and treatment of fibrosis. *Current rheumatology reports* 11(2):120-126.

44. Mammoto A, *et al.* (2009) A mechanosensitive transcriptional mechanism that controls angiogenesis. *Nature* 457(7233):1103-U1157.

45. Pathak A & Kumar S (2011) From Molecular Signal Activation to Locomotion: An Integrated, Multiscale Analysis of Cell Motility on Defined Matrices. *Plos One* 6(3).

46. Stenzel KH, Miyata T, & Rubin AL (1974) COLLAGEN AS A BIOMATERIAL. *Annual Review of Biophysics and Bioengineering* 3:231-253.

47. Roy R, Boskey A, & Bonassar LJ (2010) Processing of type I collagen gels using nonenzymatic glycation. *Journal of Biomedical Materials Research Part A* 93A(3):843-851.

48. Pederson AW, Ruberti JW, & Messersmith PB (2003) Thermal assembly of a biomimetic mineral/collagen composite. *Biomaterials* 24(26):4881-4890.

49. Whitesides GM, Ostuni E, Takayama S, Jiang XY, & Ingber DE (2001) Soft lithography in biology and biochemistry. *Annual Review of Biomedical Engineering* 3:335-373.

50. Tien J, Nelson CM, & Chen CS (2002) Fabrication of aligned microstructures with a single elastomeric stamp. *Proceedings of the National Academy of Sciences of the United States of America* 99(4):1758-1762.

51. Tan CP, *et al.* (2009) Parylene peel-off arrays to probe the role of cell-cell interactions in tumour angiogenesis. *Integrative Biology* 1(10):587-594.

52. Nelson CM, Inman JL, & Bissell MJ (2008) Three-dimensional lithographically defined organotypic tissue arrays for quantitative analysis of morphogenesis and neoplastic progression. *Nature Protocols* 3(4):674-678.

53. Raghavan S, *et al.* (2010) Decoupling diffusional from dimensional control of signaling in 3D culture reveals a role for myosin in tubulogenesis. *Journal of Cell Science* 123(17):2877-2883.

54. Pathak A & Kumar S (2012) Independent regulation of tumor cell migration by matrix stiffness and confinement. *Proceedings of the National Academy of Sciences of the United States of America* 109(26):10334-10339.

55. Tibbitt MW & Anseth KS (2009) Hydrogels as Extracellular Matrix Mimics for 3D Cell Culture. *Biotechnology and Bioengineering* 103(4):655-663.

56. Patterson J, Martino MM, & Hubbell JA (2010) Biomimetic materials in tissue engineering. *Materials Today* 13(1-2):14-22.

57. Wheeldon I, Ahari AF, & Khademhosseini A (2010) Microengineering Hydrogels for Stem Cell Bioengineering and Tissue Regeneration. *Jala* 15(6):440-448.

58. Miron-Mendoza M, Lin X, Ma L, Ririe P, & Petroll WM (2012) Individual versus collective fibroblast spreading and migration: Regulation by matrix composition in 3D culture. *Experimental Eye Research* 99:36-44.

59. Savina IN, Dainiak M, Jungvid H, Mikhalovsky SV, & Galaev IY (2009) Biomimetic Macroporous Hydrogels: Protein Ligand Distribution and Cell Response to the Ligand Architecture in the Scaffold. *Journal of Biomaterials Science-Polymer Edition* 20(12):1781-1795.

60. Romano NH, Sengupta D, Chung C, & Heilshorn SC (2011) Protein-engineered biomaterials: Nanoscale mimics of the extracellular matrix. *Biochimica Et Biophysica Acta-General Subjects* 1810(3):339-349.

61. Ehrbar M, Metters A, Zammaretti P, Hubbell JA, & Zisch AH (2005) Endothelial cell proliferation and progenitor maturation by fibrin-bound VEGF variants with differential susceptibilities to local cellular activity. *Journal of Controlled Release* 101(1-3):93-109.

62. Hanjaya-Putra D, *et al.* (2011) Controlled activation of morphogenesis to generate a functional human microvasculature in a synthetic matrix. *Blood* 118(3):804-815.

63. Nagy JA, Dvorak AM, & Dvorak HF (2012) Vascular Hyperpermeability, Angiogenesis, and Stroma Generation. *Cold Spring Harbor Perspectives in Medicine* 2(2).

64. Slevin M, Kumar S, & Gaffney J (2002) Angiogenic oligosaccharides of hyaluronan induce multiple signaling pathways affecting vascular endothelial cell mitogenic and wound healing responses. *Journal of Biological Chemistry* 277(43):41046-41059.

65. Trappmann B, *et al.* (2012) Extracellular-matrix tethering regulates stem-cell fate. *Nature Materials* 11(7):642-649.

66. Gill BJ, *et al.* (2012) A Synthetic Matrix with Independently Tunable Biochemistry and Mechanical Properties to Study Epithelial Morphogenesis and EMT in a Lung Adenocarcinoma Model. *Cancer Research* 72(22):6013-6023.

67. Kloxin AM, Kasko AM, Salinas CN, & Anseth KS (2009) Photodegradable Hydrogels for Dynamic Tuning of Physical and Chemical Properties. *Science* 324(5923):59-63.

68. Li Q, *et al.* (2006) Biodegradable and photocrosslinkable polyphosphoester hydrogel. *Biomaterials* 27(7):1027-1034.

69. Netti PA, Berk DA, Swartz MA, Grodzinsky AJ, & Jain RK (2000) Role of extracellular matrix assembly in interstitial transport in solid tumors. *Cancer Research* 60(9):2497-2503.

70. Ramanujan S, *et al.* (2002) Diffusion and convection in collagen gels: Implications for transport in the tumor interstitium. *Biophysical Journal* 83(3):1650-1660.

71. Damert A, *et al.* (1997) Up-regulation of vascular endothelial growth factor expression in a rat glioma is conferred by two distinct hypoxia-driven mechanisms. *Cancer Research* 57(17):3860-3864.

72. Cochran DM, Fukumura D, Ancukiewicz M, Carmeliet P, & Jain RK (2006) Evolution of oxygen and glucose concentration profiles in a tissue-mimetic culture system of embryonic stem cells. *Annals of Biomedical Engineering* 34(8):1247-1258.

73. Scott JG, *et al.* (2011) Production of 2-hydroxyglutarate by isocitrate dehydrogenase 1-mutated gliomas: an evolutionary alternative to the Warburg shift? *Neuro-Oncology* 13(12):1262-1264.

74. Hanahan D & Folkman J (1996) Patterns and emerging mechanisms of the angiogenic switch during tumorigenesis. *Cell* 86(3):353-364.

75. Hanahan D & Weinberg RA (2000) The hallmarks of cancer. *Cell* 100(1):57-70.

76. Dvorak HF (2010) Vascular permeability to plasma, plasma proteins, and cells: an update. *Current Opinion in Hematology* 17(3):225-229.

77. Stohrer M, Boucher Y, Stangassinger M, & Jain RK (2000) Oncotic pressure in solid tumors is elevated. *Cancer Research* 60(15):4251-4255.

78. Haessler U, Pisano M, Wu M, & Swartz MA (2011) Dendritic cell chemotaxis in 3D under defined chemokine gradients reveals differential response to ligands CCL21 and CCL19. *Proceedings of the National Academy of Sciences of the United States of America* 108(14):5614-5619.

79. Shieh AC, Rozansky HA, Hinz B, & Swartz MA (2011) Tumor Cell Invasion Is Promoted by Interstitial Flow-Induced Matrix Priming by Stromal Fibroblasts. *Cancer Research* 71(3):790-800.

80. Shields JD, *et al.* (2007) Autologous chemotaxis as a mechanism of tumor cell homing to lymphatics via interstitial flow and autocrine CCR7 signaling. *Cancer Cell* 11(6):526-538.

81. Swartz MA & Lund AW (2012) OPINION Lymphatic and interstitial flow in the tumour microenvironment: linking mechanobiology with immunity. *Nature Reviews Cancer* 12(3):210-219.

82. Basanta D, Gatenby RA, & Anderson ARA (2012) Exploiting Evolution To Treat Drug Resistance: Combination Therapy and the Double Bind. *Molecular Pharmaceutics* 9(4):914-921.

83. Stroock AD & Fischbach C (2010) Microfluidic Culture Models of Tumor Angiogenesis. *Tissue Engineering Part A* 16(7):2143-2146.

84. Whitesides GM (2006) The origins and the future of microfluidics. *Nature* 442(7101):368-373.

85. Tourovskaia A, Figueroa-Masot X, & Folch A (2005) Differentiation-on-a-chip: A microfluidic platform for long-term cell culture studies. *Lab on a Chip* 5(1):14-19.

86. Choi NW, *et al.* (2007) Microfluidic scaffolds for tissue engineering. *Nature Materials* 6(11):908-915.

87. Du Y, *et al.* (2011) Sequential Assembly of Cell-Laden Hydrogel Constructs to Engineer Vascular-Like Microchannels. *Biotechnology and Bioengineering* 108(7):1693-1703.

88. Verbridge SS, *et al.* (2010) Oxygen-Controlled Three-Dimensional Cultures to Analyze Tumor Angiogenesis. *Tissue Engineering Part A* 16(7):2133-2141.

89. Bauer M, Su G, Beebe DJ, & Friedl A (2010) 3D microchannel co-culture: method and biological validation. *Integrative Biology* 2(7-8):371-378.

90. Domenech M, Bjerregaard R, Bushman W, & Beebe DJ (2012) Hedgehog signaling in myofibroblasts directly promotes prostate tumor cell growth. *Integrative Biology* 4(2):142-152.

91. Jongpaiboonkit L, *et al.* (2008) An adaptable hydrogel array format for 3-dimensional cell culture and analysis. *Biomaterials* 29(23):3346-3356.

92. Montanez-Sauri SI, Sung KE, Puccinelli JP, Pehlke C, & Beebe DJ (2011) Automation of Three-Dimensional Cell Culture in Arrayed Microfluidic Devices. *Jala* 16(3):171-185.

93. Chung S, *et al.* (2009) Cell migration into scaffolds under co-culture conditions in a microfluidic platform. *Lab on a Chip* 9(2):269-275.

94. Chung S, Sudo R, Vickerman V, Zervantonakis IK, & Kamm RD (2010) Microfluidic Platforms for Studies of Angiogenesis, Cell Migration, and Cell-Cell Interactions. *Annals of Biomedical Engineering* 38(3):1164-1177.

95. Zheng Y, *et al.* (2012) In vitro microvessels for the study of angiogenesis and thrombosis. *Proceedings of the National Academy of Sciences of the United States of America* 109(24):9342-9347.

96. Frampton JP, Lai D, Sriram H, & Takayama S (2011) Precisely targeted delivery of cells and biomolecules within microchannels using aqueous two-phase systems. *Biomedical Microdevices* 13(6):1043-1051.

97. Miller JS, *et al.* (2012) Rapid casting of patterned vascular networks for perfusable engineered three-dimensional tissues. *Nature Materials* 11(9):768-774.

98. Chrobak KM, Potter DR, & Tien J (2006) Formation of perfused, functional microvascular tubes in vitro. *Microvascular Research* 71(3):185-196.

99. Shamloo A, Xu H, & Heilshorn S (2012) Mechanisms of Vascular Endothelial Growth Factor-Induced Pathfinding by Endothelial Sprouts in Biomaterials. *Tissue Engineering Part A* 18(3-4):320-330.

100. Verbridge SS, Chandler EM, & Fischbach C (2010) Tissue-Engineered Three-Dimensional Tumor Models to Study Tumor Angiogenesis. *Tissue Engineering Part A* 16(7):2147-2152.

101. Wong KHK, Truslow JG, & Tien J (2010) The role of cyclic AMP in normalizing the function of engineered human blood microvessels in microfluidic collagen gels. *Biomaterials* 31(17):4706-4714.

102. Liu Y, Markov DA, Wikswo JP, & McCawley LJ (2011) Microfabricated scaffold-guided endothelial morphogenesis in three-dimensional culture. *Biomedical Microdevices* 13(5):837-846.

103. Golden AP & Tien J (2007) Fabrication of microfluidic hydrogels using molded gelatin as a sacrificial element. *Lab on a Chip* 7(6):720-725.

104. Nichol JW & Khademhosseini A (2009) Modular tissue engineering: engineering biological tissues from the bottom up. *Soft Matter* 5(7):1312-1319.

105. Price GM & Tien J (2009) *Subtractive Methods for Forming Microfluidic Gels of Extracellular Matrix Proteins* pp 235-248.

106. Price GM & Tien J (2011) Methods for Forming Human Microvascular Tubes In Vitro and Measuring Their Macromolecular Permeability. *Biological Microarrays: Methods and Protocols,* Methods in Molecular Biology, eds Khademhosseini A, Suh KY, & Zourob M), Vol 671, pp 281-293.

107. Fukumura D & Jain RK (2008) Imaging angiogenesis and the microenvironment. *Apmis* 116(7-8):695-715.

108. Polacheck WJ, Charest JL, & Kamm RD (2011) Interstitial flow influences direction of tumor cell migration through competing mechanisms. *Proceedings of the National Academy of Sciences of the United States of America* 108(27):11115-11120.

109. Song JW & Munn LL (2011) Fluid forces control endothelial sprouting. *Proceedings of the National Academy of Sciences of the United States of America* 108(37):15342-15347.

110. Gerlinger M, *et al.* (2012) Intratumor Heterogeneity and Branched Evolution Revealed by Multiregion Sequencing. *New England Journal of Medicine* 366(10):883-892.

111. Ene CI & Fine HA (2011) Many Tumors in One: A Daunting Therapeutic Prospect. *Cancer Cell* 20(6):695-697.

112. Nakasone ES, *et al.* (2012) Imaging Tumor-Stroma Interactions during Chemotherapy Reveals Contributions of the Microenvironment to Resistance. *Cancer Cell* 21(4):488-503.

113. Bergers G & Hanahan D (2008) Modes of resistance to anti-angiogenic therapy. *Nature Reviews Cancer* 8(8):592-603.

114. Fukumura D & Jain RK (2007) Tumor microvasculature and microenvironment: Targets for anti-angiogenesis and normalization. *Microvascular Research* 74(2-3):72-84.

115. Folkman J (2007) Opinion - Angiogenesis: an organizing principle for drug discovery? *Nature Reviews Drug Discovery* 6(4):273-286.

116. Bergers G & Benjamin LE (2003) Tumorigenesis and the angiogenic switch. *Nature Reviews Cancer* 3(6):401-410.

117. Paez-Ribes M, *et al.* (2009) Antiangiogenic Therapy Elicits Malignant Progression of Tumors to Increased Local Invasion and Distant Metastasis. *Cancer Cell* 15(3):220-231.

118. Goel S, *et al.* (2011) NORMALIZATION OF THE VASCULATURE FOR TREATMENT OF CANCER AND OTHER DISEASES. *Physiological Reviews* 91(3):1071-1121.

119. Verbridge SS, *et al.* (2013) Physicochemical regulation of endothelial sprouting in a 3D microfluidic angiogenesis model. *Journal of Biomedical Materials Research Part A* 101(10):2948-2956.

120. Carmeliet P & Jain RK (2000) Angiogenesis in cancer and other diseases. *Nature* 407(6801):249-257.

121. Carmeliet P & Jain RK (2011) Principles and mechanisms of vessel normalization for cancer and other angiogenic diseases. *Nature Reviews Drug Discovery* 10(6):417-427.

122. Jain RK (2009) A New Target for Tumor Therapy. *New England Journal of Medicine* 360(25):2669-2671.

123. Sung JH, Esch MB, & Shuler ML (2010) Integration of in silico and in vitro platforms for pharmacokinetic-pharmacodynamic modeling. *Expert Opinion on Drug Metabolism & Toxicology* 6(9):1063-1081.

124. Scott J, Kuhn P, & Anderson ARA (2012) Unifying metastasis - integrating intravasation, circulation and end-organ colonization. *Nature Reviews Cancer* 12(7):445-446.

125. Esch MB, King TL, & Shuler ML (2011) The Role of Body-on-a-Chip Devices in Drug and Toxicity Studies. *Annual Review of Biomedical Engineering, Vol 13*, Annual Review of Biomedical Engineering, eds Yarmush ML, Duncan JS, & Gray ML), Vol 13, pp 55-72.

126. Sung JH, Kam C, & Shuler ML (2010) A microfluidic device for a pharmacokinetic-pharmacodynamic (PK-PD) model on a chip. *Lab on a Chip* 10(4):446-455.

127. Anderson ARA & Quaranta V (2008) Integrative mathematical oncology. *Nature Reviews Cancer* 8(3):227-234.

128. Chakrabarti A, Verbridge S, Stroock AD, Fischbach C, & Varner JD (2012) Multiscale Models of Breast Cancer Progression. *Annals of Biomedical Engineering* 40(11):2488-2500.

129. Borau C, Kamm RD, & Garcia-Aznar JM (2011) Mechano-sensing and cell migration: a 3D model approach. *Physical Biology* 8(6).

130. Kam Y, *et al.* (2009) Nest expansion assay: a cancer systems biology approach to in vitro invasion measurements. *BMC research notes* 2:130-130.

131. Stylianopoulos T, Diop-Frimpong B, Munn LL, & Jain RK (2010) Diffusion Anisotropy in Collagen Gels and Tumors: The Effect of Fiber Network Orientation. *Biophysical Journal* 99(10):3119-3128.

132. Anderson ARA (2005) A hybrid mathematical model of solid tumour invasion: the importance of cell adhesion. *Mathematical Medicine and Biology-a Journal of the Ima* 22(2):163-186.

133. Anderson ARA, Weaver AM, Cummings PT, & Quaranta V (2006) Tumor morphology and phenotypic evolution driven by selective pressure from the microenvironment. *Cell* 127(5):905-915.

134. Anderson ARA, Rejniak KA, Gerlee P, & Quaranta V (2009) Microenvironment driven invasion: a multiscale multimodel investigation. *Journal of Mathematical Biology* 58(4-5):579-624.

135. Quaranta V, Rejniak KA, Gerlee P, & Anderson ARA (2008) Invasion emerges from cancer cell adaptation to competitive microenvironments: Quantitative predictions from multiscale mathematical models. *Seminars in Cancer Biology* 18(5):338-348.

136. Song JW, Bazou D, & Munn LL (2012) Anastomosis of endothelial sprouts forms new vessels in a tissue analogue of angiogenesis. *Integrative Biology* 4(8):857-862.